Optimization of Transcurium Isotope Production in the High Flux Isotope Reactor

A Dissertation Presented for the
Doctor of Philosophy
Degree
The University of Tennessee, Knoxville

Susan Hogle

December 2012

© Susan Hogle 2012

All Rights Reserved

Dedication

To my father Hubert, who always made me feel like I could succeed and my mother Anne, who would always love me even if I didn't.

Acknowledgements

This research is supported by the Isotopes Program, Office of Nuclear Physics of the Oak Ridge Nuclear Laboratory, U.S. Department of Energy. ORNL is managed by UT-Battelle, LLC, for the U.S. Department of Energy under contract DE-AC05-00OR22725.

This dissertation would not have been possible without the backing I have received from my advising team of G. Ivan Maldonado, Chuck Alexander and Julie Ezold. I would like to thank my advising professor Ivan Maldonado for seeing potential in me; for providing me with the chance to pursue my studies and research under his guidance and always ensuring his students are given every opportunity to succeed. I would like to thank my technical advisor Chuck Alexander for giving me access to his astounding mind; for always being available to trade ideas, and for pointing out possibilities that I could not have envisioned. I would like to thank my mentor Julie Ezold for her overwhelming support, both personal and professional. Nearly any problem encountered can, if not be solved, be at least soothed, by a trip to Julie's office.

I would like to thank the members of my dissertation committee: Dr. Lawrence Heilbronn, Dr. Howard Hall and Dr. Robert Gryzwicz; for their guidance during my dissertation work which has helped bring this dissertation to its final form. I would like to thank all the staff at the Radiochemical Engineering Development Center, as well as at the University Of Tennessee Department Of Nuclear Engineering for their tireless support of their students. I would also like to thank my fellow students for keeping me sane over the past years. For making me wake up in the morning happy to come into work, even if I was looking at a tedious day of coding. I will miss my 6' by 4' cube in the graduate student office.

Finally I would like to thank my family, who has always given me their unconditional encouragement and support. To my parents Anne and Hubert, who did not balk at my plan to move 1000 miles away for graduate school any more than they did when I professed my undying desire to attend theatre school at the age of 12, I cannot thank you enough for all you have done for me. To my siblings Janet, Karen and Jeff, I am sorry I have missed seeing your children grow up and become the lovely people I am sure they will be. Thank you for being there to lend an ear when home seemed so far away.

Abstract

The Radiochemical Engineering Development Center at Oak Ridge National Laboratory is the world's leader in production of californium-252. This and other heavy actinides are produced by irradiation of mixed curium/americium targets in the High Flux Isotope Reactor. Due to the strong dependence of isotopic cross sections upon incoming neutron energy, the efficiency with which an isotope is transmuted is highly dependent upon the neutron flux energy spectrum and intensities. There are certain energy ranges in which the rate of fissions in feedstock materials can be minimized relative to the rate of (n,γ) absorptions. This work shows that by perturbing the flux spectrum, it is possible to alter the net consumption of curium feedstock, as well as the yields of key isotopes for the heavy element research program, such as ^{249}Bk and ^{252}Cf. This flux spectrum perturbation is accomplished by means of focused resonance shielding through the use of filter materials. This work further shows that these perturbations can alter the target yields in a significant way, increasing the amount of ^{252}Cf produced per unit curium consumption. All materials with isotopes containing appropriate energy level resonances are examined and extensive data has been obtained on the filtering effects of these materials. Neural networks and genetic algorithms are used to develop an optimization framework for evaluating the performance of filter materials. This algorithm allows for customized optimization and selection of filter materials depending upon the need of the user and the campaign conditions.

Table of Contents

1. Introduction 1

1.1 Motivation 4

1.2 Research Objective and Scope 5

2. Background 6

2.1 The High Flux Isotope Reactor and the Radiochemical Engineering Development Center 6

2.2. Californium-252 and other Heavy Actinide Isotopes 9

2.3. Actinide Radiochemistry 11

2.4. Transmutation and Losses 12

2.5. Resonance Shielding 18

2.6. Heavy Actinide Feedstock 20

2.7. Flux Spectrum Filtering 20

2.8. Benefits of Optimized Production 22

3. Literature Review 23

3.1 HFIR modeling capabilities 23

4. Methodology 24

4.1 Solving the Boltzman Transport Equation 25

4.1.1 Monte Carlo Methods 25

4.1.2 Diffusion Theory 26

4.1.3 Discrete Ordinates Methods 27

4.1.4 Bondarenko Method 27

4.1.5 Matrix Exponentiation 28

4.1.6 Neural Networks 28

4.1.7 Genetic Algorithms 30

4.2 Computer Codes and Modules 31

4.2.1 CSAS 31
4.2.2 KENO-VI 31
4.2.3 BONAMI 31
4.2.4 CENTRM 32
4.2.5 XSDRNPM 32
4.2.6 COUPLE 33
4.2.7 ORIGEN-S 33
4.2.8 Libraries 33
4.2.9 MATLAB 34
4.2.10 Perl 34
5. KENO Modeling of the High Flux Isotope Reactor 34
5.1. Fuel Elements 35
5.2. Flux Trap 36
5.3. Control Elements 38
5.4. Reflectors 39
5.5. Validation 41
5.6. Flux Variation 43
5.7. Depletion 45
6. SCALE model using CENTRM/XSDRN/BONAMI 46
7. Filtering 49
8. Transient Behavior of Filtering 56
9. Physical Limitations 59
10. Potential Filter Materials 61
10.1. Rhodium 61
10.2. Indium 63

10.3. Tellurium 64
10.4. Lanthanum 65
10.5. Promethium 67
10.6. Samarium 67
10.7. Europium 69
10.8. Dysprosium 70
10.9. Erbium 71
10.10. Lutetium 73
10.11. Hafnium 74
10.12. Tantalum 76
10.13. Rhenium 77
10.14. Iridium 78
10.15. Summary of Filter Materials 80
11. Data Uncertainties 81
12. Reaction Rate Optimization Routines 83
12.1. Problem Definition 86
12.2. Case Preparation 88
12.3. Case Evaluation 89
12.4. Analyze Transmutation Parameters 93
12.5. Analyze Fitness 94
12.6. Performance 95
13. Conclusions 100
14. Summary of Future Work 102
List of References 103
Vita 109

List of Figures

Figure 1: High Flux Isotope Reactor 7
Figure 2: Typical Target Rod for the HFIR Flux Trap 8
Figure 3: Transcurium production pathways. 13
Figure 4: Reaction rates for mid-campaign target composition 14
Figure 5: Rate of fissions per (n, γ) absorption for Cm-245, Cm-247 and Cf-251 15
Figure 6: Fission Rates per Isotope over Time 16
Figure 7: Fission Rates by Energy Range 17
Figure 8: Involute fuel plates of the HFIR core (left) and as modeled in KENO-VI (right) 35
Figure 9: Flux Trap as modeled in KENO-VI 37
Figure 10: Inner and Outer control elements, fuel elements, and flux trap experimental targets as modeled in KENO-VI 38
Figure 11: Permanent Beryllium Reflector 40
Figure 12: Reflector Regions and Experimental Sites as Modeled in KENO-VI 41
Figure 13: Flux in the flux-trap target region versus radial distance from center. 42
Figure 14: Highlighting the greater flux discrepancy in the target region, versus the moderator region, for differing target compositions 44
Figure 15: Flux Spectra Comparison between CENTRM and KENO-VI 47
Figure 16: Cross sections for key isotopes in the transcurium chain and potential filter materials 50
Figure 17: Flux Spectra for Varying Target Compositions 51
Figure 18: Reaction rates over time 56
Figure 19: Hf-176 (n,γ) absorption and Hf-177 total absorption cross sections 57
Figure 20: Os-190 (n,γ) absorption and Ir-191 total absorption cross sections 58
Figure 21: In growth of Ir-191 and Hf-177 from parent products 59
Figure 22: Total Cross section - Rhodium 103 62
Figure 23: Total Cross Sections - Indium 63
Figure 24: Total Cross Section - Tellurium 123 65
Figure 25: Total Cross Section - Lanthanum 138 66
Figure 26: Total Cross Sections - Samarium 68

Figure 27: Total Cross Sections - Europium 69
Figure 28: Total Cross Sections - Dysprosium 71
Figure 29: Total Cross Section - Erbium 167 72
Figure 30: Total Cross Sections - Lutetium 73
Figure 31: Total Cross Sections - Hafnium 75
Figure 32: Total Cross Sections - Tantalum 76
Figure 33: Total Cross Sections - Rhenium 77
Figure 34: Total Cross Sections - Iridium 79
Figure 35: Iterative optimization routine 84
Figure 36: Neural Network Layout 89
Figure 37: Neural Network Mean Squared Error 91
Figure 38: Neural Network Error Distribution 92

List of Tables

Table 1: Actinide yields from a typical target irradiation 17
Table 2: k-eff values with neutrons per generation (NPG), number of generations (Ngen), total run time and library used. 42
Table 3: Flux Variation Statistics 43
Table 4: Isotope Yields from KENO-VI five cycle depletion 45
Table 5: Comparison of Predicted Curium Isotope 48
Table 6: Transcurium yields (g) a 5-cycle irradiation for varying target compositions 54
Table 7: Production rates for Cm-244 for mixed curium targets, and for mixed curium, Ir-191 and Hf-177 targets 55
Table 8: Destruction rates for Cm-244 for mixed curium targets, and for mixed curium, Ir-191 and Hf-177 targets 55
Table 9: Actinide yields with pellet and cladding filters 60
Table 10: Isotopes of Rhodium 61
Table 11: Isotopes of Indium 63
Table 12: Isotopes of Tellurium 64
Table 13: Isotopes of Lanthanum 66
Table 14: Isotopes of Promethium 67
Table 15: Isotopes of Samarium 67
Table 16: Isotopes of Europium 69
Table 17: Isotopes of Dysprosium 70
Table 18: Isotopes of Erbium 72
Table 19: Isotopes of Lutetium 73
Table 20: Isotopes of Hafnium 74
Table 21: Isotopes of Tantalum 76
Table 22: Isotopes of Rhenium 77
Table 23: Isotopes of Iridium 78
Table 24: Reported cross section uncertainties for minor actinides as percent of total cross-section 81
Table 25: Relative Contributions to Uncertainty in Keff 82
Table 26: Neural Network Target Yields 93

Table 27: Optimized Projections weighted for Cf production with 6 g indium 96
Table 28: Optimized Projections weighted for Cf production with 3 g indium and 12 g tantalum 97
Table 29: Optimized Projection Weighted for Cf production and Cm consumption with 6 g tantalum and 5 g dysprosium 98
Table 30: Optimized Projection Weighted for Cf production and Actinide Consumption with 6 g dysprosium, 2 g hafnium and 6 g indium 99

1. Introduction

The time dependent composition of a material subject to a flux of neutrons is a complex function of the starting composition, material reaction properties, physical geometry and neutron flux characteristics. The rate of change of the concentration of each individual nuclide in a material composed of potentially hundreds of nuclides is dependent upon the rates of change of the concentrations of many other nuclides, resulting in large sets of coupled differential equations. The general equation for the concentration of one nuclide N_i can be express as the difference between the formation rate and the destruction rate:

$$\frac{dN_i}{dt} = Formation\ Rate - Destruction\ Rate$$

Any process in which ${}^{b}_{a}N$ is converted to another nuclide (or multiple nuclides) is considered a destruction of ${}^{b}_{a}N$, for example the (n,γ) reaction ${}^{b}_{a}N + {}^{1}_{0}n \rightarrow {}^{b+1}_{a}N + \gamma$, while any process in which another nuclide is converted to ${}^{b}_{a}N$ is considered a formation, for example the α decay ${}^{b+4}_{a+2}X \rightarrow \alpha + {}^{b}_{a}N$.

There are a multitude of reactions which can take place under the presence of a high neutron flux, including (n,2n), (n,p), (n,γ), (n,f), etc. However, the rates of change of nuclide concentrations are generally dominated by the (n,γ) and (n,f) reactions, as well as radioactive decay. The result is the time-dependent nuclide concentration equation which can be written as:

$$\frac{dN_i}{dt} = \int_0^\infty \left[\sum_{j \neq i} Y_j \sigma_{f,j}(E) N_j \varphi(E) + \sigma_{c,i-1}(E) N_{i-1} \varphi(E) - \sigma_{a,i}(E) N_i \varphi(E) \right] dE + \sum_k \lambda_k N_k - \lambda_i N_i$$

(Eq. 1)

Where the summation over j encompasses all nuclides N_j which may produce N_i as a result of nuclear fission with yield Y_i, and the summation over k encompasses all nuclides N_k which may produce N_i as a result of radioactive decay. The other terms account for the production of N_i from N_{i-1} via neutron capture and the destruction of N_i via neutron capture or decay. The neutron flux □(E) is a function of the neutron energy, as is the effective cross section σ(E). The key to solving this equation for every nuclide N_i is obtaining accurate estimates of the neutron flux and effective cross sections as a function of neutron energy.

Obtaining an accurate estimate of the flux in the region of interest involves modeling the particle transport process of the overall system in which the flux is generated. This can be done by solving the Boltzman neutron transport equation.

$$\frac{1}{v}\frac{\partial \Phi}{\partial t}\left(\vec{r}, E, \hat{\Omega}, t\right) + \hat{\Omega} \cdot \nabla \Phi\left(\vec{r}, E, \hat{\Omega}, t\right) + \Sigma_t\left(\vec{r}, E, \hat{\Omega}, t\right)\Phi\left(\vec{r}, E, \hat{\Omega}, t\right) = \int_{4\pi} d\hat{\Omega}' \int_0^{\infty} dE' \Sigma_s\left(\vec{r}, E' \rightarrow E, \hat{\Omega} \rightarrow \hat{\Omega}', t\right)\Phi\left(\vec{r}, E', \hat{\Omega}', t\right) + S\left(\vec{r}, E', \hat{\Omega}', t\right)$$

(Eq. 2)

This equation can be very challenging to solve even for the simplest geometries. One of the most popular approaches for modeling neutron transport is via Monte Carlo-based stochastic methods. In such methods, each interaction in the transport process is treated as a probabilistic occurrence, following a neutron from its creation, during fission or from other source, through each interaction, to its capture in, or escape from, the system. If the time dependence is ignored and the terms on the right hand side of the equation combined to create an effective source, Q, from external and internal sources, the Boltzman equation can be expressed as follows.

$$\hat{\Omega} \cdot \nabla \Phi\left(\vec{r}, E, \hat{\Omega}\right) + \Sigma_t\left(\vec{r}, E, \hat{\Omega}\right)\Phi\left(\vec{r}, E, \hat{\Omega}\right) = Q\left(\vec{r}, E', \hat{\Omega}'\right)$$

(Eq. 3)

This is one of the most important equations in reactor physics, and a variety of computer codes have been developed which can be used to obtain solutions. One such code used extensively in this research is the KENO Monte Carlo criticality program, a part of the overall SCALE code package developed and maintained by the Oak Ridge National Laboratory [1]. Using KENO one can determine the neutron flux in user-defined geometry region for a set of pre-determined energy "bins." This angular-independent parameter is referred to as the *scalar* multi-group neutron flux. Although the KENO code is capable of modeling complex 3-D geometry and performing high fidelity flux calculations, the calculation time for 3-D reactor evaluations is generally quite high.

There exists a vast amount of data on the infinitely dilute energy-dependent reaction cross sections for most nuclides. An infinitely dilute reaction cross section represents the interaction

between the neutron and a single nuclide, without the interference or influence of any other nuclides particles. In addition, the term infinitely dilute infers that there is no self-induced flux depression (such as resonance self-shielding). Such cross sections are typically presented in a multi-group format, with each group representing a weighted average of the cross section at all energies within that range. Obtaining an accurate estimate of the effective cross sections for each nuclide present in the system involves analyzing the composition of the material and the physical geometry to determine the interference on the infinitely-dilute cross section.

One of the major contributors to interference with the infinitely-dilute cross section is resonance self-shielding. When a large resonance is present within an energy region, a large number of neutrons will be absorbed at this energy, causing a flux depression. As more material is added with the same resonance band more reactions will take place, however the reaction rate per atom will decrease.

The Bondarenko method [2] is a method of cross-section processing to account for resonance self-shielding in materials. Beginning with a master data set of infinitely dilute multi group cross sections, calculations are performed to develop a set of problem-dependent effective multi-group cross sections. The BONAMI module of the SCALE code package is capable of performing iterative Bondarenko calculations for homogeneous or heterogeneous one-dimensional problems, with multizone slab, cylindrical or spherical geometry. The main advantage of the BONAMI code for cross-section processing is its simplicity and speed.

As with any method for determining multigroup resonance self-shielded cross-sections, the Bondarenko method attempts to calculate the average cross section within an energy group "g" using the following equation:

$$\overline{\sigma_g} = \frac{\int_g \sigma(E)\varphi(E)dE}{\int_g \varphi(E)dE}$$

(Eq. 4)

The Bondarenko method relies on the narrow resonance approximation, which assumes that the practical width of a resonance of an absorber nuclide is much smaller than the average energy loss due to collision with the nuclide, and that the collision density is thus constant throughout

the resonance. The self-shielded cross sections are then determined by interpolating from a series of tables of "Bondarenko factors," which are a function of the temperature, energy group, and the cross section of the mixture per atom of nuclide "i" for all nuclides in the mixture other than nuclide "i". As the BONAMI code and Bondarenko method rely on the narrow resonance approximation, this code is useful primarily in calculating effective group cross sections in the unresolved resonance region.

In the resolved resonance region a more detailed method is frequently utilized for calculating multigroup resonance self-shielded cross-sections. One such method is the Continuous Energy Transport Module (CENTRM) [3], which solves the Boltzmann neutron transport equation in one-dimension using deterministic approximation such as discrete ordinates, diffusion, homogenized infinite medium or zone-wise infinite medium calculations to compute a point-wise flux spectrum and point-wise and multigroup cross sections. The user may set the bounds for the point-wise energy region, and hence this code is particularly powerful for examining resolved resonances of particular nuclides. XSDRNPM [30] is another one-dimensional discrete ordinates transport code frequently used in conjunction with CENTRM for determining multi-group flux spectra and collapsing cross sections by cell, zone, or other parameters.

As with most applications of computing and optimization, there are no modeling and simulation approaches that may be universally "best," and applicable to all situations. Instead, the modeling and simulation process to be used is dependent upon the problem constraints and variables, the known and desired information, the accuracy required and the computing time available. As part of this research many modeling and simulation techniques have been used, with the objective being to model only what is necessary and by making assumptions and approximations where applicable.

1.1 Motivation

The Radiochemical Engineering Development Center (REDC) at the Oak Ridge National Laboratory is among the world's top suppliers of heavy actinides such as californium-252 and berkelium-249, which are produced by irradiation of actinide targets in the High Flux Isotope Reactor (HFIR) [4]. The current tools in place for modeling this process do not employ optimization methods. It is up to the user to choose the target composition and irradiation scheme. The current methods for heavy actinide yield calculations, performed using an in-house

Fortran code called TCOMP [5] in fact, use a static set of fluxes that are not dependent upon the composition of the target, and a set of two-group cross section parameters that are not dependent upon the flux spectrum within the group. These simple calculations do not take into account the impacts that one nuclide may have on another, or on the physical arrangement of the materials target. While these calculations are useful for predicting yields within an acceptable margin of error given starting masses of the key isotopes, they are not able to identify changes within the transmutation scheme as a result of inter-isotope interactions.

The overall process of generating these heavy actinides involves many losses, due to decay, fission, or transmutation to other undesirable isotopes. Currently, a simple brute force approach is employed during irradiation campaigns; whereby targets are prepared using available feed material and irradiated for as long as is necessary to produce the amount of heavy actinides necessary to meet customer demand. The supply of curium feedstock useful for heavy actinide generation is limited, and efficient use of this material is necessary in order to continue to meet customer demand in the future.

1.2 Research Objective and Scope

An initiative has recently been undertaken to analyze the transcurium isotope production process and to identify possible means of optimizing production of the heavy actinides relative to consumption of the curium feedstock. With each irradiation cycle, fission losses reduce the total actinide inventory, however, due to the energy dependence of neutron capture and fission cross sections, the likelihood of fission per capture in the target actinide is greater for certain energies of an incoming neutron. Therefore, it is proposed that by reducing the neutron flux present in the actinide targets within these key energy ranges, the total number of captures per fission can be increased, resulting in greater target yield per consumption of feedstock material. The purpose of this research is to analyze the effects of the flux spectrum on the overall transmutation rates and to identify means of perturbing the flux spectrum with the purpose of optimizing transcurium production for the REDC. By employing some of the latest simulation tools available, and by casting this problem into a generalized combinatorial optimization framework, the goal of this study is to define key control variables, as well as to establish pertinent objectives and constraints for this problem of very large dimensionality, so that optimization techniques may be

used to perform a significant and computationally intensive sweep of the optimization search space.

Primary Objectives:

1) Develop, test and assess a detailed 3-D Monte Carlo KENO model with the capability of determining high fidelity flux spectra in the actinide target region.
2) Develop, test and assess computationally efficient scoping models of the target region of the HFIR with the capability of quickly analyzing the effects on the flux spectra and effective cross sections due to small changes in target compositions.
3) Develop a fundamental understanding of the key reactions in the transmutation chain for the production of heavy actinides. Identify sources of feedstock material loss.
4) Analyze the effects on key reaction rates of inserting absorption materials for the purposes of reducing feedstock fission losses. Define the pertinent control variables, objectives, and constraints that apply.
5) Develop optimization drivers that iteratively model small changes to the target's geometry and compositions, with objectives and constraints tied to the campaign goals in order to maximize transcurium production, while minimizing (or constraining) consumption of feedstock material.

2. Background

2.1 The High Flux Isotope Reactor and the Radiochemical Engineering Development Center

The HFIR reactor at ORNL is a beryllium-reflected, light-water-cooled pressurized flux-trap-style research reactor. The HFIR is rated to a maximum operating power of 100 MW, and is currently operating at 85 MW.

As illustrated in Figure 1, at the center of the reactor is the 12.7 cm diameter flux trap containing 37 vertical target sites, which in typical operation sees a mid-plane, steady-state thermal flux on the order of 2 x10^{15} n/cm^2·s. Each of these target sites may be loaded with independent experiments, or dummy targets. Additionally, one of the targets sites contains a hydraulic tube,

which may contain up to 7 experiments, which may be moved in and out of the reactor during operation.

Surrounding the flux trap are two fuel or core regions, the inner fuel region, consisting of 171 involute-shaped fuel plates of highly enriched uranium-oxide "meat" contained within aluminum cladding, and the outer fuel region, consisting of 369 involute-shaped fuel plates. The uranium-oxide in the inner fuel element contains boron-10, a burnable poison, to help shift the power distribution to the outer fuel element.

Between the outer fuel element and the beryllium reflector is the control region which consists of two concentric poison-bearing control elements. These control elements consist of four axial regions of varying absorption characteristics, and are moved in opposite directions during operation to control reactivity.

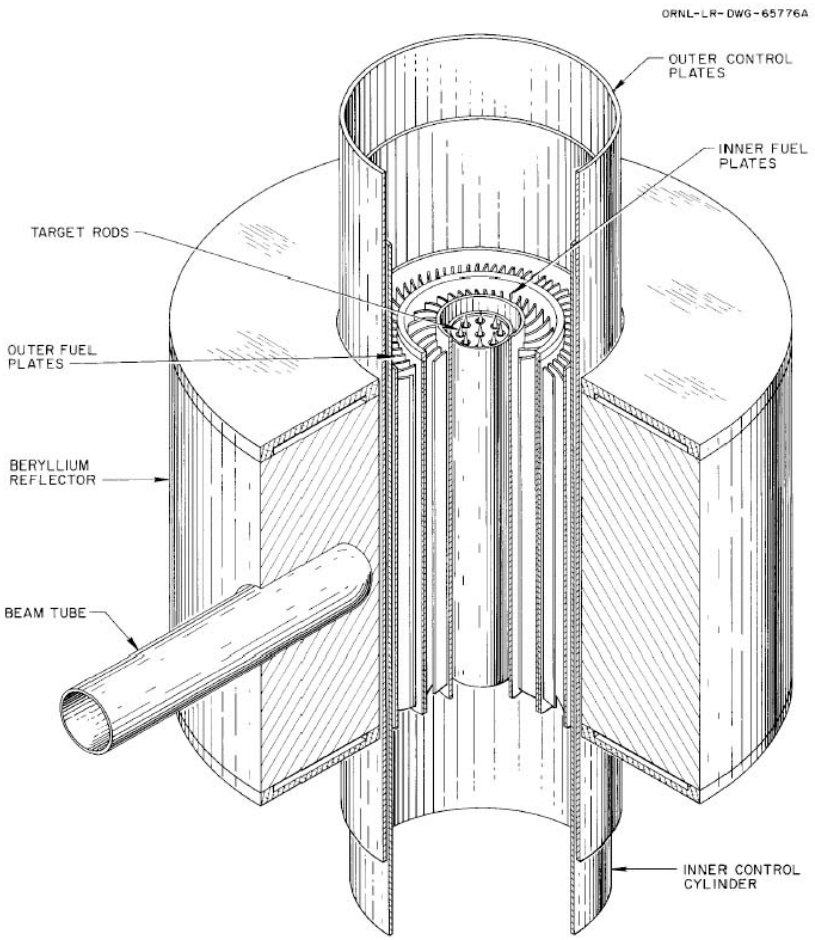


Figure 1: High Flux Isotope Reactor

The outer fuel region is surrounded by a beryllium reflector, which is subdivided into three regions: the removable, semi-removable, and permanent beryllium reflector regions. The reflector region sees a steady-state thermal flux on the order $2x10^{12}$ n/cm^2·s. This region of the HFIR also contains 42 experimental target sites of varying size and location that are used extensively for research and development, most recently being evaluated for the production of Pu-238.

The reflector is surrounded by water of effectively infinite thickness, and the core is also reflected by water in the axial direction. The entire assembly is contained within a 244 cm diameter steel pressure vessel immersed within a pool of water.

For a typical transcurium isotope production campaign, the REDC at ORNL prepares new target rods, principally composed of mixed curium isotopes, for irradiation in the HFIR flux trap target sites. The cylindrical target rods, such as that depicted in Figure 2, contain typically between 30-35 pellets, with aluminum powder end caps and contained within an aluminum cladding. When inserted into the target shroud, these pellets compose the 506 mm active length of the 889 mm rod.

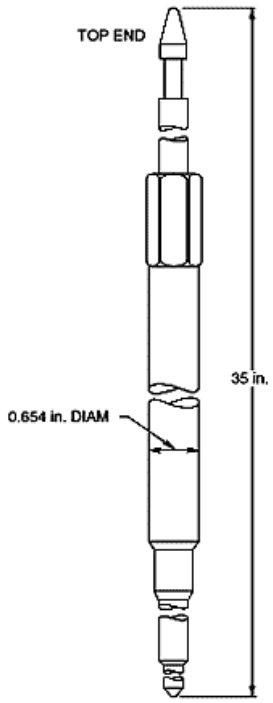


Figure 2: Typical Target Rod for the HFIR Flux Trap

The target rods produced by the REDC are irradiated in the HFIR for a number of cycles which depends upon the initial target composition, number of targets, and production goals. Typically, in recent campaigns, four to six targets containing eight grams of heavy curium per target have been irradiated for five to seven irradiation cycles. Each irradiation cycle lasts approximately 22-25 days, with downtime of 10-50 days between cycles.

After irradiation, the targets are left to cool before being transferred to the REDC hot cell facilities. The Al target holders (referred to as hex cans) are removed, and the target clad, pellet clad, the pellet Al matrix and the irradiated curium oxide are placed in a caustic nitrate dissolver. The Al and caustic-soluble fission products dissolve leaving behind, primarily, the rare earth fission products and the actinides. The rare earth fission products and the actinides are dissolved in nitric acid and are separated by batch extraction and anion and cation exchange chromatography. The remaining purified mixed curium, plutonium and americium are recycled and re-fabricated into new targets.

The current production goal of the REDC is to produce 150 mg of Cf-252 every two years. The current operating schedule does not typically involve simultaneous target fabrication, irradiation and processing, resulting in a fairly linear process. Target fabrication requires approximately three months, and target processing requires another three months, allowing up to 18 months for irradiation and cooling.

2.2. Californium-252 and other Heavy Actinide Isotopes

Californium, atomic number 98, is a soft, dense silvery-grey metal and like all transuranium isotopes it is entirely artificially produced. Californium is named after the state of California, where it was discovered at UC-Berkley in the 1950s by bombarding curium-242 with helium ions. The main isotopes of californium are Cf-249 through Cf-252, with other isotopes (Cf-253 and Cf-254) existing only for much shorter periods of time. Cf-249 through Cf-252 all primarily decay by alpha emission, with half-lives ranging from 900 years for Cf-251 to 2.645 years for Cf-252. Cf-249 through Cf-252 also decay through a spontaneous fission branch [6].

While the fraction of spontaneous fission decays is very small for most of the Cf isotopes, for Cf-252 the spontaneous fission fraction is approximately 3% of all total decays, with a combined half-life of 2.645 years, losing approximate 2% of its mass every month. This results in Cf-252

being a very powerful neutron emitter, with one microgram emitting approximately 170 million neutrons per minute, with an energy spectrum similar to that of a fission rector.

Cf-252 is useful as a neutron source for various industrial, research and medical purposes. One of the primary applications of Cf-252 is prompt gamma neutron activation analysis, or PGNAA, which involves exposing a sample to a flux of neutrons and examining the resulting gamma spectrum from the sample. As atoms in the sample capture a neutron, they will achieve an excited state (compound nucleus) and almost instantaneously emit high energy prompt gamma photons. The energies of the photons are unique to the element, and analyses of the prompt gamma spectrum provide a measure of the elemental content of the sample. PGNAA is used extensively in the coal and cement industries for on-line analysis of feed materials, slurries and laboratory samples [8].

Cf-252 has also been shown to be effective in the treatment of advanced cervical cancer. This brachytherapy involves inserting a neutron source directly into the region of the cancer, and may also involve providing external doses. Because of the high linear energy transfer of fast neutrons, they are able to deliver high radiation damage directly to the tumor site [9].

Cf-252 is also used extensively for neutron radiography, providing initial neutrons when starting up a fresh fuel core in a power reactor, calibration standards, and production of fission fragments for research.

At the REDC, the separated and purified Cf-252 is distributed in a palladium matrix shaped into thin wire or pellets for encapsulation at other commercial operations. In the past californium-oxide has also been encapsulated into compact portable neutron sources, typically about the size of a pinky finger, or smaller.

Production of californium is typically achieved by bombarding curium rich in Cm-246 and Cm-248 with a high flux of neutrons, transmuting Cm-248 into Bk-250 via two neutron captures and one beta decay, which quickly beta decays (half-life of 3.2 hours) to Cf-250.Additional neutron captures by Cf-250 lead to the higher isotopes of Cf-251 and Cf-252, with losses due to fission and decay during the process. Cf-252 itself has a total thermal capture cross section of approximately 50 barns, leading transmutation into heavier actinide isotopes during the irradiation.

Berkelium-249 is another major isotope produced by the REDC, both as an intermediary step for the production of Cf-252, and as a target for international super-heavy element research programs. Berkelium, like californium, is a soft, dense silvery-grey metal, named after the location of its discovery in 1949 at UC-Berkeley in California. Berkelium-249 does not have any known industrial purposes, and hence is not produced in great amounts, other than along the pathway to the production of heavier actinides. However, Bk-249 is used extensively in scientific-research for the synthesis of super-heavy elements.

In 2009 the REDC produced a 22 milligram batch of Bk-249 which was then sent to the Joint Institute for Nuclear Research in Dubna, Russia. This sample was exposed to a Ca-48 beam at the Dubna Gas Filled Recoil Separator for 150 days and resulted in the synthesis of the element ununseptium, atomic number 117, for the first time [10].

2.3. Actinide Radiochemistry

The actinide elements; actinium, atomic number 89, through lawrencium, atomic number 103; are 5f transitional elements having partially filled f and d orbitals in the valence states. The chemical and physical properties of an element are determined by the configuration of the valence electrons, the 5f and 6d electrons for the actinide elements. Since the configurations of these valence electrons are similar to the configurations of the 4f and 5d valence electrons for the lanthanide elements, they display similar properties. The ionic radii of the actinides decrease with increasing atomic number, meaning that the effective charges of the heavier actinides are relatively larger than those of the lighter actinides of the same valence. This difference, as well as the amount of energy required to promote an f electron to a d orbital, differentiates the behavior of the different actinide elements [11], [12].

Ion exchange is the main tool employed for separating actinides both from the lanthanide elements, and from each other. The actinide elements all have multiple valence states, however a valence of 3 is dominant for all actinides from curium to nobelium. The differences in the complexation properties between actinides and lanthanides in LiCl allows for group separation of the actinides from the lanthanides. Historically, separation of the actinide elements from each other has been performed using a variety of techniques involving organic acids as eluting agents, including citric, glycolic, tartaric, lactic, and α-hydroxyisobutyric acids [13], [14].

2.4. Transmutation and Losses

A typical actinide target initially consists of mixed curium, plutonium, and americium isotopes. As the target is irradiated, individual atoms of these isotopes may 1) capture a neutron and transmute into a heavier isotope, 2) capture a neutron and fission, 3) beta decay and transmute into a higher element of the same mass, or 4) alpha decay into a lighter element of lower mass. Throughout the transmutation process, the feedstock materials, as well as their daughter products which include the heavier actinides of berkelium, californium, einsteinium, and fermium, are both created and destroyed. The time-dependent composition of the target is a complex function, where the rate of change of the concentration of each isotope is dependent upon the concentrations of all other isotopes preceding it in the transmutation chain, its cross sections and half-life, and the energy dependent neutron flux. As discussed in the introduction, the rate of change of the nuclide concentration (N_i) for any given actinide isotope "i" can be described by the following balance, with the yield from fission being neglected:

$$\frac{dN_i}{dt} = \int_0^\infty \left[\sigma_{c,i-1}(E)N_{i-1}\varphi(E) - \sigma_{a,i}(E)N_i\varphi(E)\right]dE + \sum_{k\neq i}\lambda_k N_k - \lambda_i N_i$$

Eq. (5)

Where the two terms in the integral represent, respectively, production and destruction of N_i via neutron capture, the summation over "k" represents all nuclides N_k, which may produce N_i as a result of radioactive decay, and $\lambda_i N_i$ represents the decay of N_i. The neutron flux $\varphi(E)$ is a function of the neutron energy, as is the cross section $\sigma(E)$.

In order to produce transcurium isotopes, primarily Bk-249 and Cf-252, a series of (n,γ) neutron captures are required in the feedstock material. By a series of neutron captures and beta decays, the desired isotopes can be produced from lighter isotopes, with losses due to fission and decay along the way. The multiple pathways for the production of Bk-249 and Cf-252 from mixed feedstock are shown in Figure 3 with the primary, or most likely, path being highlighted in blue.

Each time a neutron is absorbed in the feedstock material it may induce fission or be captured to produce a heavier isotope. Heavier isotopes subsequently beta-decay to produce the next heaviest element with the same atomic number, or may absorb another neutron before beta decay occurs. The direction of each possible decay and capture is shown in Figure 3.

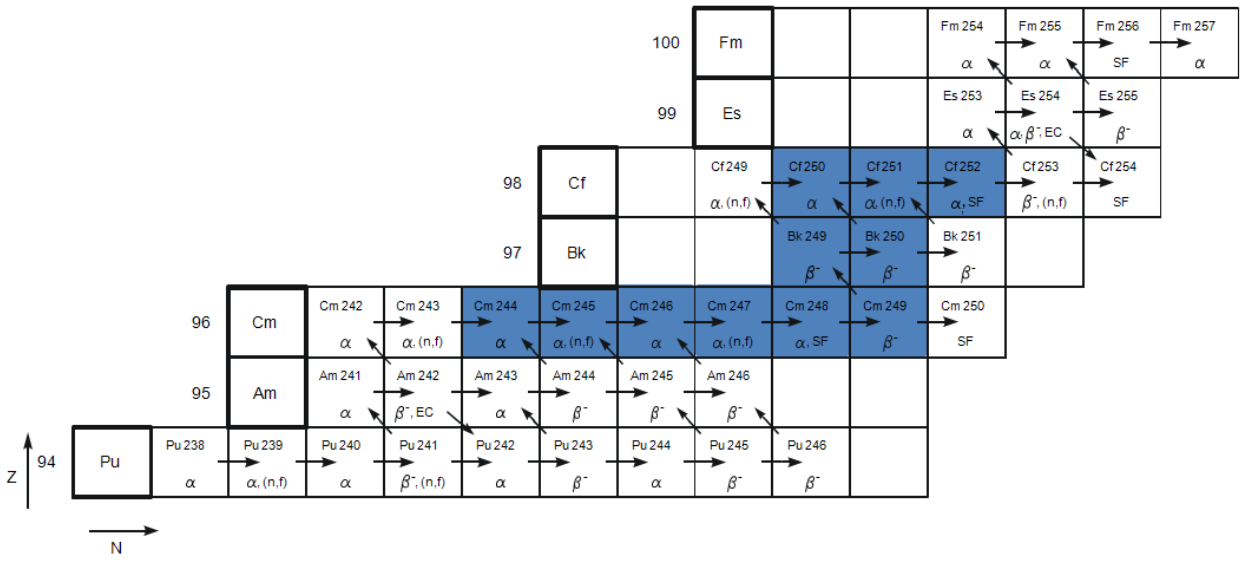


Figure 3: Transcurium production pathways.

As can be seen from the main pathway shown in Figure 3, a series of at least eight neutron captures and two beta decays is required to produce Cf-252 from Cm-244, with no fission or alpha decay. As the half-lives for these alpha emitters are all relatively long, compared to the irradiation times, the primary means for removing an atom from the transmutation path shown in Figure 3 is by fission. For each of the neutron captures, there is the potential for fission, removing the atom from the transmutation chain and reducing the total feedstock material available for transcurium isotope production.

Increasing the overall neutron flux by a constant value (that is, retaining the same energy profile but increasing the magnitude) will result in an increase to the neutron capture rates. This includes both (n,γ) capture, which is necessary for production of heavy actinides, and fission, which is destruction of feedstock material. The key to studying the feedstock losses is to examine the ratio of fission captures to non-fission-captures. Minimizing this ratio will result in less feedstock material destroyed per atom of heavy actinide generated. The term "potential californium," describes the maximum amount of californium that can be produced from a given batch [15]. Thus, the key to optimizing the potential californium entails reducing the number of fissions per neutron capture in the feedstock material, thus increasing the total amount of californium that could be created from a given batch of feedstock material.

By examining the fission and capture rates for each isotope in the main pathway, the isotopes for which feedstock losses are most significant can be identified. The fission and (n,γ) capture rates are shown below in Figure 4 for a typical 8 gram target, with a composition that would be expected after three irradiation cycles, which is approximately mid-way through a production campaign.

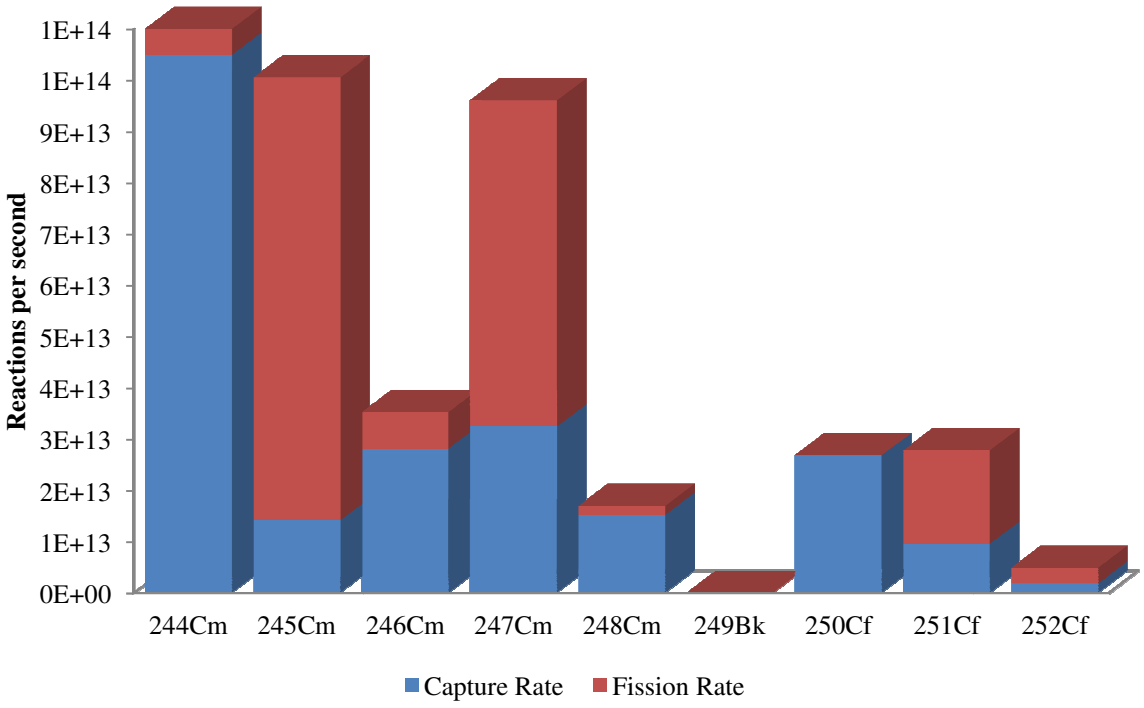


Figure 4: Reaction rates for mid-campaign target composition

It can be seen in Figure 4 that the ratio of fission captures to non-fission captures is highest for the isotopes Cm-245, Cm-247 and Cf-251, in decreasing order, and that these three isotopes also have the highest fission rates in the target, also in decreasing order (note that although the fission cross section for Cf-251 is higher than that of Cm-247, Cm-247 is present in much greater amounts in the target, resulting in a higher total fission rate). This would indicate that these isotopes have both the lowest "conversion ratio" and also the highest total loss rate, making them the primary sources of feedstock loss.

Figure 4 represents a 1-group reaction rate for capture and fission for each main isotope in the transmutation chain, however, as it has been noted that both the cross-sections and the flux are a function of energy, these capture and fission rates, and the resulting ratios, are also a function of

neutron energy. Investigating the reaction rates of each of these isotopes in further detail reveals that the ratio of fission-captures to non-fission-captures (ratio of the fission cross-section to the capture cross-section) varies with energy and that it is significantly greater in certain energy ranges. The energy dependence of the ratio between fission and capture is illustrated in Figure 5 for the primary isotopes of interest with the lowest conversion ratio: ^{245}Cm, ^{247}Cm and ^{251}Cf.

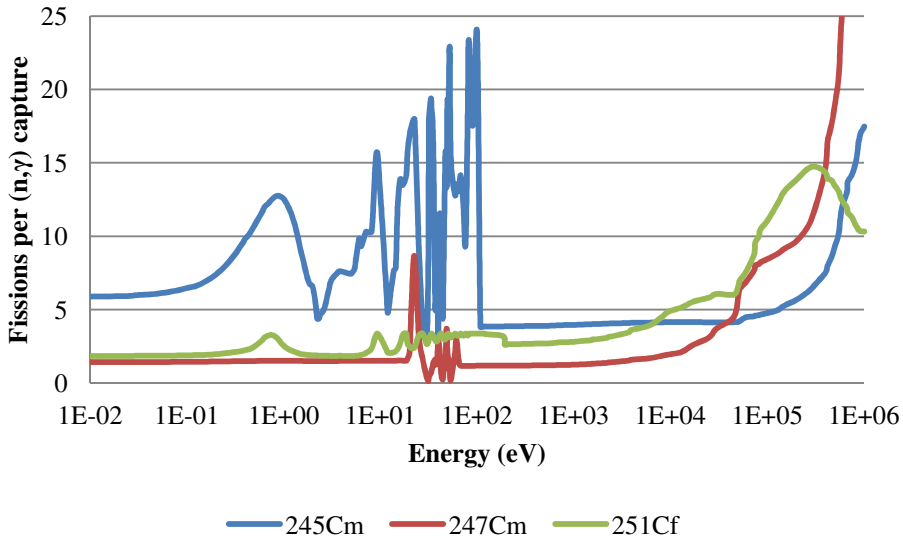


Figure 5: Rate of fissions per (n, γ) absorption for Cm-245, Cm-247 and Cf-251

It can be seen from Figure 5 that the rate of fissions per capture varies with the energy of the absorbed neutron, and there are clear energy ranges or bands where this rate is significantly higher. The more neutron captures which occur at energies where the ratio of fissions per capture is high, the greater the resulting loss of feedstock material per unit of heavy actinide produced. Therefore, reducing feedstock losses may be possible by promoting captures at energies where the ratio of fissions per capture is low. Although Figure 5 displays extremely high ratios of fissions per (n,γ) capture at energies greater than 1E5 eV, it should be noted that the overall cross sections are very low in this region, as is the flux, and hence minimal efficiency gains would be expected from flux perturbations in this region.

The ratio of fissions per capture for an isotope also varies with time, as the composition of the target changes, which in turn changes both the flux spectrum and the effective cross sections of the isotope. Figure 6 illustrates the fraction of the fission rate accounted for by each isotope in the target, over the course of five cycles.

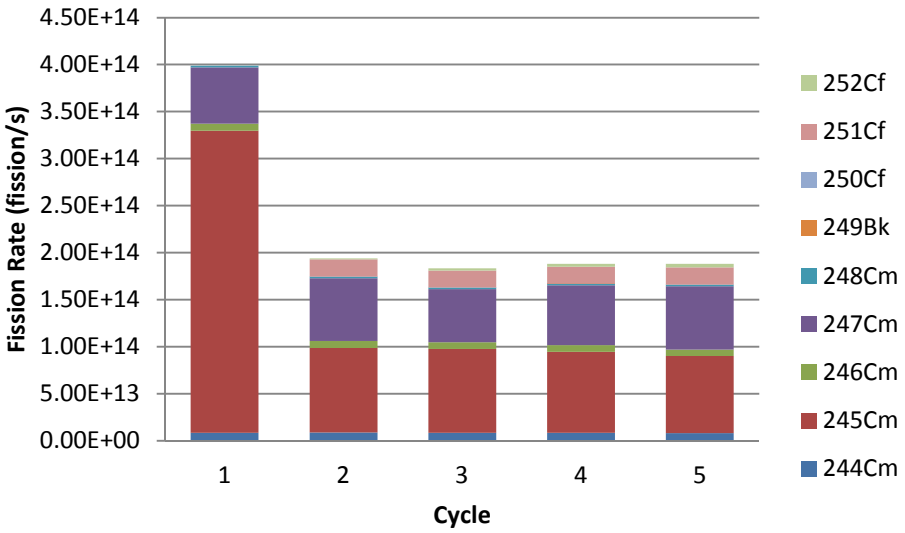


Figure 6: Fission Rates per Isotope over Time

As can be seen from Figure 6 the fission rate typically starts out quite high, drops quickly, and remains relatively stable for the rest of the campaign. The reason for this is that a typical target includes a significant amount of Cm-245 and Cm-247, which quickly burns out. Another key observation is that the contribution from Cm-247 increases from cycle 1 to cycle 2, decreases from cycle 2 to cycle 3, and then increases again from cycle 3 to cycle 4. If this irradiation were examined longer, it would be seen that the contribution from Cm-247 then slowly decreases after the 4^{th} or 5^{th} cycle. The reason for this is that the concentration of Cm-247 builds up from two different precursor isotopes, first from Cm-246 transmuting directly to Cm-247, peaking around cycle 2, and then from Cm-244 transmuting to Cm-247 through Cm-245 and Cm-246, peaking around cycle 4 or 5. Overall though, after the first cycle, the contributions to the fission rate from each isotope remain relatively stable, slowly decreasing as the actinide feed material is depleted. On average, Cm-245, Cm-247 and Cf-251 account for 50%, 35% and 10% of the fission losses, respectively.

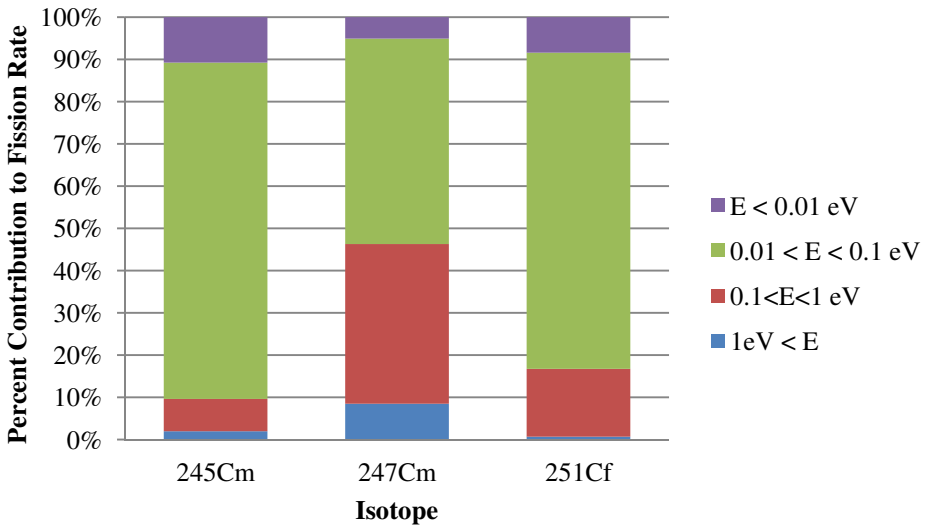
Irradiating a typical target for five irradiation cycles of 24 days each, with down-time of 19 days between each cycle results in the yields shown in Table 1, as modeled with the SCALE modules CENTRM and ORIGEN (see chapter 6 for details on SCALE models using CENTRM and ORIGEN). Total actinide losses over the five irradiation cycles are 1.703 grams or 21.46% of the initial mass. Using our previous estimates, this means that Cm-245, Cm-247 and Cf-251

account for 0.85, 0.60 and 0.17 grams of feedstock material loss respectively, or just over 95% of the total actinide losses.

Table 1: Actinide yields from a typical target irradiation

	Initial Mass (g)	Final Mass (g)
Cm-244	1.580	1.196
Cm-245	0.049	0.014
Cm-246	4.043	3.805
Cm-247	0.117	0.075
Cm-248	0.858	0.856
Bk-249	0	0.004
Cf-252	0	0.024
Total Actinides	7.937	6.111

Investigating even further, it can be estimated what fraction of these feedstock losses happen within specific energy bands. Integrating the fission cross sections of Cm-245, Cm-247 and Cf-251 with a typical flux spectrum for mid-campaign conditions the overall fission rates as a function of energy can be determined, which are shown in Figure 7.



.

Figure 7: Fission Rates by Energy Range

From Figure 7 it is observed that the greatest contribution to fission losses occurs in the energy range of 0.01 eV to 0.1 eV, with 0.1 eV to 1 eV being a close second for ^{247}Cm.

2.5. Resonance Shielding

As discussed in section 2.4, feedstock losses occur due to fission, which is also dominated by the isotopes Cm-245, Cm-247 and Cf-251. These fission rates are a function of the flux energy spectrum and the effective cross sections of the fissionable isotopes, while the ratio of fission captures to non-fission captures is a measure of the inefficiency of the transmutation. Reducing this ratio, by changing either the effective cross sections or the flux spectrum, is the means to increasing the efficiency of the transmutation process.

Energy self-shielding is the effect whereby the flux spectrum is attenuated in the presence of a large resonance. The neutron capture cross section around a large narrow resonance rises sharply as the energy approaches the resonance peak, and then falls rapidly. Neutrons which are scattered into this energy range will have a higher probability of capture than neutrons outside this energy range. Neutrons scattered past the energy range will not be affected by the resonance at all. This results in a flux depression over the range of the resonance from the increased capture at this energy, with the flux returning to its unperturbed value outside the resonance's range. This reduces the effective capture of the resonance, compared to what it would be if the resonance did not cause a flux depression; the higher the flux depression, the less effective the capture resonance.

The flux in the epithermal range can be determined from the transport equation as follows:

$$\varphi(E)\Sigma_t(E) = \sum_i \int_{E_2}^{E_1} dE' \, \frac{\Sigma_s^i(E')\varphi(E')}{E'(1-\alpha_i)}$$

(Eq. 6)

Where the summation on the right hand side is performed over all nuclides present, i. If we assume that the nuclides present are primarily hydrogen (α=0) and very heavy nuclei ($\alpha \approx 1$) this equation becomes:

$$\varphi(E)\Sigma_t(E) = \int_E^{\infty} dE' \frac{\Sigma_s^H(E')\varphi(E')}{E'} + \sum_i \int_E^{E/\alpha_i} dE' \frac{\Sigma_s^i(E')\varphi(E')}{E'(1-\alpha_i)}$$

$$\varphi(E)\Sigma_t(E) \cong \int_E^{\infty} dE' \frac{\Sigma_s^H(E')\varphi(E')}{E'} + \sum_i \Sigma_s^i(E)\varphi(E)$$

$$\varphi(E)\left[\Sigma_t(E) - \sum_i \Sigma_s^i(E)\right] \cong \int_E^{\infty} dE' \frac{\Sigma_s^H(E')\varphi(E')}{E'}$$

$$\varphi(E)[\Sigma_a(E) + \Sigma_s^H(E)] \cong \int_E^{\infty} dE' \frac{\Sigma_s^H(E')\varphi(E')}{E'}$$

(Eq. 7)

This results in an exponential attenuation of the flux of the form:

$$\frac{\varphi}{\varphi_0} = \exp\left(-\int_{E_2}^{E_1} \frac{\Sigma_a(E')dE'}{(\Sigma_a(E') + \Sigma_s^H)E'}\right)$$

(Eq. 8)

Applying this formula to an energy resonance it can be assumed that the width of the resonance ($E_1 - E_2$, or ΔE) is much more narrow than the energy of the resonance (E), and also that the resonance capture cross section is much larger than the hydrogen scattering cross section. This results in the following approximation for the attenuation factor due to energy shielding [16]:

$$\frac{\varphi}{\varphi_0} = \exp\left(-\int_{E_2}^{E_1} \frac{\Sigma_a(E')dE'}{(\Sigma_a(E') + \Sigma_s^H)E}'\right) \cong \exp\left(-\int_E^{E+\Delta E} \frac{dE'}{E'}\right) \cong \frac{E}{E + \Delta E}$$

Eq. (9)

Spatial self-shielding is the effect whereby a large mass of a highly absorbing material results in attenuation of the flux spectrum in the region of the material. Much like with energy self-shielding, this results in the overall capture in the region of the material being lower than it would otherwise be without the effects of the spatial self-shielding. The effect of spatial self-

shielding is dependent upon multiple factors, including the material density, rod or sphere diameter and lattice spacing.

It is this spatial self-shielding effect which made criticality possible in early graphite moderated reactors, increasing the probability that a neutron would "escape" the resonance energy region without being absorbed, in order to be absorbed in the thermal region where fission of uranium is much more likely.

2.6. Heavy Actinide Feedstock

The current production of heavy actinides at the REDC is performed using a feedstock material composed of heavy curium. A heavier feedstock, containing higher amounts of isotopes such as Cm-248 and Cm-246, as opposed to Cm-244, produces heavy actinides such as berkelium and californium faster, and results in fewer fission losses, as fewer neutron captures are required. The existing heavy curium feedstock available to the heavy element production program is not unlimited, and once that supply is depleted, targets must instead be fabricated from lighter curium stocks.

There are two inventories of light curium available for production of targets. This material may be used once heavy curium stocks are depleted, or may be used supplemental to the use of heavy curium in order to prolong its lifetime. These two light curium stocks would require significant pre-processing in order to prepare the material for target fabrication. These materials, even after pre-processing, could not be irradiated directly in the flux trap, unless blended with other materials, as the high concentration of Cm-245 would lead to heat generation beyond the design limitations.

It is desirable to prolong the use of heavy curium feedstock for as long as possible to reduce reliance upon lighter curium feedstocks, which are both less efficient to irradiate, due to the higher number of neutron captures required to produce Bk-249 and Cf-252, and also require more processing prior to irradiation in the flux trap.

2.7. Flux Spectrum Filtering

Flux spectrum filtering is the process of altering the overall magnitude and/or spectrum of the flux by the addition of filter materials within a specific energy range of the flux. These filter materials will absorb neutrons, removing them from the flux. The number and energy of

neutrons which are absorbed by these materials will depend upon the nature and physical placement of the filter material.

The attenuation of the neutron flux through a material can be expressed as:

$$\frac{\varphi}{\varphi_0} = \exp(-\Sigma t)$$

(Eq. 10)

Where φ is the transmitted flux φ_0 is the incident flux, Σ is the macroscopic cross section of the material and t is the thickness of material. As the cross section for the material varies with neutron energy, so does the flux transmission and attenuation.

The concept behind flux spectrum filtering is to make use of materials whose cross sections are higher in the region(s) where flux depression is desirable. As was described in section 2.4, the ratio of fission to non-fission capture is particularly high for Cm-245 in the region of 0.5 eV to 2 eV. If it was desired to depress the flux spectrum in this region, a filter material with a high cross section in that same energy band might be beneficial.

An ideally "perfect" filter material would have a high cross section in the energy region where the flux is to be depressed, and a negligible cross section everywhere else. Unfortunately, filter materials such as these do not exist. One of the difficulties encountered with flux spectrum filtering is that usually there will be a reduction of the flux throughout the entire energy spectrum. This effect can be minimized by selecting appropriate materials with cross sections that are significantly lower than those of the target material.

Another issue with flux spectrum filtering is that as the filter material absorbs neutrons and removes them from the flux, the filter material is depleted; each neutron capture removes an atom from the concentration of the filter material. One way of dealing with depletion of the filter material is by utilizing multi-layered filters of varying materials, each designed to depress the flux in a different energy region. Another method is to use filter materials which transmute by neutron capture into other filter materials, or using filter materials which "grow in" from other materials.

Flux spectrum filtering can be a very powerful tool for generating the local flux spectrum that is desired for a target irradiation. Flux spectrum filtering, as it has been examined as part of this research, does not generally increase the flux in any energy bin, it only removes neutrons from the flux in regions where flux depression is desired. To locally increase the flux in a particular energy region would require specifically designed scattering, which at this time has not been investigated.

2.8. Benefits of Optimized Production

The main benefit of optimizing the production of transcurium isotopes is that the current stock of heavy curium feedstock will not be consumed as quickly. As the material used to fabricate the targets was initially made nearly 40 years ago at the Savannah River Site, in facilities that have since been decommissioned and are no longer available, conserving this material for the foreseeable future is a necessary component to the ongoing operation of the heavy actinides production program at ORNL [7].

As the current inventory of heavy curium is depleted, light curium may be used as a supplemental feedstock material. However, as mentioned in section 2.6, this material is also of finite supply. Additionally, the material is not currently readily available for target fabrication and irradiation. Prolonging the use of the existing supply of heavy curium will provide the heavy actinide production program more time to develop new target feeds and designs, and would also allow for the potential to pre-irradiate the light curium to burn out high heat generating isotopes such as Cm-245 and Cm-247, and to increase the overall weight of the curium feedstock. Less supplemental light curium will be necessary to maintain current production rates if the transmutation efficiency is increased.

Processing of the irradiated targets, and fabrication of new targets, is also costly. If new targets are able to be irradiated for longer periods of time, before the feedstock material is depleted, irradiation and target fabrication costs may be reduced. Although at this time cost estimates have not been performed, these estimates would need to take into account any additional cost required to make the more efficient targets.

Finally, developing the tools necessary to analyze the irradiation efficiency will allow the pursuit of campaign-specific irradiations, which would depend upon the goals of each campaign.

3. Literature Review

3.1 HFIR modeling capabilities

The HFIR staff at ORNL currently makes an MCNP model available via their public website [17], which was validated against HFIR fuel cycle number 400 in 2004 by N. Xoubi [18] and published as part of a dissertation by Xoubi in November 2005[19]. The main research objectives of Xoubi's work were to study the difference between a predicted and actual eigenvalue at critical reactor conditions (the "eigenvalue drift"). As such, the focus of this model included depletion of the fuel, control and reflector regions, as opposed to the target island.

This work was continued by D. Chandler as part of a dissertation published in August 2011[20]. In this work Chandler investigated the dynamic behavior of the nuclear core in response to reactivity-induced perturbations. Chandler expanded upon the MCNP model developed by Xoubi and further developed a depletion model using the TRITON module of the SCALE code package and KENO-VI geometry. Though this model was capable of calculating target rod yields following irradiation [21] this was not the primary focus of the model. In order to perform depletion calculations in a reasonable timeframe, the geometry of the flux trap and control region was simplified.

At the REDC, calculation of target rod yields following irradiation is currently performed using an in-house developed code TCOMP [4]. TCOMP is a Fortran computer code calculates the analytical solution to the neutron concentration equation. The software is qualified to calculate critical safety parameters only for initial target compositions explicitly identified in the manual, which do not include some of the target compositions analyzed as part of this research. The software requires user input of the thermal and epithermal flux, as well as the cross sections, and the currently available data does not account for any sort of flux filtering or shared-resonance shielding.

Thermal flux filtering has long been used in the research and development world for experiments concerned with the epithermal and/or fast flux. This is particularly true of experimental work concerned with the actinide elements. In 2010, experiments were performed in the Advanced Test Reactor and Idaho National Laboratory for the purpose of examining the effective neutron capture cross sections of a variety of actinide elements, including Cm-244 and Cm-248 [25]. In

this experiment, boron and cadmium filters of varying thicknesses were employed in order to reduce the thermal neutron flux to a sufficient level such that the capture cross sections at higher energies could be analyzed. As usual, this experiment was modeled and simulated with MCNP prior to being carried out.

Similarly, simulations have been performed by Ellis, et.al [26] in an attempt to filter out the thermal range of the neutron flux spectrum so to approximate a fast flux spectrum for possible irradiations at HFIR that would be representative of the spectra within a liquid metal fast reactor. Given that the fast flux (> 0.1 MeV) in the target region of HFIR actually exceeds 1×10^{15} $n/cm^2.s$. The combination of this high fast flux and the use of a highly absorbing europium-oxide (Eu2O3) liner designed to filter thermal neutrons mimics an irradiation environment that closely approximates that of a fast reactor.

Filter materials can also be used to filter epithermal and fast neutron fluxes, as is the case in thermal neutron imaging. It was proposed in 2010 to use a sapphire (Al_2O_3) filter at the 2.0 MW TRIGA MARK-II reactor at Maamora Nuclear Research Center in Morocco in order to filter the epithermal and fast neutron flux [26] and enhance the neutron thermal beam neutron imaging. The beam line was simulated using GEANT4, another Monte Carlo transport code, and it was determined that a 5cm layer of sapphire permitted the filtration of epithermal neutrons as well as fast neutrons in a considerable way without perturbing the thermal neutron flux.

As of yet, no research has been found which deals specifically with the filtering of the neutron flux within the specific energy range of a resonance for the purposes of reducing fission captures. Therefore, this specific area of research constitutes a new and original component of this dissertation.

4. Methodology

A key objective of the research herein presented includes to accurately model the spatial and transient behavior of the energy-dependent neutron field in the target sites of the High Flux Isotope Reactor, in order to identify and quantify the principal effects upon the target isotopic yields. This involves using a variety of modeling techniques in an attempt to isolate primary factors affecting the yields. At different points in the computational process, the modeling

technique to be used is dependent upon the known and desired parameters as well as the accuracy required and the computing time required (or tolerable). As part of this research, many modeling techniques have been used, with the objective being to model only what is necessary when it is necessary, making assumptions and approximations where applicable. This section documents the types of calculations performed, the various codes employed in this research, the calculations performed with said codes, and the assumptions and data required to make use of them.

4.1 Solving the Boltzman Transport Equation

When determining the flux spatial distribution and its energy spectrum, and the resulting effective cross sections for a given arrangement, regardless which modeling technique is employed, the main goal is to solve the Boltzman neutron transport equation, with any number of assumptions. These assumptions may or may not be appropriate to a given situation, which is why it is essential to understand the assumptions that are employed by various codes. In general, the methods for solving the Boltzman transport equation can be divided into two types, stochastic techniques, such as Monte Carlo, and deterministic techniques,

4.1.1 Monte Carlo Methods

Monte Carlo methods are a type of computational technique that involves the stochastic solution of problems. These methods perform a repeated experimental sampling to determine the expected value of parameters of interest. These methods can be employed in particle transport by modeling the physical properties of the experiment and applying a probability distribution to the interactions with each particle in the system. By tracking each particle from birth to death (by either capture or escape) and tallying the outcomes of interactions, over many generations of particles a statistical behavior or solution to the transport equation can be determined. This solution however is only as accurate as the accuracy of the physical model and the probability distributions, and is still susceptible to the randomness of the process if poor counting techniques or insufficient particles are sampled. Monte Carlo methods are incredibly powerful, capable of simulating the most complex 3-D geometries and large domains that are not feasible with deterministic systems [23], however, they also require significant computing time. The Monte Carlo N-Particle code (MCNP) is a popular three-dimensional general purpose Monte Carlo code developed by Los Alamos National Laboratory [23]. A similar three-dimensional general-

purpose code Monte Carlo transport code is included in the SCALE code system; this is the KENO-VI functional module [21].

4.1.2 Diffusion Theory

Diffusion theory is an approximation to the transport equation that involves simplifying the treatment of the directional components of the neutron flux, to assume that particles will "diffuse" from areas of high concentration to areas of low concentration following Fick's law. Derivation of the diffusion equation from the transport equation makes a number of assumptions in order to apply Fick's law, which means that there are many situations where the equation breaks down. These assumptions include [28]:

- The medium is effectively infinite: Within a few mean-free paths of the boundary Fick's law is no longer valid due to the high contribution of exponential terms.
- The contribution to the flux is mostly from scattering collisions: Locations within a few mean free paths of sources (fission) or sinks (absorbers) do not follow the diffusion approximations.
- The cross sections are independent of position: At the boundary between two media with differing scattering properties Fick's law may break down. If the flux becomes rapidly ferrying this invalidates the Taylor series expansions of the flux used to derive the diffusion equation.
- Scattering is isotropic in the Laboratory Coordinate System: This is typically true at low energies but may not necessarily be true at higher energies.
- The neutron flux varies slowly throughout the medium: If the medium is strongly absorbing this may lead to rapidly varying fluxes, which again invalidates the Taylor series expansions of the flux.
- The neutron density is slowly varying with time: It is assumed that the change to the flux during the time for a neutron to travel a few mean free paths is very small.

CENTRM [3] is a module of the SCALE code package, which may be run using 2-D diffusion approximations.

4.1.3 Discrete Ordinates Methods

Discrete ordinates methods to the solution of the transport equation treat spatial dependencies of the neutron flux by utilizing a finite difference grid, and handle angular dependencies of the neutron flux by discretizing the angular behavior of the flux into a fixed number of directions, or ordinates, using numerical integration "quadratures" to tie the angular solution to the scalar flux [29]. Discrete ordinates calculations are generally able to provide a more accurate approximation to the flux solution of the transport equation than diffusion methods, but are computationally more expensive, calculating more information than is typically necessary [23].

Discrete ordinates methods are particular to the choice of directions, quadrature weights, differencing schemes and iterative solution procedures. These techniques are commonly used in such areas as "lattice physics" to help generate spatially homogenized and energy collapsed (few group) cross sections that can be used in diffusion theory applications. CENTRM [3] and XSDRNPM [30] are modules of the SCALE code package that may be run using 1-D discrete ordinates approximations.

4.1.4 Bondarenko Method

The Bondarenko method [2] relies on the narrow resonance approximation, which assumes that the practical width of a resonance of an absorber nuclide is much smaller than the average energy loss due to collision with the nuclide, and that the collision density is thus constant throughout the resonance. This method breaks down the contribution to the total cross section into two pieces, the contribution from the resonance nuclide, and the contribution to scattering from other nuclides. Group cross sections are pre-calculated for a variety for σ_0 values (where σ_0 is the cross section of the mixture per atom of nuclide "i" for all nuclides in the mixture other than nuclide "i") based upon the problem materials, and then the flux solution is calculated by iteratively interpolating between these values. The benefit to the Bondarenko method is that it requires significantly less cross-section pre-processing than other deterministic methods, requiring little computational time. The BONAMI module of the SCALE code package employs the Bondarenko method for processing resonance cross sections in the unresolved resonance range.

4.1.5 Matrix Exponentiation

The time dependent nuclide concentration equation described in the introduction (Eq. 1) can be written in matrix notation as:

$$\dot{\bar{N}} = \bar{\bar{A}}\bar{N}$$

(Eq. 11)

In this equation the vector N represents the nuclide concentrations, and A represents the transition matrix from each nuclide to each other nuclide, and is a combination of problem dependent transmutation, destruction and decay rates. The solution to this equation is:

$$\bar{N} = exp\left(\bar{\bar{A}}t\right)\bar{N}_0$$

(Eq. 12)

Matrix exponentiation is a method of solving for the nuclide concentrations N in the previous equation by expressing the exponential term as the series expansion for the exponential function. Matrix exponentiation is employed by the SCALE module ORIGEN [35].

4.1.6 Neural Networks

Neural networks represent a type of empirical modeling in which exemplar, or historical data are used to "train" the neural network (or model) and determine relationships between variables. Once the network has been trained, it uses those relationship functions in order to quickly predict responses to new sets of data inputs. The main advantage to neural networks, and empirical modeling in general, is that the bulk of the computation time is a one-time-only cost, to train the model, and future computations are performed in a fraction of a second. Neural networks in particular are highly adept at analyzing sparse data, where not every variable carries a value within individual data sets. Neural networks are more accurate the more data that is provided to train the model, and are only appropriate for making predictions within the range of the data used to train the model.

A neural network consists of a network of individual "neurons", each one of which performs a basic functional operation. A neuron receives a vector "p" of the input variables. These inputs

are multiplied by a weight vector “w”, and added to a bias “b”, to form the net “n”. The net input “n” is evaluated by a transfer function “f” to produce the output “a”.

These neurons are arranged in the neural network as a series of layers, where the input to each neuron in a layer consists of a vector of the outputs of the neurons in the previous layer (or the supplied inputs, for the case of the first layer). The number of layers and number of neurons within a layer are typically problem-dependent and often designed to optimize the performance of the neural network, so each layer may have different numbers of neurons, and these need not coincide to the number of inputs, however the number of neurons in the final layer must equal the number of total predictor outputs for the problem.

For example, a problem with 5 inputs and two outputs might have a two layer neural network with 10 neurons in the first layer and two in the second layer. Each of the 10 neurons in the first layer would receive 5 inputs and produce one output. Each of the neurons in the second layer would receive 10 inputs (one from each of the ten neuron in the first layer) and produce one output. These two outputs (one from each of the two neurons in the second layer) from the second layer would comprise the solution.

The neural network used in this research is trained in a batch mode, using all available data at once to determine the network relationships. The training method used in this research is the Widrow-Hoff learning algorithm, a Least-Mean-Square algorithm which adjusts the weights and biases of the neurons to minimize the mean square error (MSE) for the training data [36]. Given a batch of training vectors and initial weights and biases, each individual vector is evaluated, and the weights and biases corrected such as to minimize the MSE. After each vector is evaluated the network is adjusted with the sum of the corrected weights and biases. This process is then iterated until a certain tolerance on the total MSE of the training data is reached. Each iteration is called an epoch.

For the purposes of this research, neural networks are employed as a means of making quick predictions of isotopic yields, when sufficient data is available. Rapid and accurate predictions are a necessary component of efficient optimization models.

4.1.7 Genetic Algorithms

Genetic Algorithms are a type of evolutionary algorithm which can be used to solve optimization problems. In a genetic algorithm a single set of variables for a solution is called an "individual". The ranges and boundary conditions for the individual must be set by the user. These can include simple bounds, such as minimum and maximum values for each variable, as well as complex relationships between the variables which must be satisfied in each solution. When a genetic algorithm is initiated, a "population" of individuals is selected at random, where the number of individuals in the population is set by the algorithm parameters. The solution for each individual in the population is determined, and these solutions are then compared using a user fitness function, which must be coded into the algorithm. The fitness function determines which individuals in the population resulted in a more optimal solution. If a certain stopping criteria is met, and the optimal solution is found, the algorithm stops. If not, a new generation of individuals is created.

The population of the new includes the individuals from the previous population with the best fitness function evaluation, as well as "children" of the individuals in the previous population with the best fitness. These "children" are produced by making random changes to the individual "parents" based upon a Gaussian distribution, called a mutation operator, and by combining pairs of individual "parents", called a crossover operator. Over subsequent generations, the diversity of the population, that is, the average distance between individuals within the population, decreases, as the algorithm converges upon an optimal solution. Parameters affecting the production of subsequent populations, such as the number of mutations and crossover children, and the distribution of random changes, are defined in the algorithm.

The genetic algorithm determines whether the optimal state has been achieved by analyzing the change in fitness of the population over many generations. In each generation the average fitness for the population is calculated and over subsequent generations, the change in the average fitness for the population is compared. When the total change in the average fitness function over a certain number of generations is less than a set tolerance the genetic algorithm ends and returns the solution with lowest fitness function evaluation. The genetic algorithm also employs a stopping criteria based on the number of generations. If the stopping criteria for the change in the average fitness of the population is not met within a set number of generations the algorithm

will end and return the solutions with the lowest fitness function evaluation determined so far, and will indicate that the fitness function stopping criteria was not met.

For the purposes of this research genetic algorithms are employed as a means of searching for the optimal filter composition and irradiation time for a given user supplied target. The genetic algorithm employs neural networks, as described in the previous sub-section, for making fast isotopic yield predictions [37].

4.2 Computer Codes and Modules

4.2.1 CSAS

CSAS [31], [32] are the Criticality Safety Analyses Sequences, a module of the SCALE code package [1]. These sequences are effectively a control module which allow for simplified user input, and which call a sequence of other SCALE codes such as KENO, BONAMI, CENTRM and XSDRNPM (see following sections for details on these and other codes).

CSAS uses a block style input typical of most scale control modules where the user enters the material compositions, and the zone in which they are located, followed by the celldata, indicating the lattice type and boundary conditions.

4.2.2 KENO-VI

KENO-VI [21] is a module of the SCALE code package which performs three-dimensional Monte Carlo transport calculations. The KENO module can be using within other modules such as CSAS. The KENO code uses Monte Carlo method to solve the Boltzmann transport equation (Equation 2) for the entire system. The three dimensional geometry is constructed using quadratic equations, intersections, rotations, and hexagonal and dodecahedra arrays, allowing for extremely versatile and complex configurations. Particles of interest are tracked from their birth until death in the system, using continuous energy or multigroup cross section data for the probability distribution to determine the parameters of particle interaction.

4.2.3 BONAMI

BONAMI [2] is a module of the SCALE code package which calculates resonance corrected cross sections in the unresolved resonance range. Within the scope of this research BONAMI is called from the control module CSAS. BONAMI utilizes the Bondarenko method, described in

section 3.1.4, to produce problem-dependent data from a master library of AMPX cross sections and Bondarenko factors. The user specifies a one-dimensional geometry in either spherical, cylindrical, or slab geometry. This geometry may contain multiple zones, with each zone containing a homogenous mixture. Self-shielded cross sections are calculated for each zone, with Dancoff expressions used to account for heterogeneous effects. The Dancoff expressions account for leakage of neutrons between homogenous zones. These expressions add an effective cross section to the σ_0 values (cross section of the mixture per atom of nuclide "i" for all nuclides in the mixture other than nuclide "i").

4.2.4 CENTRM

CENTRM [3] is a module of the SCALE code package which calculates continuous energy neutron spectra. Within the scope of this research CENTRM is called from the control module CSAS. CENTRM utilizes various deterministic approximations to the Boltzman transport equation, such as diffusion and discrete ordinates, described in sections 3.1.2 and 3.1.3, to produce problem dependent fluxes for processing resonance-shielded multi-group data. The user specifies a one-dimensional geometry in either spherical, cylindrical or slab geometry, with multiple homogenous zones, similarly to what is done for BONAMI. CENTRM can also be used for an infinite homogenous region, which is referred to as zero-dimensional geometry. Solving the transport equation CENTRM produces the flux per unit lethargy over a discrete energy mesh, assuming a linear variation of the flux between energy points, as well as the spherical harmonic moments of the angular flux.

4.2.5 XSDRNPM

XSDRNPM [30] is a module of the SCALE code package which calculates continuous energy neutron spectra, and can be used to generate multi-group cross sections. Within the scope of this research XSDRNPM is called both from CSAS, and independently using the FIDO input system. XSDRNPM utilizes discrete ordinates, described in section 3.1.3, to produce problem dependent collapsed cross sections and neutron spectra. XSDRNPM can also be used for eigenvalue determination, shielding analysis and adjoint calculations, although these features are not utilized in this research. The user specifies a one-dimensional geometry in either spherical, cylindrical or slab geometry, with multiple homogenous zones, similarly to what is done for BONAMI and CENTRM. The user may also specify fixed sources if present, but only by calling XSDRNPM

directly, this functionality is not available through the CSAS control module. Solving the fixed-source transport equation XSDRNPM produces the multi-group flux spectrum and utilizes it to collapse input AMPX cross sections from a master library into a problem-specific multigroup cross section library, accounting for resonance self-shielding and other spectral effects.

4.2.6 COUPLE

COUPLE [34] is a module of the SCALE code package which is used for generating ORIGEN-S libraries. This data processing code reads AMPX working libraries, such as those produced by CENTRM and XSDRNPM, or multigroup infinite dilute problem-independent cross sections and generates binary format 1-group problem specific nuclear data libraries for use in the depletion code ORIGEN-S. COUPLE may make use of user specified flux spectra, or those contained within standard AMPX libraries. COUPLE combines these problem-dependent cross sections with ENDF/B-VII nuclear decay data and energy-dependent fission product yields.

4.2.7 ORIGEN-S

ORIGEN-S [35] is a module of the SCALE code package which is used to calculate time dependent concentrations, activities and radiation source terms as a result of irradiation and decay. ORIGEN-S uses a matrix exponential expansion model, described previously in section 4.1.5, and a binary data library containing both cross section and decay data. ORIGEN-S analyzes the full isotopic transition matrix to solve the rate of change equations for nuclide concentrations. ORIGEN-S includes options for continuous removal or feed of streams.

4.2.8 Libraries

Each of the codes used in this research require input of a cross-section library [34]. Development of a cross section library begins with a generic library of infinite dilute cross sections. For the purposes of this research the ENDF/B-VII library "scale.rev07.xn238v7" released with SCALE version 6.1 was used to generate problem dependent libraries with CENTRM and XSDRN, and collapsed down and combined with the decay library "origen.rev01.yields.data", also released with SCALE version 6.1, to generate problem dependent 1-group ORIGEN-S libraries with COUPLE.

ENDF stands for "Evaluated Nuclear Data File" and the ENDF/B-VII library contains evaluated (recommended) cross sections, fission product yields, and other data with emphasis on neutron-

induced reactions [39]. These data are based on a combination of experimental results, nuclear physics theory, and are coupled with the most advanced fitting methods. Most nuclides in these libraries have resonance data in the resolved resonance region and Bondarenko factors in the unresolved resonance region. The ENDF/B-VII library was developed has been tested using a suite of benchmarks and is acceptable for general use in criticality and reactor physics applications.

4.2.9 MATLAB

MATLAB is a commercial software programming language designed for numerical analysis (version R2012a, The MathWorks Inc., Natick, MA, 2000) [40]. MATLAB includes a number of built in tools and scripts for use in matrix manipulation and empirical modeling. For the purposes of this research MATLAB was used to generate neural networks to predict irradiated target yields, as well as developing genetic algorithms to search for the global minimum to the transcurium production optimization problem.

4.2.10 Perl

Much of the programming done in support of this research was performed in Perl [41], a high-level dynamic programming language. Although Perl is a very powerful and flexible language, it is inelegant. Perl scripts were developed as part of this research mainly as a way to call SCALE routines, analyze the output data, and prepare and call new SCALE routines in an iterative manner.

5. KENO Modeling of the High Flux Isotope Reactor

Much of the work presented in this section was documented in [42] and presented at the American Nuclear Society Annual Meeting in June 2011. The CSAS-6 module from the SCALE package, incorporating KENO-VI geometry, was used in this work for analyzing the beginning of cycle 400 for the HFIR. A counterpart model had previously been developed and analyzed using MCNP, which yields a BOC k-effective within 1% of the expected value [18]. Much of the KENO-VI model's detail has been adapted from the MCNP model, and the results of the simulations of both models have been compared to each other and also against the data reported in the HFIR design report by Cheverton and Sims [50].

5.1. Fuel Elements

The inner and outer fuel elements of the HFIR are composed of involute plates in the inner and outer fuel elements each containing 15.18 ± 1% and 18.44 ± 1% grams of U-235, respectively. This fuel meat is distributed along the arc of the fuel plate in varying thickness and the plates are separated by .050 inch water gaps. This involute plate geometry results in a fuel-to-water ratio that varies with the radial distance from the flux trap. Although there have recently been attempts to model the detailed geometry of the HFIR fuel plates, for the purposes of this research, the individual plates were not modeled, but instead the fuel region itself was represented by a series of cylinders, with axial and radial layers, each approximating the average fuel-water ratio in that region of the fuel element.

The inner and outer fuel element were modeled as a series of homogenous concentric rings; eight for the inner fuel elements and nine for the outer fuel element, each with 7 axial fuel layers, for a total of 56 "cells" in the inner fuel region and 63 in the outer fuel region. Each homogenous ring accounts for the uranium fuel, aluminum plate cladding, and water between each plate, as well as any axial variations which result from uneven burnup. The involute fuel plate geometry as well as the concentric cylinders as modeled in KENO-VI are both shown in Figure 8, below.

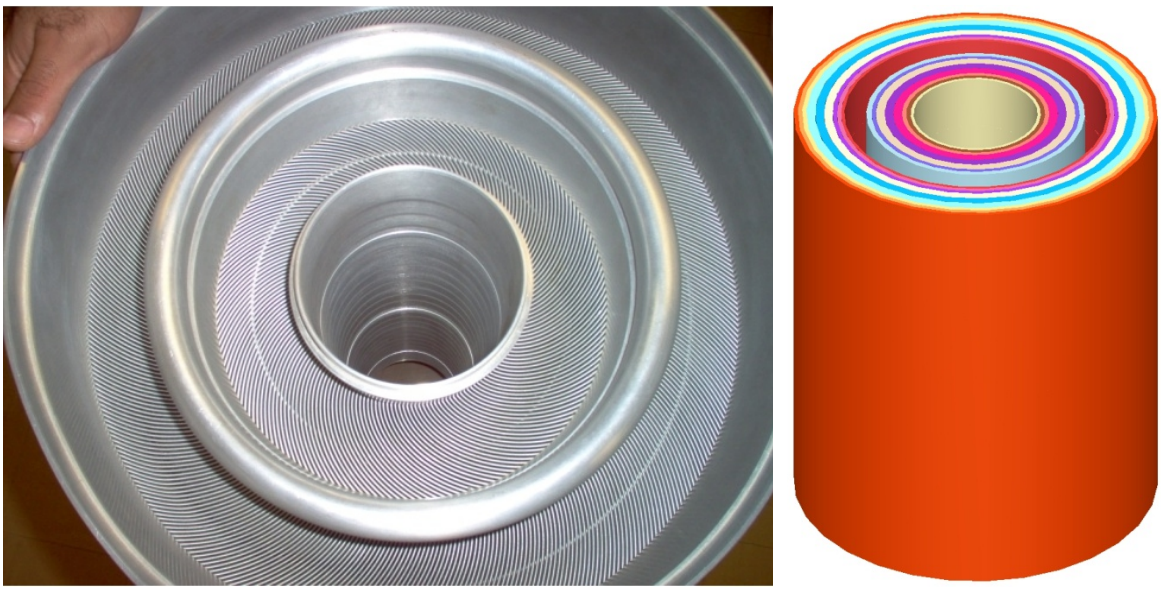


Figure 8: Involute fuel plates of the HFIR core (left) and as modeled in KENO-VI (right)

5.2. Flux Trap

The flux trap is the central region of the HFIR core, surrounded by the fuel element region. The flux trap region consists of a cylindrical basket and 37 vertical experimental target sites that typically contain heavy actinide curium production targets, solid aluminum dummy targets, shrouded aluminum dummy targets, stainless steel targets, and other experiments. The flux trap is the area of primary interest to this research, as it is the location of the production of heavy actinides.

Of the 37 target sites, 6 are located on the periphery of the basket, hence called the peripheral target positions (PTP). The six PTP are spaced symmetrically around the flux trap at 60 degree intervals. Each of these six regions consists of an approximately 1cm radius cylindrical region. The targets within these regions contain seven axial regions, containing experimental targets of approximately 0.5 cm radius, inside an aluminum cladding.

The 31 interior target sites have radii of 0.835 cm and are arranged in a triangular pitch with spacing of 1.6891 cm. One of these target locations contains a hydraulic tube. The hydraulic tube contains nine axial regions that can host small targets called “rabbits”. These rabbits can be loaded into, or removed from the reactor, via the hydraulic tube, during operation. The nine target specimens are surrounded with compressed air within an aluminum cladding. The remaining 30 target sites contain shrouded experimental targets or solid rods. Shrouded experimental targets are composed of a small diameter specimen pellets cladded and shrouded in aluminum, with space between the cladding and the shroud for coolant flow. When experimental targets are not in place, the target region may be filled with a shrouded aluminum target of similar design, or solid aluminum rods.

In the KENO VI model the shrouded target sites are modeled as six regions per target: two regions for the experimental specimen (one for collection of centerline data, and one for the remaining axial region), one for the specimen cladding, one for the target shroud, one for the target site cylinder, and two for coolant (one between the specimen cladding and target shroud and one between the target shroud and the target site cylinder). Axial separation of the individual specimen pellets is not included, as these targets are typically homogenous in nature, however the aluminum target holder above and below the target was modeled. Solid targets are homogenized to include the target, cladding and target region cylinder. The PTP sites are

modeled similarly to the interior shrouded target sites, however the axial regions are individually modeled to allow for loading of different targets in the periphery. The hydraulic tube is also modeled similarly to the interior shrouded target sites, containing nine regions for the axial rabbit positions, one for the tubing, one for the compressed air, one for the cladding, and one for the coolant between the cladding and the target site cylinder. All of the coolant within the flux trap is homogenized with the structural materials of the flux trap basket and target site cylinders.

The flux trap, as modeled for cycle 400 of HFIR operation, is shown below in Figure 9. This cycle contained 9 solid and 21 shrouded targets in the interior target sites, in addition to the hydraulic tube and PTP sites. The image is cut away at the top, as well as from the front quarter, to show both axial and radial cross sectional views.

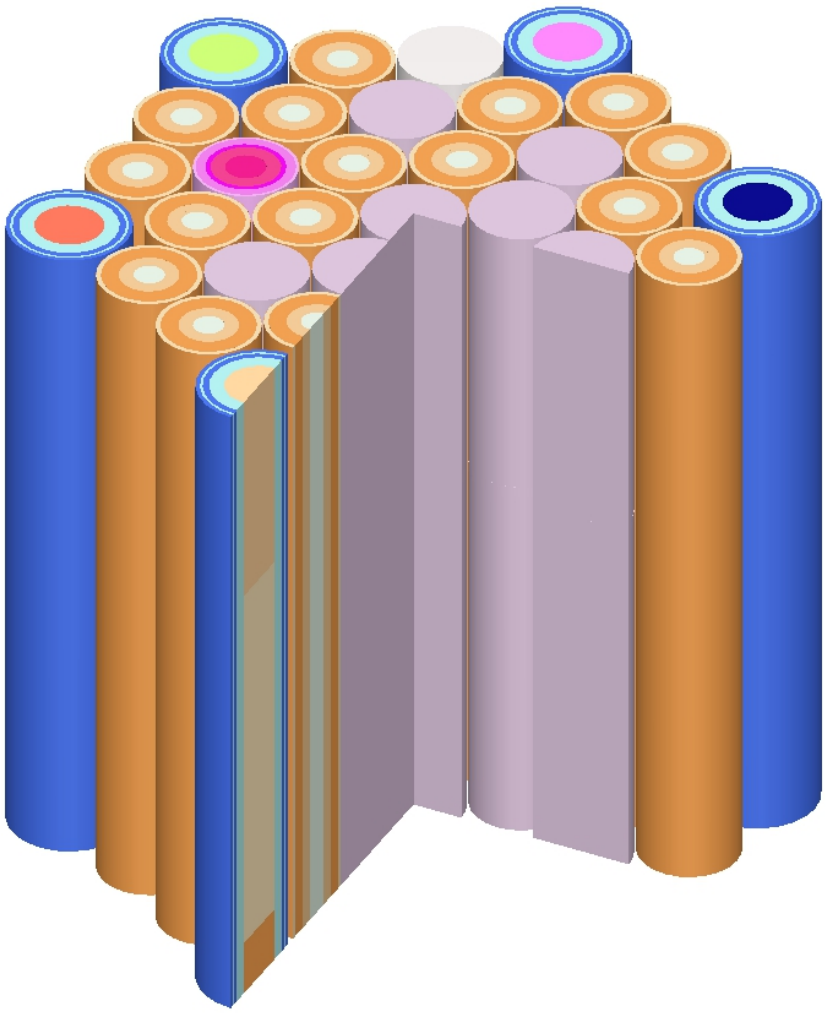


Figure 9: Flux Trap as modeled in KENO-VI

5.3. Control Elements

The control element region consists of two concentric cylinders, the inner control element (ICE) region and outer control element (OCE) region surrounding the fuel. Each element is composed of four radial arc segments comprising a cylinder with small gaps between each radial arc. Each element is also composed of four axial control regions, aluminum at the top and bottom, a black control region composed of aluminum with europium oxide, and a grey control region composed of aluminum with tantalum oxide. The control elements are moved vertically in opposite directions over the course of the reactor cycle, the ICE moving down and the OCE moving up. This movement reduces the amount of negative reactivity being provided by the control elements for the duration of the cycle.

The control elements were modeled in KENO-VI as two cylinders with four axial regions each. Each axial region was homogenized with the flow-through holes and spaces between the radial arcs. An image of the control elements surrounding the experimental target sites of the flux trap and the fuel elements, as modeled in the KENO-VI geometry is shown below in Figure 10.

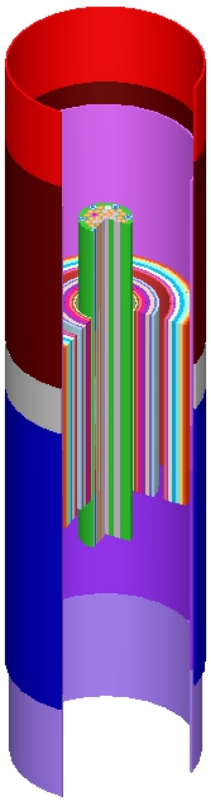


Figure 10: Inner and Outer control elements, fuel elements, and flux trap experimental targets as modeled in KENO-VI

The atom densities for the control elements beginning of cycle 400 have been previously calculated via simulation of the irradiation and decay history using the point depletion and decay code ORIGEN-S. It is expected that variations in the control element composition over time will have minimal effect on the results [51]. Future depletion calculations will require re-start and repositioning of the control elements, as there is currently no functionality in KENO-VI depletion via TRITON for changing geometries, so as to move the elements over the duration of the cycle.

5.4. Reflectors

The HFIR contains three reflector regions: the removable, semi-removable, and permanent beryllium reflector regions. The removable beryllium reflector (RB region) is a 5 cm thick cylindrical region surrounding the control element region. This area contains eight large experimental facilities, placed in pairs of two every 90 degrees around the region, and four small experimental facilities, placed every 90 degrees around the region, offset from the large experimental facilities by 45 degrees. The RB is replaced after every 40 operating cycles.

The semi-permanent reflector region is a 3 cm thick cylindrical region surrounding the RB region. This area contains eight control rod access plug facilities, placed in pairs of two every 90 degrees around the region similarly to the large experimental facilities in the RB region. The semi-permanent reflector region is replaced after every 80 operating cycles.

The permanent reflector region is a 20 cm thick cylindrical region surrounding the semi-permanent reflector region. This area contains 6 large VXF, 11 inner small VXF, 5 outer small VXF, two vertical slant tubes, two horizontal beam tubes, a radial beam tube and a tangential beam tube. An image of the permanent reflector is show below in Figure 11 where the VXF experimental facilities can be seen.

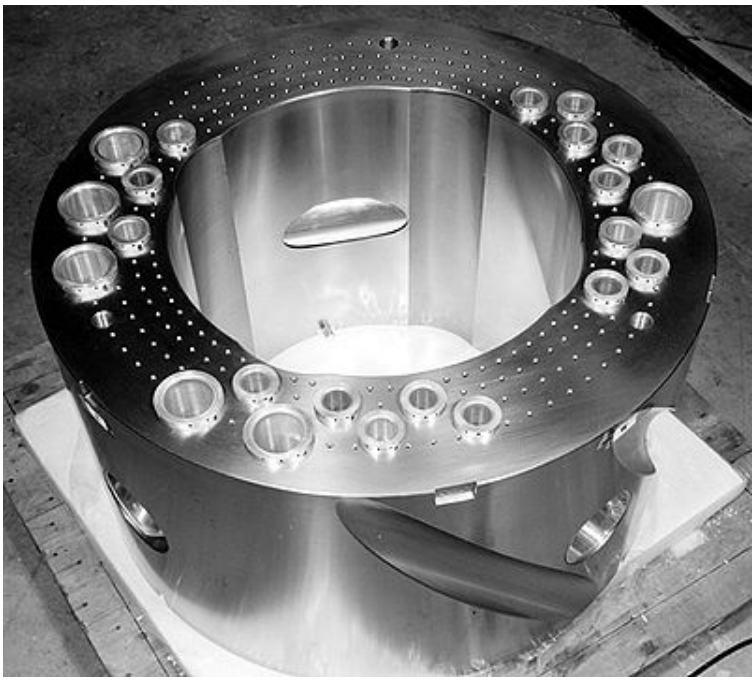


Figure 11: Permanent Beryllium Reflector

The reflector regions are modeled in KENO-VI as a series of concentric cylinders, three reflector regions and three water gaps for the removable, one for the semi-permanent, and seven for the permanent reflector. Although the composition of the beryllium used in each reflector region is identical, the presence of structural materials and flow holes, with which the beryllium is homogenized, results in varying atomic densities. The reflector regions may also include poisons, depending on the operating cycle, which are homogenized with the beryllium.

The large and small experimental facilities in the RB region are modeled as a two region cylinder, an inner region for the experiment and an aluminum lining. Each of the experimental sites is filled with beryllium, although other experimental targets could be modeled. The control rod access plug facilities in the semi-permanent reflector region are modeled as single region cylinders, and are again filled with beryllium. The VXF experimental facilities in the permanent reflector region are modeled as two region cylinders, an inner region for the experiment (filled with beryllium in this model) and an aluminum lining. The vertical slant tubes, horizontal beam tubes, radial beam tube and tangential beam tube are not modeled. If future research is to be performed using this model for the purposes of investigating the reflector region, these facilities would need to be accounted for, however, for the purposes of investigating the flux trap

characteristics, it is not expected to have significant impact. The reflector regions, as modeled in KENO-VI, are shown below in Figure 12.

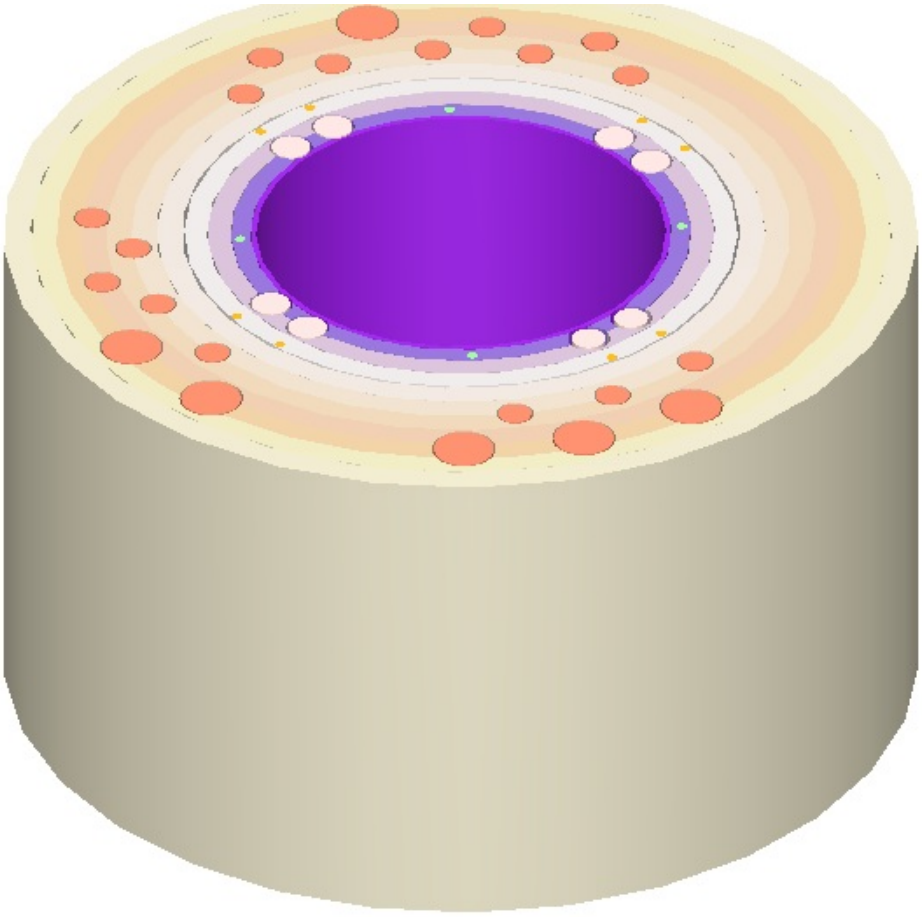


Figure 12: Reflector Regions and Experimental Sites as Modeled in KENO-VI

5.5. Validation

Cycle 400 of the HFIR took place from April 27, 2004 at 2:55 am until May 21, 2004 at 5:35 pm for a total life cycle of 24d, 14h, 40m. The reactor contained 9.43 kg of 93.1% enriched U-235. This is typical for a HFIR irradiation cycle. There were no curium targets loaded during this cycle of the reactor.

The main parameter of interest in the validation is the value of k-effective, which in principle should be as close to 1.0000 as possible. A variety of KENO-VI input parameters were tested so as to optimize the model for accuracy and computation requirements. Additionally, two different

standard SCALE libraries were utilized: a 238-group ENDF/B-VII.0 library (V7-238) and a 44-group ENDF/B-V library (44 Group). The results are summarized below in Table 2.

Table 2: k-eff values with neutrons per generation (NPG), number of generations (Ngen), total run time and library used.

Ngen	NPG	Library	Time (m)	K-eff
10000	2000	V7-238	4029	1.00683 ± 0.00019
10000	2000	44 Group	4211	1.01049 ± 0.00019
2000	2000	V7-238	844	1.00706 ± 0.00045
2000	2000	44 Group	840	1.01009 ± 0.00047
2000	1000	44 Group	421	1.01086 ± 0.00062

Another key parameter obtained from the KENO-VI model tallies and could be compared to the available MCNP model is the flux in the flux-trap target region. This flux profile is shown below in Figure 13.

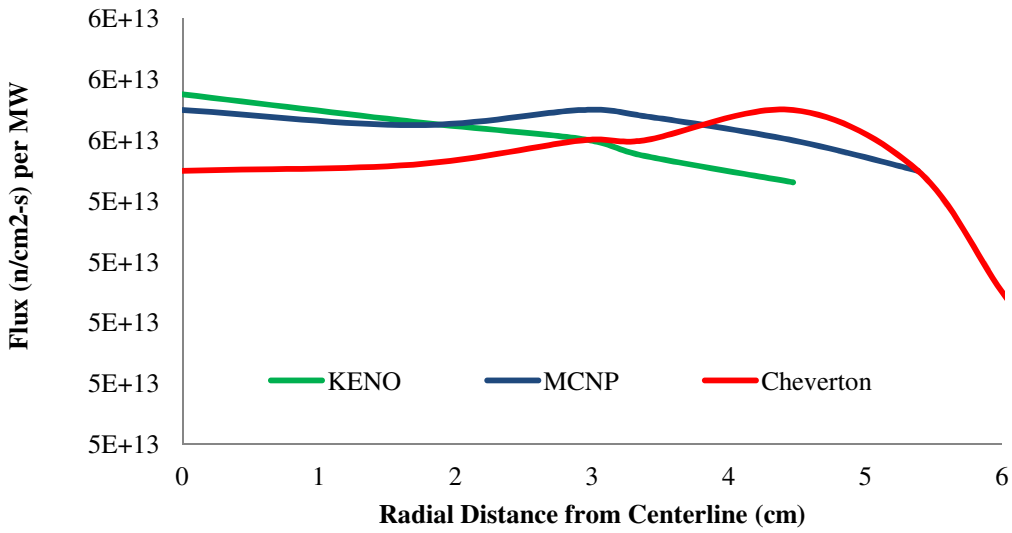


Figure 13: Flux in the flux-trap target region versus radial distance from center.

The flux profile for the KENO-VI model was determined by summing the tallied fluxes per source neutron over all 238 energy groups and multiplying by the HFIR overall source strength of 6.4234E18 n/s. The uncertainty for the flux tallies determined in the KENO-VI model were in

the range of 2% to 5%, with slightly higher uncertainties for energy bins at the endpoint of the spectrum which contained significantly lower tallies.

The results presented in Figure 13 show that the calculated total flux in the flux trap is similar to that calculated in the MCNP model, and that documented by Cheverton and Sims. As can be observed from Table 2, all calculations are within approximately 1% of the expected k-effective value of 1.0000 and in the same range of statistical accuracy as the previously analyzed MCNP model. Reducing the library from 238 to 44 groups does not significantly reduce the run time, however this decreases the accuracy of the calculated k-effective value. Increasing the number of generations results in a small increase in accuracy, from 0.71% to 0.68%, and more than halves the standard deviation, from 0.05% to 0.02%, but at the cost of a run-time increase that is proportional to the increase in number of generations.

5.6. Flux Variation

The key data obtained from the KENO-VI model for use in this research was the 238-group neutron flux spectrum at various locations in and around the flux-trap. The KENO-VI model was run using the V7-238 library, with 2000 generations and 2000 neutrons per generation, for varying target compositions, and it was observed that the flux spectrum surrounding the flux trap remained relatively constant, although the flux in the target itself varied with target composition. This is highlighted in Table 3 summarizing the flux variations in the shrouded target interior versus the flux variations in the flux trap moderator when the KENO-VI model was run with aluminum "dummy" targets versus typical mixed curium targets.

Table 3: Flux Variation Statistics

	Average group Δ	**S. Dev. group Δ**	**Total flux Δ**
Target	19.66 %	19.97 %	4.06 %
Moderator	11.33 %	18.65 %	1.32 %

It can be observed that in the moderator, the average delta between the fluxes for differing target compositions is significantly lower than inside the target. This can also be seen from a graph of the flux spectra inside the target, and inside the moderator, for the two target cases, shown in

Figure 14. Only the thermal range (the location of greatest discrepancy) is shown for ease of viewing.

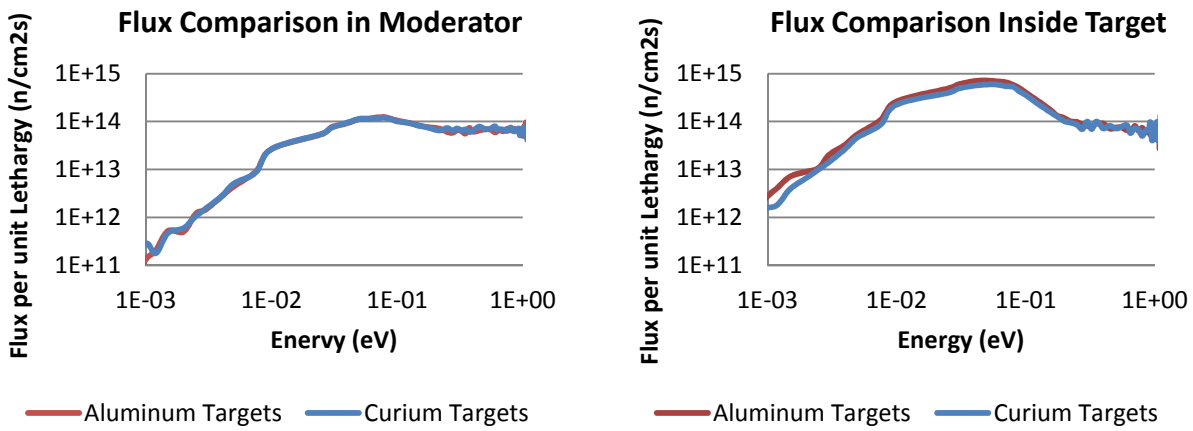


Figure 14: Highlighting the greater flux discrepancy in the target region, versus the moderator region, for differing target compositions

This information is of great importance when it comes to making approximations and assumptions regarding the conditions in the flux trap. This is because for the purpose of optimization studies it is typically necessary to examine a very large number of consecutive cases in serial, in order to converge upon a global optimum of a certain fitness function or optimization objective. Since the KENO-VI model required a run time of more than 400 minutes to analyze a static-state condition on a single multi-core node on the CPILE2 cluster at ORNL, it is expected that many days of would be required to compute a depletion over time with appropriate statistics. Although this execution time could be reduced by running the problem on multiple cores/nodes, it is unlikely that the processing time can be reduced to a small enough time to allow potentially upwards of thousands of calculations in serial. As such, it was not considered practical to utilize this model within an iterative optimization framework. However, the fact that the flux spectrum was relatively constant in the moderator and on the outer boundary of the flux trap provided the opportunity to model only the flux trap, and apply a fixed-source to simulate this constant flux. This assumption becomes less accurate over time, and as the composition (and number) of the in the flux trap changes. Shorter duration analysis of small changes will yield more accurate results using this assumption.

5.7. Depletion

Although the KENO model is used primarily to obtain the static flux within the moderator of the flux trap, and was determined to be non-practical for use within an iterative optimization framework, the KENO model, being of high fidelity, is very useful for validating results of lower fidelity models used within the optimization framework. In order to validate depletion results it was necessary to modify the KENO model to perform depletion over time. The control region, consisting of two concentric cylinders which move over the duration of the irradiation, were replaced with a single material containing burnable poison of an density that would provide the same effective rate of absorption as the control plates. This technique was previously developed and validated by D. Chandler [43].

The KENO depletion model was run to simulate a five cycle irradiation, using a target composition representative of the current heavy curium feedstock. Each cycle consisted of a 25-day irradiation in a ring-1 flux trap position, with 19 days of decay following each cycle. This target irradiation is representative of typical operations during a californium production campaign. The purpose of these depletion calculation was to set a "baseline" against which other models, to be discussed later in this dissertation, could be compared. The initial target composition and final yields were as shown in Table 4:

Table 4: Isotope Yields from KENO-VI five cycle depletion

Isotope	Charge (g)	Yield (g)		Isotope	Charge (g)	Yield (g)
Pu-238	0.002	0.000		**Cm-245**	0.049	0.017
Pu-239	0.001	0.000		**Cm-246**	4.043	3.860
Pu-240	0.565	0.006		**Cm-247**	0.117	0.065
Pu-241	0.000	0.001		**Cm-248**	0.858	0.838
Pu-242	0.016	0.080		**Bk-249**	0	0.004
Am-243	0.706	0.107		**Cf-252**	0	0.024
Cm-244	1.580	1.291		**Total**	7.937	6.291

6. SCALE model using CENTRM/XSDRN/BONAMI

Much of the work in this section was documented in [44] and presented at the American Nuclear Society Annual Meeting in June of 2012. A simple model of the flux trap was developed consisting of a triangular pitch lattice of multi-region cylinders; typically aluminum-cladded, curium oxide and aluminum targets within a water moderator. This model was developed for use with the SCALE modules CENTRM and XSDRNPM. The CENTRM module employs various deterministic approximations to the Boltzman transport equation in one-dimension and was used to compute self-shielded multi-group cross sections. The XSDRNPM module employs one-dimensional discrete-ordinates transport and was used to compute problem-specific fluxes. By only modeling a small portion of the HFIR reactor, the location where small variations in the flux spectrum are expected to take place, it is possible to significantly reduce the complexity of the problem, so that many small perturbations can be simulated in a short period of time.

To simulate the constant flux incumbent upon the flux trap, a fixed source was applied in the outer most layer of the lattice with the same energy spectrum as the observed constant flux in this region from the KENO-VI model. A calibration was then performed to adjust the normalization factor for the source, until the flux observed within the target matched that observed within the target in the KENO-VI model. This was repeated for a variety of target compositions to check the calibration. A comparison of the flux spectrum as calculated in the KENO-VI model and the CENTRM model is show below in Figure 15 for both a typical mixed curium target, and for a typical mixed curium with a small amount of added Ir-191.

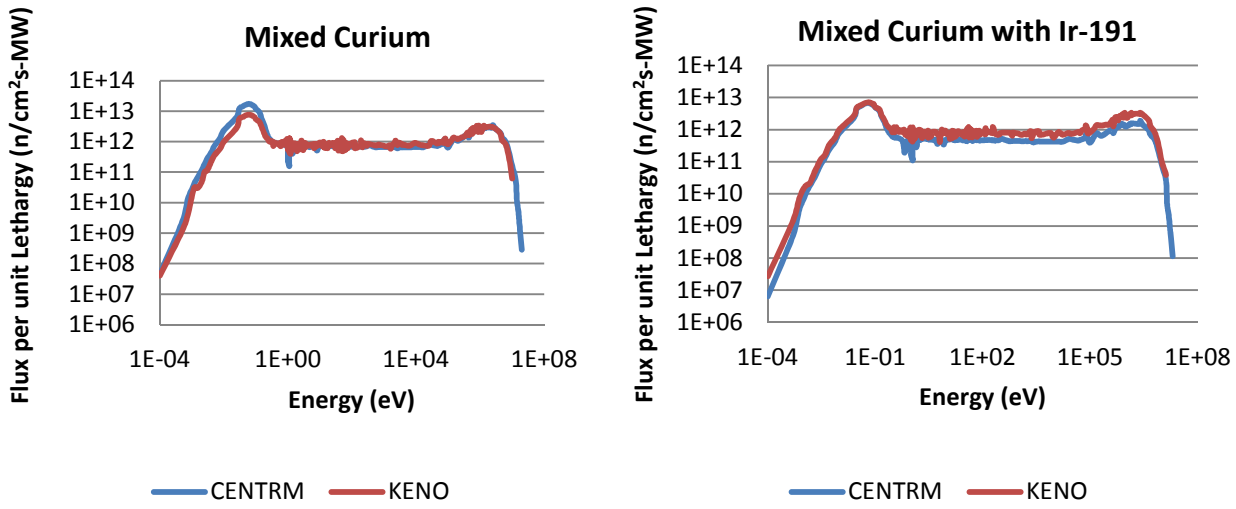


Figure 15: Flux Spectra Comparison between CENTRM and KENO-VI

Using the 238-group flux and effective cross sections generated by the CENTRM model, the SCALE module COUPLE was used to collapse the cross sections down and combine them with the ENDF-VII/B decay data to create a 1-group effective cross section binary library for use in depletion calculations. The SCALE module ORIGEN-S was then used to perform an irradiation and decay of the target materials with the 1-group library, and the total neutron flux obtained from the CENTRM model.

The SCALE cross section processing, transport and irradiation/decay calculations were called from a customized Perl script which requires user input of the target composition, target geometry and irradiation history. The script then cycled through the CENTRM and ORIGEN calculations for each irradiation step, with re-processing of effective cross sections and neutron flux and CENTRM and XSDRNPM to reflect the changing targets. Yields were read from the ORIGEN-S output, converted to the proper format, and used to populate new data for the CENTRM model. It has been previously shown, via a comparison between TCOMP and ORIGEN-S models, that during typical target irradiation, re-processing of the target constituent cross sections was only required approximately once per irradiation cycle [45].

The iterative model and the previously discussed KENO model were run to simulate the most recent transcurium isotope production campaign 75 using the actual target compositions and irradiation history. This campaign consisted of nine cycles of irradiation, for durations of 24 to

26 days each, for 4 targets with periods of decay ranging from 18 to 53 days in between each irradiation, as well as 6 additional targets for 1 irradiation cycle for 25 days. A post-irradiation decay period of 101 days was included for both sets of targets. The cross sections and flux spectrum were processed prior to each 24 to 26 day irradiation period. The transcurium isotope yields from both models are compared in Table 5. As of the date of this writing the analytical isotopics have not yet been obtained.

Table 5: Comparison of Predicted Curium Isotope

Isotope	KENO-VI (g)	CENTRM/ORIGEN (g)
Cm-244	1.291	1.196
Cm-245	0.017	0.014
Cm-246	3.860	3.805
Cm-247	0.065	0.075
Cm-248	0.838	0.856
Bk-249	0.004	0.004
Cf-252	0.023	0.024
Total Actinides	6.291	6.111

As can be seen from Table 5, the CENTRM model is able to calculate the transcurium yields with a reasonable accuracy when compared to the KENO simulation of campaign 75 data, within approximately 5 to 10% for all key isotopes as well as for total actinides. The CENTRM program was also compared to the campaign 67 data, however, the predictions became less reliable over longer campaigns. Campaigns during the 1970's and 1980's were not for the main purpose of Californium production, and were much longer in duration, with campaign 67 lasting 18 cycles over nearly four years. As discussed in section 5, the assumption that the flux in the moderator is essentially static becomes less accurate over time, and as more significant changes to the flux trap configuration take place.

7. Filtering

Much of the work presented in this section was documented in [46] and presented at the PHYSOR 2012 conference in April 2012. In order to suppress the flux spectrum in the energy ranges where the ratio of fissions to neutron captures is greatest, it is proposed that filter materials with high total capture cross sections in these energy regions be sought out. The ideal filter material will have a high capture cross section in the energy bands where it is desirable to reduce the overall reaction rate in the target (energy bands where fissions are significantly higher than (n,γ) captures, relative to the overall fission to capture ratio, as shown in Figure 5) but where it will not greatly suppress the overall flux in the remainder of the energy spectrum. Overly suppressing, or "poisoning" the flux spectrum will result in a reduction of the overall transmutation process as well as faster burnout of the filter material.

As discussed in Section 2, Cm-245, Cm-247 and Cf-251 are the isotopes most affected by fission losses during the transmutation processes. Looking back to Figure 5 in section 2.4, it was observed that in the energy range surrounding 1 eV the fission rates are significantly greater than (n,γ) absorption rates. The cross sections for the key isotopes contributing to fission losses were compared with the cross sections for a variety of potential filter materials, and a few isotopes were identified that displayed potentially useful properties: namely; ^{191}Ir and ^{177}Hf. The cross sections for the total capture cross sections of these materials are shown in Figure 16 along with the fission cross sections of Cm-245, Cm-247 and Cf-251.

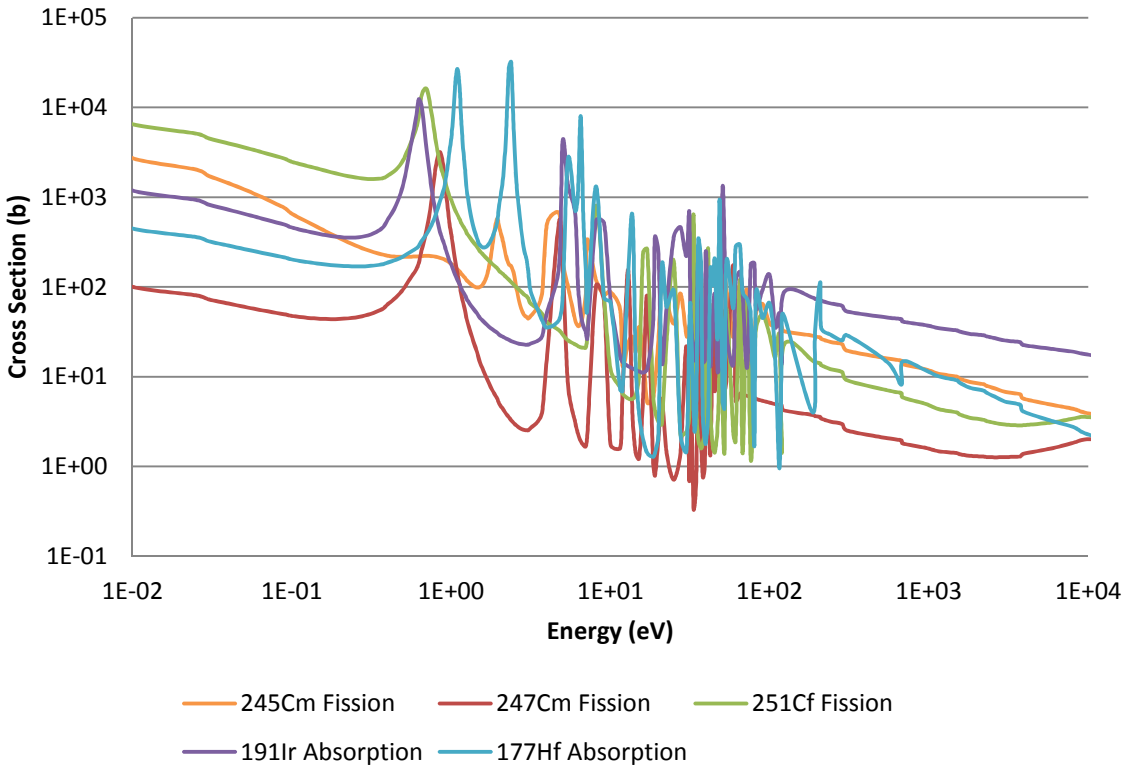


Figure 16: Cross sections for key isotopes in the transcurium chain and potential filter materials

As can be seen from Figure 16, both Hf-177 and Ir-191 display some of the characteristics desirable in a filter material for flux spectrum perturbation. Hf-177 contains a very high resonance near 1eV which partially overlaps with the resonances of Cm-247 and Cf-251. Hf-177 also contains an even higher resonance near 5eV, which completely encases the Cm-245 fission resonance in this region. Ir-191 contains a large resonance just below 1 eV which almost fully overlaps the Cf-251 resonance in this region. Ir-191 also contains a number of resonances in the epithermal range, including one at 7eV which overlaps a similar resonance in Cm-247, and another near 50 eV which corresponds to a region of high fission to capture ratio for Cm-247. Both Hf-177 and Ir-191 have low overall thermal cross sections, well below those of Cm-245 and Cf-251, such that they will not be quickly depleted and will not overly suppress the flux outside of the desired range for perturbation. Both isotopes also have cross sections that are much higher than those of Cm-245, Cm-247 and Cf-251 in the fast-energy range, which may be desirable, given than the rate of fissions per (n,γ) absorption is higher in the fast region than in

the thermal and epithermal regions. However, given the overall low flux in the fast-energy region, impact may be minimal.

With some potential materials identified, the 238-group flux spectrum in the region of the actinide target was analyzed using the 1-D discrete ordinates code CENTRM. Simple triangular-pitch three-region targets, containing the actinide target, cladding, and moderator, were simulated using CENTRM using a constant volumetric source in the moderator to simulate the unperturbed flux spectrum produced by the HFIR. The compositions of the targets were then varied in order to observe the resulting flux spectrum in the actinide target as a function of the composition and presence of filter materials. The observed flux spectra in the actinide target are shown in Figure 17 for four different compositions: standard mixed curium oxide (8g per target), mixed curium oxide with 1g Ir-191 per target, mixed curium oxide with 1g Hf-177 per target, and mixed curium oxide with 1g If-191 and 1g Hf-177 per target. The reductions in the flux spectrum are clearly visible around the resonances, and the thermal flux, while reduced, hasn't been completely poisoned.

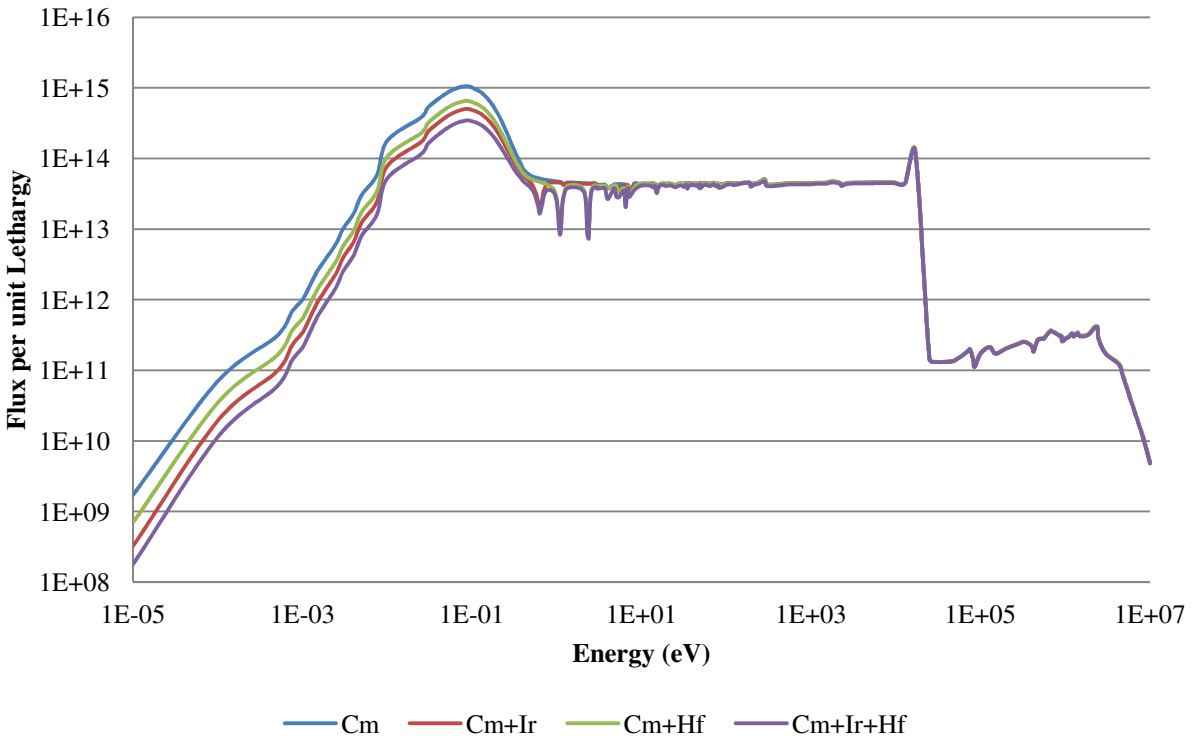


Figure 17: Flux Spectra for Varying Target Compositions

With the flux spectra and the cross sections from the CENTRM model, a five-cycle irradiation, typical of the irradiation period for a current campaign, was simulated. The irradiation history file used for iterating the model via Perl was as follows:

```
Irradiate 1 2 5 10 24 Decay 43
Irradiate 1 2 5 10 24 Decay 43
Irradiate 1 2 5 10 24 Decay 43
Irradiate 1 2 5 10 24 Decay 43
Irradiate 1 2 5 10 24 Decay 43
```

This history instructs the iterative script to run the transport calculation to obtain fluxes and effective cross sections, then deplete in ORIGEN-S with time steps of 1, 2, 5, 10, and 24 cumulative days, followed by decay to a total time of 43 days. The beginning of a new line then instructs the script to iterate and recalculate the flux and effective cross sections, and perform another depletion calculation. Overall the transport calculation was performed five times, and five depletion calculations were performed with 6 time-steps for each calculation.

The composition files used for this calculation differed, depending on the presence of filter materials. The composition file used to calculate the yields from a typical unfiltered curium target (representative of what would have been used in the most recent campaign) was as follows:

```
pu-238 1 2 0.001722
pu-239 1 2 0.000851
pu-240 1 2 0.565094
pu-241 1 2 0.000255
pu-242 1 2 0.016042
am-243 1 2 0.706215
cm-244 1 2 1.579877
cm-245 1 2 0.048613
cm-246 1 2 4.043418
cm-247 1 2 0.117259
cm-248 1 2 0.857666
bk-249 1 2 1.10000E-10
cf-250 1 2 1.10000E-10
```

```
cf-251 1 2 1.10000E-10
cf-252 1 2 1.10000E-10
al-27  1 1 19.3000
o-16   1 1 18.0000
al-27  2 1 122
si-28  2 1 0.306
mn-55  2 1 0.0307
fe-56  2 1 0.308
cu-63  2 1 0.119
cu-65  2 1 0.0525
h-1    3 1 6.52
o-16   3 1 52.2
```

This composition file instructs the Perl script to populate the SCALE input files with the appropriate atom densities for the target, cladding and moderator materials. Looking at the first line, this instructs the Perl script to include 0.001722 grams of the isotope pu-238 in region 1 (the target), and that this isotope is a type-2 isotope (actinide) for the purposes of ORIGEN-S depletion. Three other composition files were run for the target compositions as discussed previously, including 1 gram of Ir-191, 1 gram of Hf-177, and 1 gram of each combined.

In Table 6, the overall results on the transmutation chain for the different target compositions are shown as are the amounts of ^{252}Cf and ^{249}Bk produced per loss of feedstock material, which are the key parameters of interest for optimization of feedstock consumption.

The results in Table 6 show clearly that the transmutation rates are very sensitive to the influence of flux spectrum perturbation. Specifically, the results show that the transcurium production rate of the overall process is slowed down by the perturbed flux spectrum but that potential californium, the efficiency with which ^{252}Cf is created, is increased.

Table 6: Transcurium yields (g) a 5-cycle irradiation for varying target compositions

Isotope	Cm (g)	Cm + Ir (g)	Cm + Hf (g)	Cm + Ir + Hf (g)
Total ^{244}Cm	1.20E+00	1.27E+00	1.32E+00	1.39E+00
Total ^{246}Cm	3.80E+00	3.82E+00	3.82E+00	3.83E+00
Total ^{248}Cm	8.56E-01	8.57E-01	8.63E-01	8.63E-01
Total ^{249}Bk	4.09E-03	4.16E-03	4.08E-03	4.14E-03
Total ^{252}Cf	2.45E-02	2.44E-02	2.32E-02	2.28E-02
Cm loss	7.01E-01	6.09E-01	5.44E-01	4.64E-01
^{252}Cf /Cm loss	5.83E-03	6.83E-03	7.50E-03	8.92E-03
^{249}Bk /Cm loss	3.50E-02	4.01E-02	4.26E-02	4.91E-02

Because there is a significant reduction in the total flux, the overall reaction proceeds more slowly. For example, with the addition of 1 g of each If-191 and Hf-177, the production rate slowed down such that the Cf-252 yield was only 93% that of the base mixed curium target. However, the amount of curium consumed during the irradiation was only 66% that of the base mixed curium target due to the lower reaction rates. The result is that the amount of Cf-252 produced per unit of curium consumed was 53% higher for this case, and the amount of Bk-249 produced per unit of curium consumed was 40% higher. The majority of the feedstock savings comes in the form of increased retention of Cm-244, however there is also increased retention of the heavier curium isotopes. Some of the retention of Cm-244 may be due to increased production from Pu-240 and Am-243, which are present in the target in significant (>0.5 g) amounts. The production and destruction rates for Cm-244 at the mid-point of the campaign for a mixed curium target, and for a mixed curium target blended with 1g of each If-191 and Hf-177 are shown in Tables 7 and 8 below:

Table 7: Production rates for Cm-244 for mixed curium targets, and for mixed curium, Ir-191 and Hf-177 targets

Precursor	Production Rate in mixed Cm (/s)	Production Rate in mixed Cm,Ir,Hf (/s)
Cm243	3.75E+09	4.33E+09
Cm245	3.37E+08	4.02E+08
Cm246	3.00E+08	3.48E+08
Cm247	2.89E+04	3.39E+04
Total	4.39E+09	5.08E+09

Table 8: Destruction rates for Cm-244 for mixed curium targets, and for mixed curium, Ir-191 and Hf-177 targets

Successor	Destruction Rate in mixed Cm (/s)	Destruction Rate in mixed Cm,Ir, Hf (/s)
Pu241	6.10E+05	7.13E+05
Am244m	7.84E+05	9.07E+05
Am244	1.75E+06	2.02E+06
Cm242	5.68E+07	6.70E+07
Cm243	8.25E+09	9.73E+09
Cm245	2.63E+14	2.14E+14
Fission	1.41E+13	1.24E+13
Total	2.77E+14	2.26E+14

Subtracting the destruction rate from the production rate for Cm-244 yields a net destruction rate of 2.77E14 atoms per second for the mixed Cm target, and 2.26 atoms per second for the mixed Cm,Ir,Hf target. The net Cm-244 destruction rate in the filtered target is only 80% of the net destruction rate in the unfiltered target. Although the filters were originally chosen to reduce losses from Cm-245, Cm-247 and Cf-251, it appears that they are providing an added benefit of increasing retention of the most common feedstock material, Cm-244.

8. Transient Behavior of Filtering

The amount of flux depression caused as a result of resonance shielding is dependent upon the amount of material causing the flux depression; hence the effects of the resonance shielding will change over time as the composition of the target and filter materials change. As a result modeling a lengthy transmutation process requires continuous updating of the flux and cross-sections to account for changes in reaction rates which will affect the transmutation.

Ir-191 and Hf-77 are the two primary filter materials used in phase two of this research for investigating the effects of flux spectrum perturbations through filtering on the overall transmutation of heavy actinides. Looking at the reaction rates for the target over the duration of a typical 5-cycle campaign irradiation when Hf-177 and Ir-191 are employed as filter materials shows the transient behavior of resonance shielding.

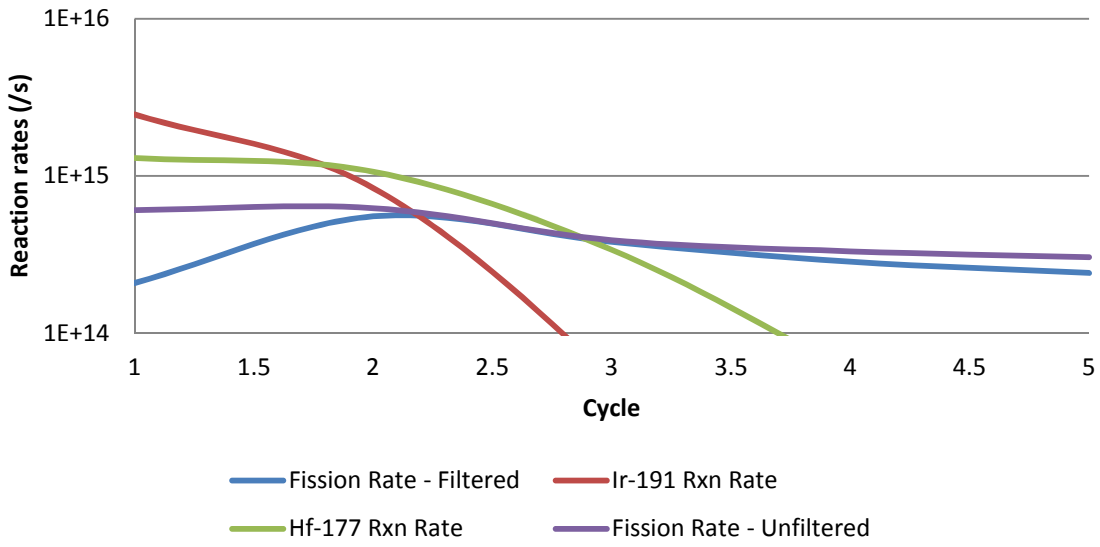


Figure 18: Reaction rates over time

As can be seen from Figure 18, the total reaction rates of Hf-177 and Ir-191 drop exponentially over the course of the irradiation as the material is consumed. During the first few cycles, as a large portion of this material is consumed, the fission rate increases, before slowly decreasing, though never back to the original rate. Looking at the fission rate for an unfiltered target, there is no such reduction at the start. It is expected that the fission rate would slowly decrease over irradiation as fissionable material is burnt up, particularly initial seeds of Cm-245 and Cm-247 and that is indeed observed in the unfiltered target. The bulk of the reduction in the fission rate

for the filtered target happens within the first two cycles, with the fission rate slowly decreasing, similar to the unfiltered target, over the remainder of the campaign.

While this initial decrease in the fission rate is of great benefit, it may be desired to continue to decrease the fission rate for the duration of the campaign. To achieve this, one must either load a great deal more filter material, or take other actions to ensure that a higher concentration of filter material remains during the duration of the cycle. This may be accomplished either by slowing the consumption of the filter material (filtering the filter so to say), or by utilizing a filter material that, upon capture of a neutron, transmutes to another useful filter material.

Using the two previously studied filter materials Hf-177 and Ir-191, the potential parent and daughter products of these isotopes were examined. The main parent isotope of Hf-177 is Hf-176, whose (n,γ) cross section is plotted in Figure 19 along with the total cross section of Hf-177. It can be seen that as Hf-176 does not display any resonance structure in the 1eV range, it may not be a particularly useful filter material. However, the significant overall cross section would allow slow in-growth of Hf-177 over time.

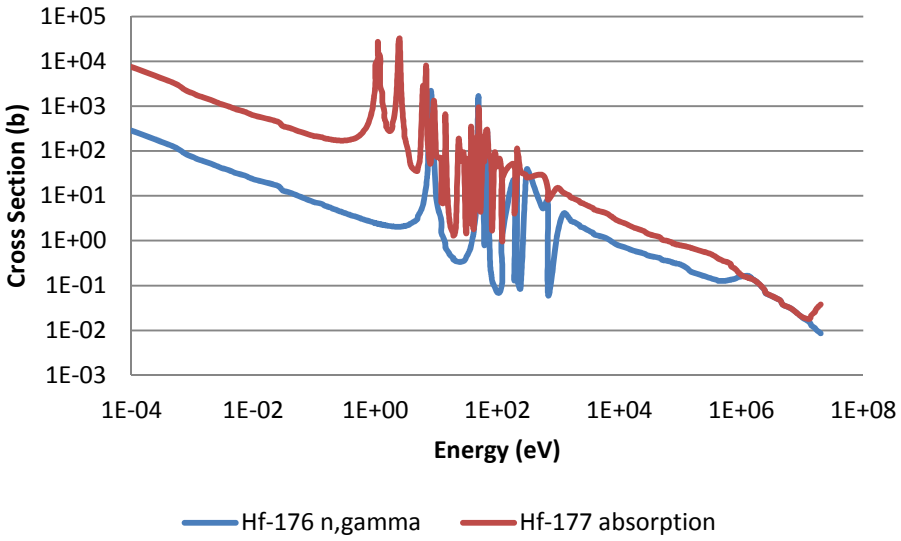


Figure 19: Hf-176 (n,γ) absorption and Hf-177 total absorption cross sections

The main parent product of Ir-191 is Os-190, whose (n,γ) cross section [47] is plotted in Figure 20 along with the total capture cross section of Ir-191. Os-190 absorbs a neutron to transmute to the relatively short lived Os-191, which then beta decays to Ir-191 with a half-life of 15.4 d.

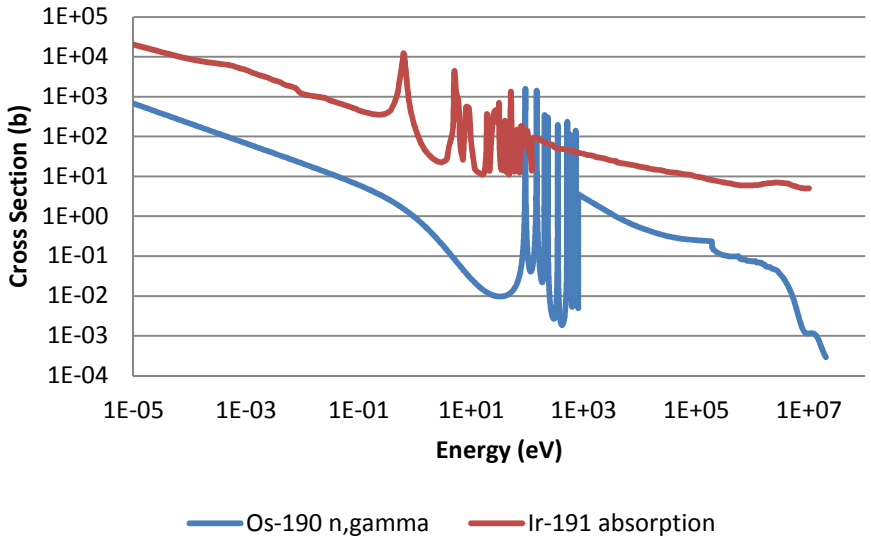


Figure 20: Os-190 (n,γ) absorption and Ir-191 total absorption cross sections

Again, although Os-190 does not display the cross-sectional properties that would be desirable in a filter material, the strong thermal cross section may allow for stable in-growth of Ir-191 over a longer duration irradiation.

The growth rate of Ir-191 and Hf-177 from these two parent isotopes was examined by running a simple depletion calculation, consisting of a mixed curium target filtered with 1 gram of Os-190 and 1 gram of Hf-176. The concentrations of the daughter filter materials over time are shown below, in Figure 21.

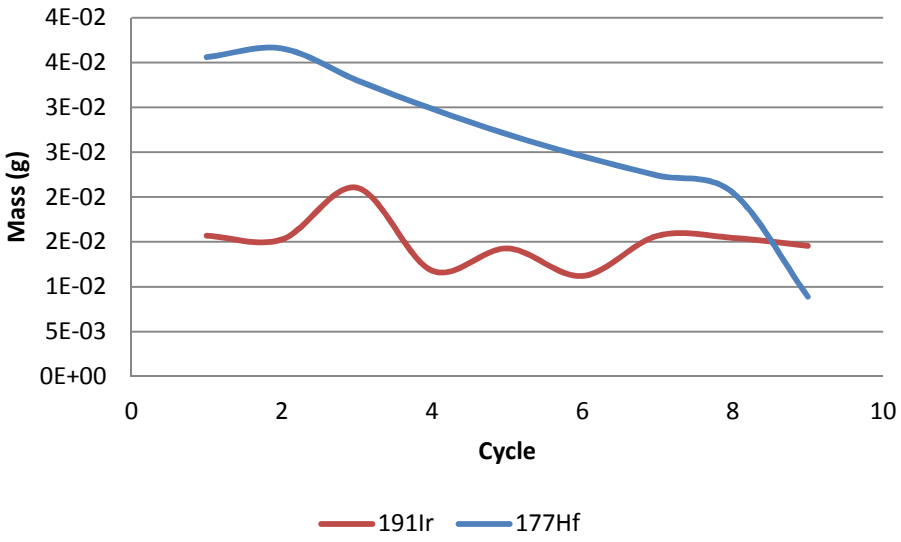


Figure 21: In growth of Ir-191 and Hf-177 from parent products

From Figure 21 it can be seen that the amount of daughter filter product produced from in-growth from Os-190 and Hf-176 is small, approximately 2% to 4% of the original charge, meaning that a very large amount of the daughter filter product must be added in order to grow in either iridium or osmium in significant amounts. This introduces physical limitations, such as the maximum amount of material that can be blended in, either in the target, or in the cladding.

9. Physical Limitations

As mentioned in the previous section, there are physical limitations that must be considered when developing new target compositions and configurations. The first of these is heat conduction in the target. Current safety assessment documentation allows for a total allowable "void" within the target of 12%, where "void" is considered any material other than aluminum oxide [48]. If a target configuration were proposed which included greater than 20% void, a new safety assessment of the heat conduction would be required. If a non-homogenous target configuration were proposed, incorporating layering of filter materials, each layer would also need to satisfy the 12% void requirement.

The other main limitation is the difficulty of target fabrication and/or post-irradiation processing. Any materials which are incorporated into the pellet or pellet cladding will be dissolved with the

cladding during post-irradiation processing. The chemical processing of this solution must be assessed to ensure these materials are soluble and do not interfere with the actinide separations.

Incorporation of the filter materials into the target cladding however allows for greater loading of filter materials, as the 12% void condition no longer applies. Additionally, as the cladding is removed and dissolved separately from the actinide target, chemical separation during post-processing is no longer an issue. It remains to be seen if incorporation of filter materials into the cladding however provides the same level of fission reduction and feedstock retention as incorporation into the target pellet.

Another irradiation case was run with similar configuration as that used to initially analyze the effects of Ir-191 and Hf-177. One gram of each of Ir-191 and Hf-177 was added, however, this time the materials were homogenized with the aluminum of the target cladding. The mixed curium target was irradiated, using the filtered target cladding, for five irradiation cycles, and the yield results compared to both an unfiltered target and to a target with in-pellet filter materials. The results are shown below in Table 9.

Table 9: Actinide yields with pellet and cladding filters

Isotope	Unfiltered	Pellet Filtered	Cladding Filtered
Total ^{244}Cm	1.20E+00	1.33E+00	1.32E+00
Total ^{246}Cm	3.80E+00	3.82E+00	3.82E+00
Total ^{248}Cm	8.56E-01	8.64E-01	8.61E-01
Total ^{249}Bk	4.09E-03	3.90E-03	3.95E-03
Total ^{252}Cf	2.45E-02	2.27E-02	2.31E-02
Cm loss	7.01E-01	5.41E-01	5.57E-02
^{252}Cf /Cm loss	5.83E-03	7.21E-03	7.09E-03
^{249}Bk /Cm loss	3.50E-02	4.20E-02	4.15E-02

As can be seen from Table 9, moving the filter materials from the pellet to the cladding has only a small effect on the overall transmutation efficiency. The total yield of both Bk-249 and Cf-252 is slightly increased, while the feedstock consumption is similarly slightly increased. The overall yields per unit of feedstock consumed are within 2% of the pellet filtered target. As such, it would be expected that target filtering through material addition to the cladding would be a more economical and feasible option.

10. Potential Filter Materials

The previous three sections have looked at the potential for filtering the flux spectrum, and have looked primarily at two isotopes, Ir-191 and Hf-177 as a proof of concept. In order to explore the potential for filtering the flux spectrum, all isotopes with a major low lying resonance were examined, both for their individual potential as a filter isotope, as well as for the practicality of using the naturally occurring form of the element. Factors considered included the cross sections and resonances of the individual isotopes, overall thermal cross sections, ability to grow in the filter material, or ability to transmute to other potential filter materials, availability and natural abundances.

10.1. Rhodium

- Atomic weight: 102.9055
- Density: 12.45 g/cm^3
- Valance: 6

Table 10: Isotopes of Rhodium

Isotope	Abundance	Half-life	Major Resonances (eV)
Rh-103	100%	Stable	1.26

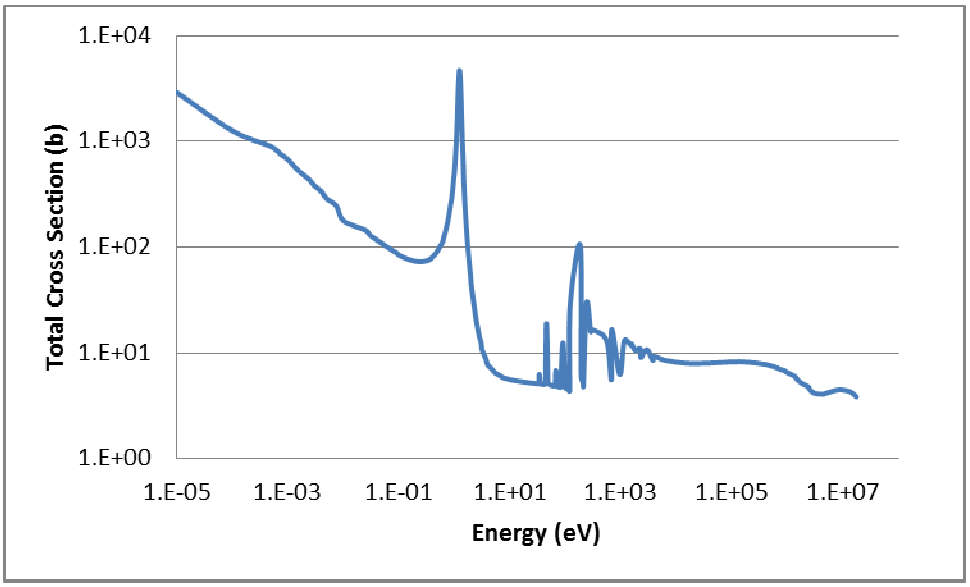


Figure 22: Total Cross section - Rhodium 103

Rhodium, atomic number 45, appears to be a potential candidate as a filter material due to the presence of a single resonance at 1.26 eV with a maximum height that is significantly greater than the cross section at the surrounding energies. Rh-103, the isotope containing the resonance, is the sole constituent component of natural Rhodium.

Rh-103 transmutes to Rh-104, which decays to Pd-104 with a half-life of 42.3s. Ph-104 is a stable isotope with no significant reaction cross-sections. It is therefore unlikely that Rh-103 would transmute to another suitable filter material in any significant quantity. Rh-103 can be produced from (n,γ) absorption in Rh-102, from beta decay of Ru-103 with half-life of 39 d, or from electron capture decay of Pd-103 with half-life of 17 d. As Rh-102 has no natural abundance and no significant cross section, production of Rh-103 from Rh-102 is unlikely. Production of Rh-103 via decay of Ru-103 or Pd-103 is also unlikely, due to the long half-lives of these isotopes, relative to the irradiation time, and the low cross-sections of their own parent isotopes.

Rhodium would be expected to be used as a stand-alone filter material; neither being produced, nor producing any other suitable filter materials, in any significant quantities.

10.2. Indium

- Atomic weight: 114.818
- Density: 7.31 g/cm^3
- Valance: 3

Table 11: Isotopes of Indium

Isotope	Abundance	Half-life	Major Resonances (eV)
In-113	4.29%	Stable	1.80
In-115	95.71%	4.408x10^{14} y	1.46, 3.85, 9.07

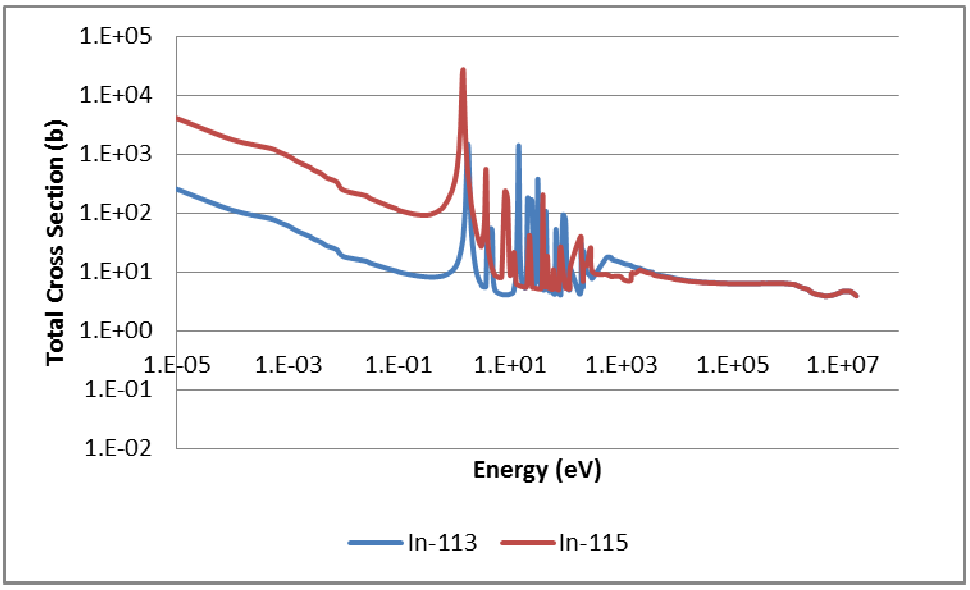


Figure 23: Total Cross Sections - Indium

Indium, atomic number 49, is composed of two naturally occurring isotopes, In-113 and In-115, both of which contain major resonances in the region of 1 eV with a max height significantly greater than the cross section at the surrounding energies.

The daughter products of In-113 and In-115 are In-114 and In-116 respectively. In-114 decays to Sn-114, a stable isotope with no significant cross section, with a half-life of 1m. In-116 decays to Sn-116, a stable isotope with no significant cross section, with a half-life of 14 s. It is therefore unlikely that Indium would transmute to another suitable filter material in any significant quantity.

In-113 can be produced from neutron absorption in In-112, from beta- decay of Cd-113 with a half-life of 7.5E15 y, or from beta+ decay of Sn-113 with a half-life of 115 d. Production of In-113 via decay is therefore unlikely due to the long half-lives of these isotopes, relative to the irradiation time. As In-112 has no natural abundance, production of In-113 via (n,γ) absorption is also unlikely.

In-115 can be produced from (n,γ) absorption in In-114, or from a 7-stage decay chain from Mo-115, itself primarily produced via fission. As In-114 has no natural abundance, production of In-115 via (n,γ) absorption is unlikely, as is production from decay.

Indium would be expected to be used as a stand-alone filter material; neither being produced, nor producing any other suitable filter materials, in any significant quantities.

10.3. Tellurium

- Atomic weight: 127.6
- Density: 6.24 g/cm^3
- Valance: 6

Table 12: Isotopes of Tellurium

Isotope	Abundance	Half-life	Major Resonances (eV)
Te-123	0.89%	5.99 y	2.33
Te-120, 122, 124, 125, 126, 128, 129	99.08%	~stable	none

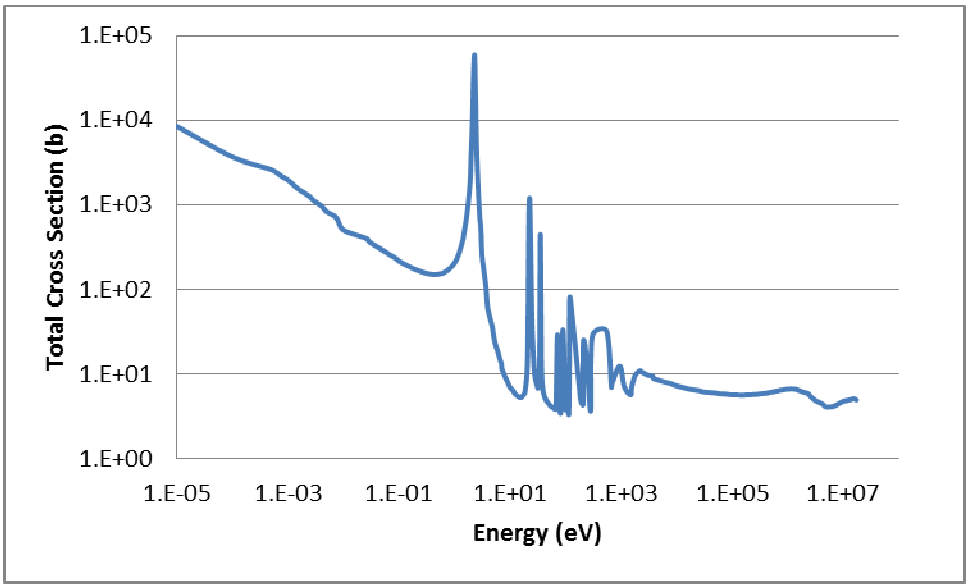


Figure 24: Total Cross Section - Tellurium 123

Tellurium, atomic number 52, is composed primarily of stable isotopes containing no major resonances below 5 eV. One isotope however, Te-123, which exists in natural abundance just shy of 1%, contains a major resonance at 2.3 eV with a max height significantly greater than the cross section at the surrounding energies.

The daughter product of Te-123 is Te-124, a stable isotope with no significant cross section. It is unlikely that Te-123 would transmute to another suitable filter material in significant quantities.

Te-123 can be produced from neutron absorption in Te-122 or from a decay 7-stage decay chain from Pr-123, primarily produced via fission. Te-122 exists with a natural abundance of 2.55%, and has no significant cross-section, other than a resonance in the region of 70 eV. It is therefore unlikely that Re-123 would be produced in any significant quantities during irradiation.

Due to the low natural abundance of Te-123, it is not expected to be a practical material for flux filtering. If used it would be expected to be used as a stand-alone filter material; neither being produced, nor producing any other suitable filter materials, in any significant quantities.

10.4. Lanthanum

- Atomic weight: 138.9055
- Density: 6.146 g/cm^3
- Valance: 3

Table 13: Isotopes of Lanthanum

Isotope	Abundance	Half-life	Major Resonances (eV)
La-138	0.09%	1.02E11 y	2.99
La-139	99.91%	Stable	none

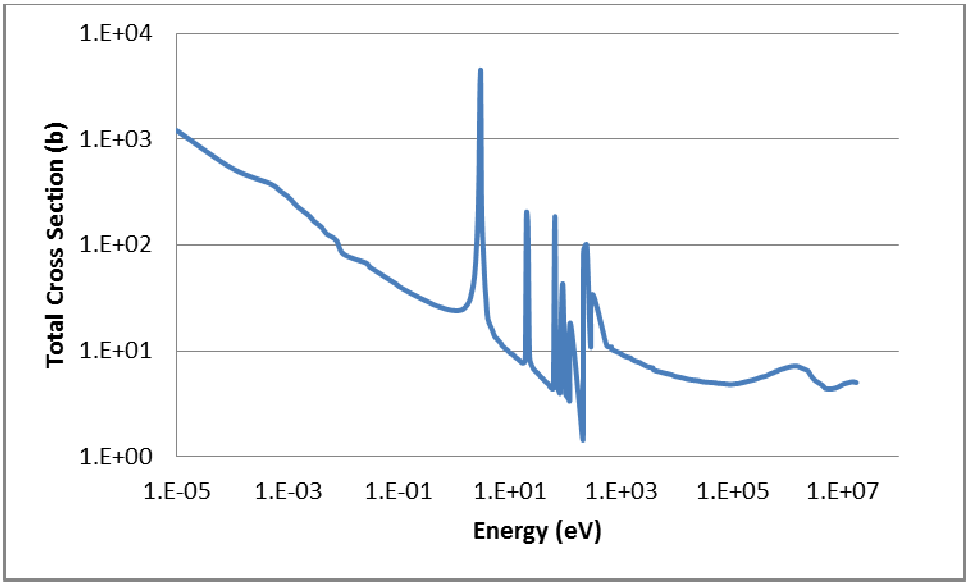


Figure 25: Total Cross Section - Lanthanum 138

Lanthanum, atomic number 57, is composed primarily of the stable isotope La-139, which contains no major resonances below 5 eV. One isotope however, La-138, which exists in natural of only 0.09%, contains a major resonance at 2.99 eV with a max height significantly greater than the cross section at the surrounding energies.

The daughter product of La-138 is La-139, the naturally abundant stable isotope of Lanthanum with no significant cross section. There are no known decay-chains for the production of La-138 and no natural abundance of the parent isotope La-137. Therefor it is unlikely that La-138 could be produced in any significant quantities during irradiation.

Due to the low natural abundance of La-138, it is not expected to be a practical material for flux filtering. If used it would be expected to be used as a stand-alone filter material; neither being produced, nor producing any other suitable filter materials, in any significant quantities.

10.5. Promethium

- Atomic weight: 145
- Density: 7.264 g/cm^3
- Valance: 3

Table 14: Isotopes of Promethium

Isotope	Abundance	Half-life	Major Resonances (eV)
Pm-148	0%	5.3681 d	0.169

Promethium, atomic number 61, contains no stable isotopes and exists only via synthetic production. Pm-148 contains a major resonance at 0.169 eV with a max height significantly greater than the cross section at the surrounding energies. There are no known decay modes for production of Pm-148, and production of the precursor, Pm-147, is only via lengthy decay chains of fission products. It is considered highly impractical however to produce Pm-148 during irradiation and it is deemed unsuitable for flux filtering.

10.6. Samarium

- Atomic weight: 150.36
- Density: 7.353 g/cm^3
- Valance: 3

Table 15: Isotopes of Samarium

Isotope	Abundance	Half-life	Major Resonances (eV)
Sm-144	3.07%	Stable	None
Sm-147	14.99%	1.062E11 y	3.40, 18.30
Sm-148	11.24%	6.98E15 y	None
Sm-149	13.82%	Stable	0.097, 0.872, 4.95, 8.95
Sm-150	7.38%	Stable	None
Sm-151	0%	88.8 y	1.09, 2.03, 6.39, 10.43, 11.13, 16.80, 17.33, 18.43
Sm-152	26.75%	Stable	8.05
Sm-153	0%	1.928 d	1.94
Sm-154	22.75%	Stable	None

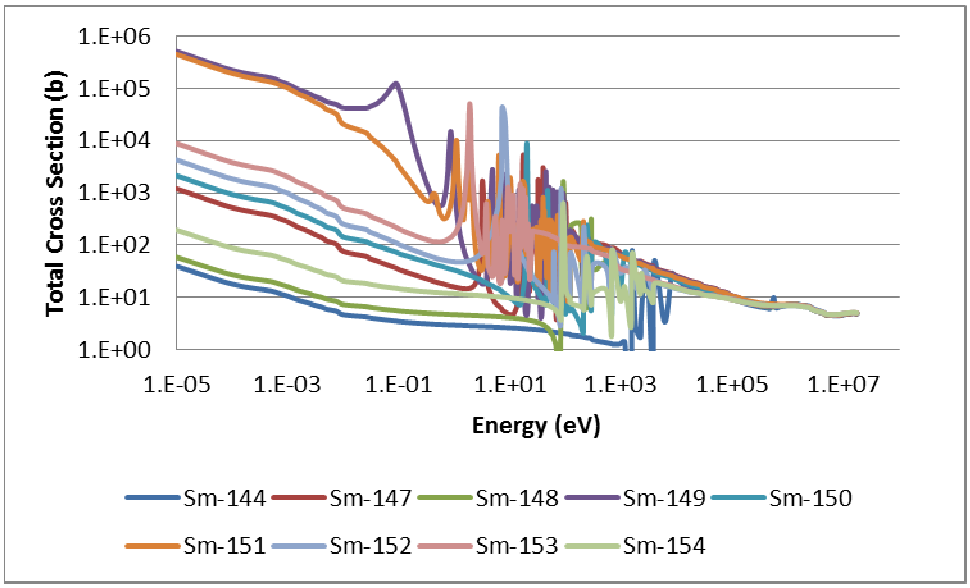


Figure 26: Total Cross Sections - Samarium

Samarium, atomic number 62, is composed of seven naturally occurring isotopes. One of these isotopes, Sm-147, which occurs with natural abundance of 15%, contain a major resonance at 3.4 eV with a max height significantly greater than the cross section at the surrounding energies. A second isotope, Sm-149, which occurs with natural abundance of 14%, contains a major resonance at 0.097 eV, however, the overall thermal resonance in this energy range is also quite high. Sm-149 also contains a major resonance at 2.03 eV with a max height significantly greater than the cross section at the surrounding energies. Four of the naturally occurring isotopes, Sm-144, Sm-148, Sm-150 and Sm-154, contain no major resonances below 5 eV. Samarium-152 does not contain any major resonances below 5 eV, but does contain a major resonance with max height significantly greater than the cross section are the surrounding energies at 8.05 eV. Two additional isotopes, Sm-151 and Sm-153, do not occur naturally, but have major resonances below 5 eV.

Sm-153 and Sm-147 both display potential as filter materials, due to the low lying resonances with max heights much greater than the overall thermal cross sections of these materials. However, the thermal cross sections of Sm-149 and Sm-151 are extremely high, and may cause unacceptable reduction in the thermal flux. Samarium isotopes are typically produced as transient fission products that are strong neutron poisons in power fission reactors, similarly to isotopes of xenon.

Samarium may be useful as a filter material, but care will need to be exercised to ensure that excessive thermal flux poisoning does not occur. It will also need to be determined the cost and difficulty of separating isotopes of Samarium if particular isotopes, such as Sm-152 and/or Sm-153 are desired.

10.7. Europium

- Atomic weight: 151.964
- Density: 5.244 g/cm^3
- Valance: 3

Table 16: Isotopes of Europium

Isotope	Abundance	Half-life	Major Resonances (eV)
Eu-151	47.81%	Stable	0.321, 0.460, 3.37, 7.29
Eu-152	0%	13.5461 y	0.884, 1.34, 1.37, 1.89, 4.13, 4.92, 6.35, 6.74, 9.61, 9.94
Eu-153	52.19%	Stable	2.46, 3.29, 3.94, 8.85, 11.61, 18.01, 20.02
Eu-154	0%	8.5997 y	0.192, 4.14, 5.22, 6.82, 9.32, 9.48
Eu-155	0%	4.7644 y	0.603, 2.04, 7.19

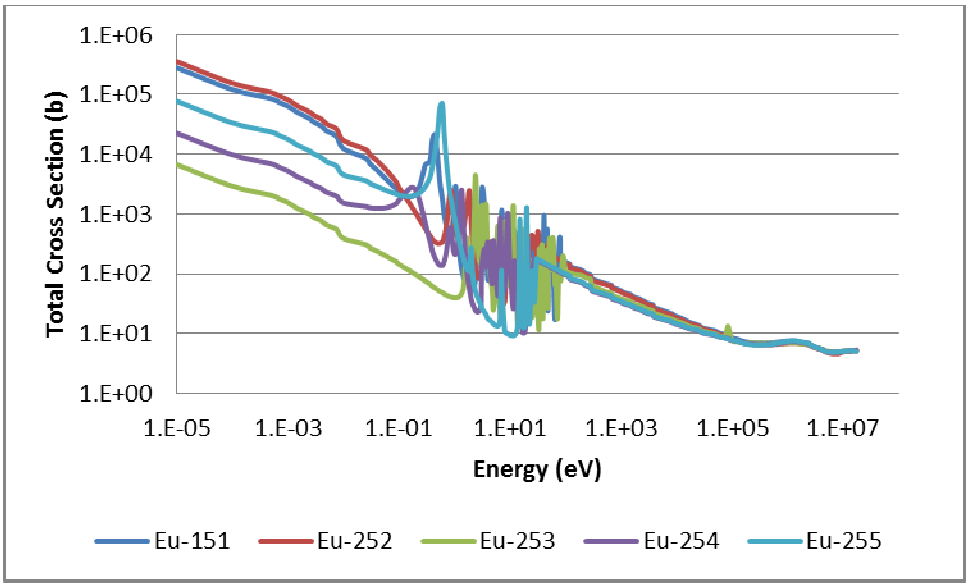


Figure 27: Total Cross Sections - Europium

Europium, atomic number 63, is composed of two naturally occurring isotopes, Eu-151 and Eu-253. Eu-151, which occurs with natural abundance of slightly less than 50%, contain major

resonances at 0.321, 0.460, 3.37 and 7.29 eV. However, Eu-151 is an extremely strong thermal neutron absorber, used as a poison in many thermal fission power reactors. The daughter product of Eu-151, Eu-152, is an even stronger thermal neutron absorber. The heavier isotopes, naturally occurring Eu-153, and daughter product Eu-153 have lower thermal cross sections, similar to that of Cm-245, however the second daughter product, Eu-155 is again a much stronger thermal neutron absorber.

It may be possible to use the low energy resonances of Eu-153 and Eu-154 without producing significant quantitates of Eu-255, if used in combination with the low level resonances of Sm-152 and Sm-153, the latter of which decays by beta emission to Eu-153.

10.8. Dysprosium

- Atomic weight: 162.5
- Density: 8.551 g/cm^3
- Valance: 3

Table 17: Isotopes of Dysprosium

Isotope	Abundance	Half-life	Major Resonances (eV)
Dy-156	0.06%	Stable	3.21
Dy-158	0.1%	Stable	None
Dy-160	2.34%	Stable	None
Dy-161	18.81%	Stable	3.68, 4.33
Dy-162	25.51%	Stable	5.44, 5.80
Dy-163	24.9%	stable	1.71
Dy-164	28.18%	stable	none

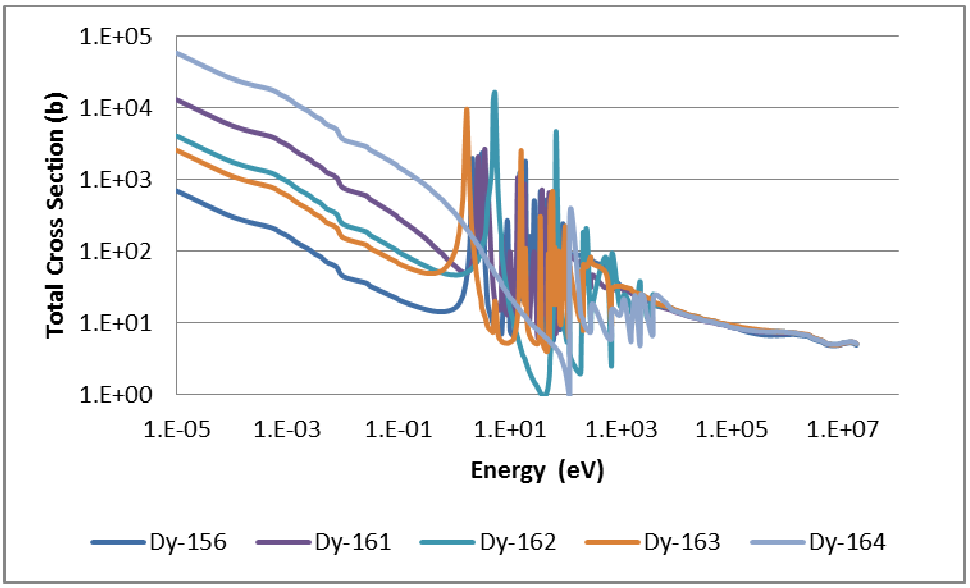


Figure 28: Total Cross Sections - Dysprosium

Dysprosium, atomic number 66, is composed primarily of four naturally occurring elements, with small quantities of three others. Of these isotopes, Dy-163, which occurs in natural abundance of 28.18% contains a major resonance at 1.71 eV, and three other isotopes, Dy-156, Dy-161 and Dy-162 contain major resonances near or below 5 eV. Three isotopes contain no major low energy resonances, however, two of these isotopes occur in very small natural abundances.

Dysprosium displays potential as a filter material due to containing multiple isotopes with low energy resonances, allowing for the potential of Dy-161 and Dy-162 to transmute to Dy-163 as they absorb neutrons. The heaviest isotope, Dy-164, however, is a fairly strong thermal neutron absorber, which transmutes into the radioactive isotope Dy-165, itself having a thermal cross section of 3500 b in the ground state and 2000 b in the metastable state [49].

Dysprosium in its natural form may be a potential filter material for the transcurium production targets, however, care would need to be taken that excessive amounts of thermal flux poisoning by Dy-164 do not occur.

10.9. Erbium

- Atomic weight: 167.259
- Density: 9.066 g/cm^3
- Valance: 3

Table 18: Isotopes of Erbium

Isotope	Abundance	Half-life	Major Resonances
Er-162	0.14%	Stable	
Er-164	1.61%	Stable	
Er-166	33.61%	Stable	
Er-167	22.93%	Stable	0.460, 0.584, 5.98, 9.3
Er-168	26.78%	Stable	
Er-170	14.93%	stable	

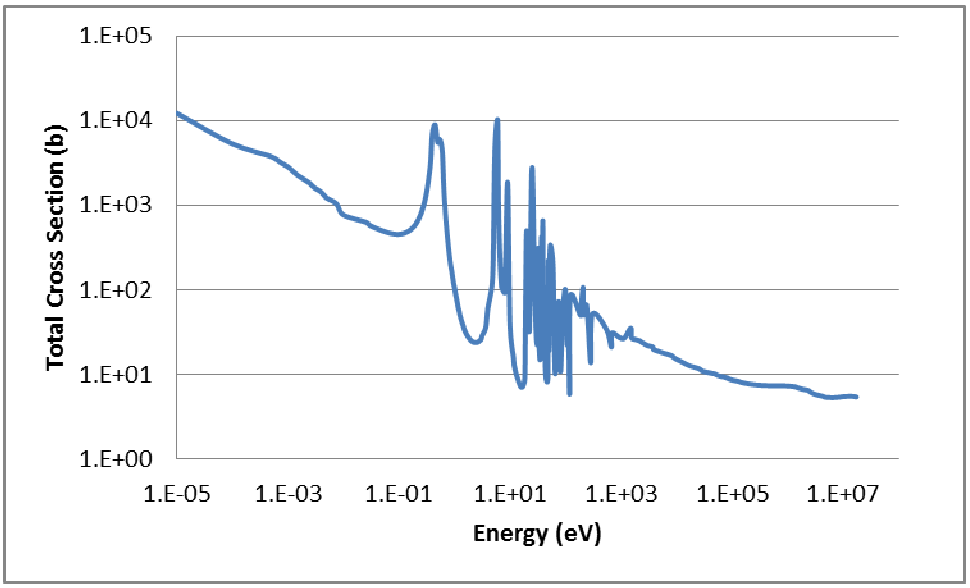


Figure 29: Total Cross Section - Erbium 167

Erbium, atomic number 68, is composed primarily of four naturally occurring isotopes, and contains two other isotopes is minor abundances. One of these isotopes, Er-167m contains two major resonances near 0.5 eV with max heights significantly greater than the cross sections at the surrounding energies. The remaining isotopes of erbium have neither major low energy resonances, nor significant neutron cross sections.

The daughter product of Er-167 is Er-168, a stable isotope with no significant neutron cross section. It is therefore unlikely that erbium would transmute to another suitable filter material in any significant quantity.

Er-167 can be produced from neutron absorption in Er-166, or from fission product decay chains. Although the cross section of Er-166 is not particularly suitable for flux filtering, containing no major low energy resonances, the overall thermal cross section is with an appropriate range where Er-167 may be grown in, without significantly poisoning the thermal flux.

Erbium in its natural form may be a potential filter material for the transcurium production targets, with initial flux depression caused by Er-167, and additional grown in from Er-166 and potentially Er-164 and Er-165. However, an erbium synthetically enriched with Er-167 may be more effective.

10.10. Lutetium

- Atomic weight: 174.967
- Density: 9.841 g/cm^3
- Valance: 3

Table 19: Isotopes of Lutetium

Isotope	Abundance	Half-life	Major Resonances
Lu-175	97.41%	Stable	5.22, 13.97, 14.16
Lu-176	2.59%	3.837E10	0.141, 1.56, 6.13,

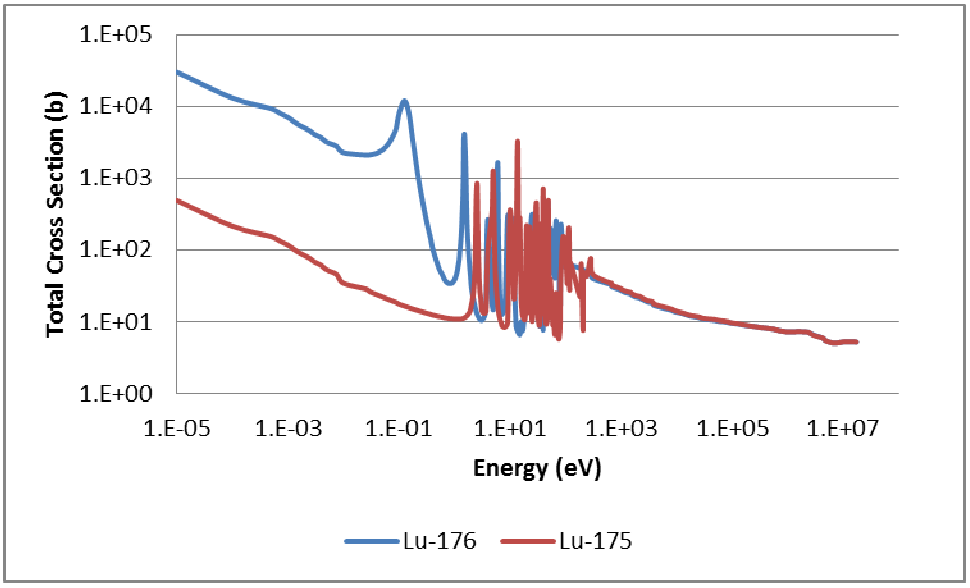


Figure 30: Total Cross Sections - Lutetium

Lutetium, atomic number 71, is composed primarily of Lu-175, with secondary component Lu-176 occurring in natural abundance of less than 3%. Lu-176 contains major resonances at 0.141 and 1.56 eV, with max heights significantly greater than the cross sections at the surrounding energies. Lu-175 contains a major resonance at 5.22 eV.

The daughter product of Lu-176 is Lu-177, an isotope with neutron cross section of the same order of magnitude as Lu-176, with a large resonance near 3 eV. Lu-177 decays to hafnium-177 with a half-life of 6.6 days. Hafnium-177 itself is a promising filter material, as discussed below.

Lu-176 is produced from neutron absorption in Lu-175, the much more abundant isotope of Lutetium. Although the cross section of Lu-175 is not particularly suitable for flux filtering, with lowest energy major resonance occurring at 5.22 eV, the overall thermal cross section is with an appropriate range where Lu-176 may be grown in, without significantly poisoning the thermal flux. Additionally, the resonances in Lu-175 may prove to be significant as more study is performed.

Lutetium in its natural form may be a potential filter material for the transcurium production targets, with initial flux depression caused by Lu-176, and additional grown in from Lu-175, as well as minor in-growth of Hf-177 from Lu-176 and Lu-177. However, a lutetium synthetically enriched with Lu-176 may be more effective.

10.11. Hafnium

- Atomic weight: 178.49
- Density: 13.31 g/cm^3
- Valance: 4

Table 20: Isotopes of Hafnium

Isotope	Abundance	Half-life	Major Resonances
Hf-174	0.16%	2E15 y	4.25, 13.38
Hf-176	5.26%	Stable	7.93
Hf-177	18.6%	Stable	1.10, 2.39, 5.89, 6.60, 8.88
Hf-178	27.28%	Stable	7.78
Hf-179	13.62%	Stable	5.68
Hf-180	35.08%	stable	

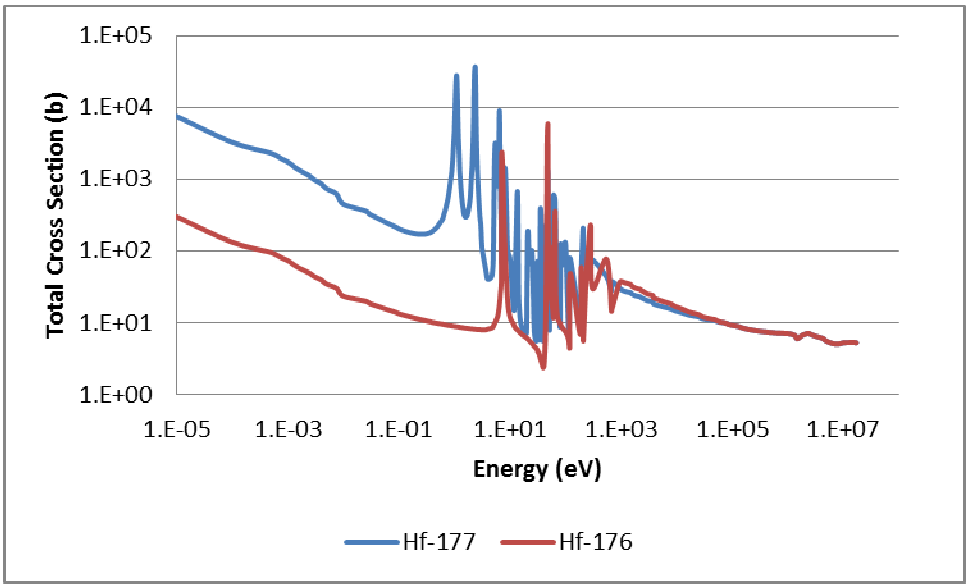


Figure 31: Total Cross Sections - Hafnium

Hafnium, atomic number 72, is composed primarily of four naturally occurring isotopes, with two additional isotopes occurring in small amounts. One of these isotopes, Hf-177, contains major resonances at 1.10 and 2.39 eV, which align well with corresponding resonances in Cm-247. Four other isotopes, Hf-174, Hf-176, Hf-178 and Hf-179 contain major resonances at 4.25, 7.93, 7.78 and 5.68 eV respectively. The two heaviest isotopes, Hf-179 and Hf-180 contain no major low energy resonances.

The daughter product of Hf-177 is Hf-178, a stable isotope with an overall neutron cross section within one order of magnitude of Hf-177, with a major resonance near 8 eV. Hf-178 then transmutes to Hf-179, again, a stable isotope with an overall neutron cross section within one order of magnitude of Hf-177, with a major resonance near 6 eV.

Hf-177 is produced from (n,γ) absorption in Hf-176. Although the cross section of Hf-176 is not particularly suitable for flux filtering, with lowest energy major resonance occurring at 7.93 eV, the overall thermal cross section is with an appropriate range where Hf-177 may be grown in, without significantly poisoning the thermal flux. Hf-177 is also produced from decay of Lu-177, which is produced during irradiation of Lu-176, as discussed in the previous section.

Hafnium in its natural form may be a potential filter material for the transcurium production targets, with initial flux depression caused by Hf-177 and additional grown in from Hf-176.

However, a hafnium synthetically enriched with Hf-177 may be more effective. A combination of shielding with Hafnium and lutetium may also prove to be effective, with lutetium providing both filtering of its own, and ingrowth of hafnium.

10.12. Tantalum

- Atomic weight: 180.9479
- Density: 16.65 g/cm^3
- Valance: 5

Table 21: Isotopes of Tantalum

Isotope	Abundance	Half-life	Major Resonances
Ta-180	0%	8.15 h	0.200, 0.435, 2.06, 5.93, 11.92, 18.19,
Ta-181	99.9888%	Stable	4.28, 10.36,
Ta-182	0%	114.431 d	0.148, 1.82, 12.93

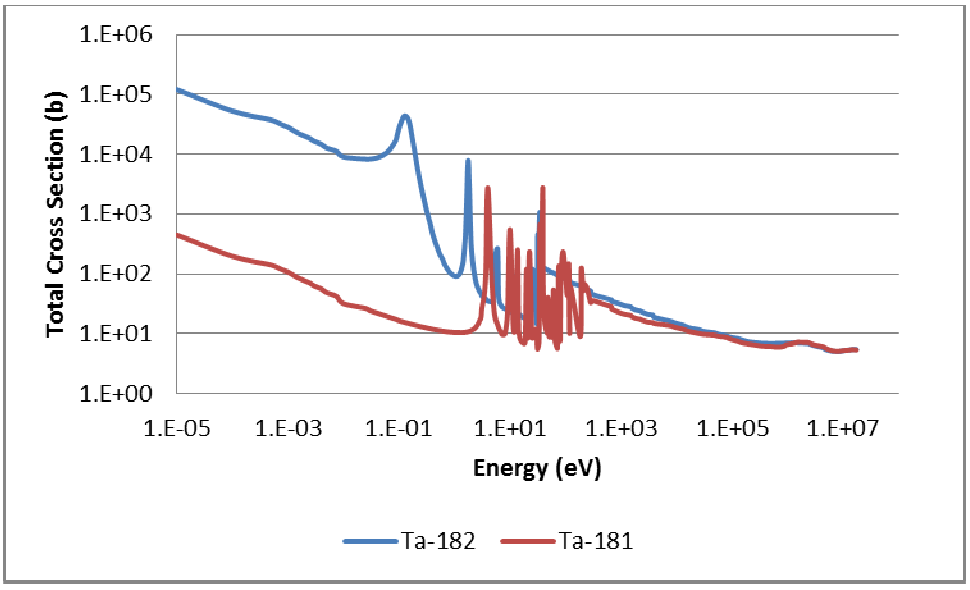


Figure 32: Total Cross Sections - Tantalum

Tantalum, atomic number 73, is composed primarily of Ta-181, with trace amounts of Ta-180m. Ta-181, as well as two isotopes of tantalum which do not occur naturally, Ta-180 and Ta-182, contain major resonances below 5 eV. Ta-180 has a half-life of 8 hours with no easy means of production, so despite the prevalence of a number of well suited low energy resonances, is not practical for use as a filter material. Ta-182 however is produced from (n,γ) absorption in Ta-

181 with significant cross section, so the potential exists to in-grow this material from a loading of Ta-180.

Ta-182 transmutes to Ta-183, which beta decays to the stable isotope W-183 with a half-life of 5 days. The thermal cross section of Ta-183 is approximately two order of magnitude below that of Ta-182, with little data on the resonances.

Tantalum in its natural form may be a potential filter material for transcurium production targets, providing little flux depression initially, from Ta-181, with in-growth over time from Ta-182.

10.13. Rhenium

- Atomic weight: 186.207
- Density: 21.02 g/cm^3
- Valance: 7

Table 22: Isotopes of Rhenium

Isotope	Abundance	Half-life	Major Resonances
Re-185	37.4%	Stable	2.16
Re-187	62.6%	4.12E10 y	

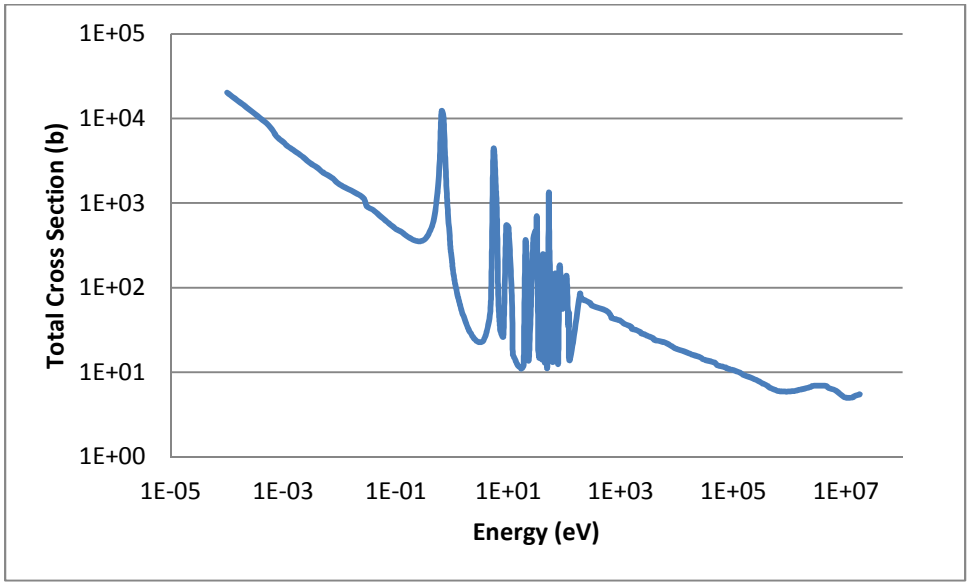


Figure 33: Total Cross Sections - Rhenium

Rhenium, atomic number 75, is composed of two isotopes, Re-185 and Re-187. Re-185, comprising about one third of natural Rhenium, contains a major resonance at 2.16 eV, while the heavier isotope, Re-187, does not contain any major low energy resonances.

Re-185 is produced by beta decay of W-185 with half-life of 75 days as well as by electron capture by Os-185 with half-life of 94 days. Due to the long half-lives of these parent isotopes relative to the irradiation time, it is unlikely that Re-185 would be produced in any significant amount in the reactor.

Re-185 transmutes to Re-186, which decays primarily to Os-186 with half-life of 3.7 days. Re-186 also transmutes to Re-187 if a neutron is captured before the isotope decays.

Rhenium in its natural form may be a potential filter material for the transcurium production targets, with flux depression caused by Re-185, and lessening over time. However, rhenium synthetically enriched with Re-185 may be more effective.

10.14. Iridium

- Atomic weight: 192.217
- Density: 22.56 g/cm^3
- Valance: 6

Table 23: Isotopes of Iridium

Isotope	Abundance	Half-life	Major Resonances
Ir-191	37.3%	Stable	0.653, 5.36, 6.13, 9.07
Ir-192	0%	73.827 d	0.256, 0.546, 1.57, 2.07, 3.13, 4.39, 7.83, 12.75, 14.56
Ir-193	62.7%	stable	1.30, 9.07

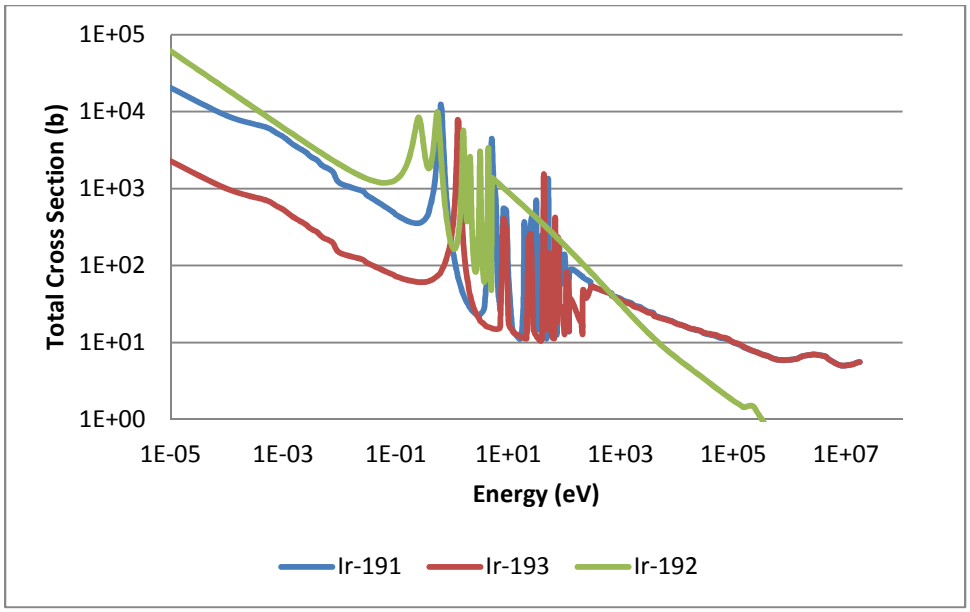


Figure 34: Total Cross Sections - Iridium

Iridium, atomic number 77, is composed of two natural isotopes, Ir-191 and Ir-193. Ir-191, comprising about one third of natural iridium, contains a major resonance at 0.653 eV, while the heavier isotope, Ir-193, contains a major resonance at 1.30 eV. The intermediary isotope, Ir-192, which does not occur naturally and has a half-life of 74 days, has major resonances at 0.256, 0.546, 1.57, 2.07, 3.13 and 4.39 eV.

Ir-191 is produced by beta decay of Os-191 with a half-life of 15.4 days and by electron capture of Pt-191 with a half-life of 2.8 days. Os-191 is produced via (n,γ) absorption in Os-190, which comprises 26% of natural osmium. Pt-191 is produced via (n,γ) absorption in Pt-190, which comprises only 0.014 % of natural platinum. It may be possible then to generate Ir-191 in the reactor from a loading of Osmium, although the loading would need to contain a large amount of Os-190 to produce Ir-191 in any significant quantity.

Ir-191 transmutes to Ir-192, which transmutes to Ir-193 if another neutron is absorbed before it decays, primarily to Pt-192, whose first major resonance occurs near 20 eV. Ir-194, the daughter product of Ir-193, has an overall thermal cross section in the same order of magnitude as that of Ir-193, however, little information is known on the presence of any resonances. Ir-194 decays to

Pt-194, an isotope with overall thermal cross section more than an order of magnitude smaller than that of Ir-193, with a half-life of 19 hours.

Iridium in its natural form is very promising as a filter material, due to the low energy resonances in both the naturally occurring isotopes, as well as those in the intermediary isotope. The usefulness of the filter material will be extended due to the transmutation of Ir-191 to other useful isotopes. Neutron capture by Ir-193 however produced no additional useful isotopes for filtering. It may also be possible to produce Ir-191 from a loading of Os-190, although it would require either highly enriched, or large amounts, of osmium.

10.15. Summary of Filter Materials

Rhodium and indium have been identified as possible stand-alone filter materials in their natural forms; neither being produced, nor producing any other suitable filter materials, in any significant quantities.

Samarium and europium are two elements that show potential as filter materials, but contain isotopes which may excessively poison the neutron flux. It may be possible to employ the heavier isotopes of samarium and transmuting to the higher isotopes of europium, if the higher isotopes of samarium and heavier isotopes of europium can be avoided in large quantities. However, this would require isotopic separation of samarium, which may not be financially prudent.

Dysprosium is another element that has been identified as a possible stand-alone filter material usable in its natural form, however the heavier isotope of Dy-164 may cause excessive thermal flux poisoning.

Erbium, lutetium and hafnium have been identified as possible filter materials which may be effective in their natural forms, but would be more effective if enriched with their heavier naturally occurring isotopes. A combination of hafnium and lutetium also displays potential, due to the ability to in-grow hafnium from lu-176.

Tantalum was identified as a potential filter material that would be required to grow-in over time, as the naturally occurring isotope Ta-181 provides little benefit, while its daughter isotope, Ta-182 contains two prominent low energy resonances

Rhenium has been identified as a possible filter material which may be effective in its natural form, but would be more effective if enriched with the lighter naturally occurring isotope.

Iridium has been identified as a possible filter material in its natural form due to the low energy resonances in both the naturally occurring isotopes, as well as those in the intermediary isotope. The usefulness of the filter material will be extended due to the transmutation of Ir-191 to other useful isotopes. It may also be possible to produce Ir-191 from a loading of Os-190, although it would require either highly enriched or large amounts of osmium.

11. Data Uncertainties

When performing calculations involving heavy actinides, the issue of uncertainties in the cross sections is a matter of some significance. In the report "Present Status of Minor Actinide Data" [52] the cross sectional data available for Cm-244 and Cm245 were discussed, and in the report "Impact of Nuclear Data Uncertainties on Transmutation of Actinides in Accelerator-Driven Assemblies", [53] these data were analyzed to estimate the uncertainty in the available cross sections. Aliberti et al reported the following uncertainties expressed as a percent of the total cross-section:

Table 24: Reported cross section uncertainties for minor actinides as percent of total cross-section

	Am-241 and Am-243		**Am-242m**		**Cm242,Cm243, Cm245,Cm246**		**Cm244**	
	Capture	Fission	Capture	Fission	Capture	Fission	Capture	Fission
Thermal	.2	.2	.04	.2	.04	.3	.04	.3
Epithermal	.4	.2	.4	.2	.4	.3	.4	.3
Fast	.4	.2	.4	.2	.4	.3	.4	.4

As can be seen from Table 24, the uncertainties in the minor actinide cross sections, determined by comparing the reported data from different sources, is on the order of 20% to 30%, with the exception of thermal capture in Cm242 through Cm-246.

The program Tsumani-1D [54] was used for performing an uncertainty analysis on the target configuration used in the CENTM model. TSUNAMI-1D is a module of the SCALE code

system for sensitivity and uncertainty analysis and utilizes the previously discussed CENTRM and BONAMI modules for cross-section processing, and the XSDRNPM module to perform both forward and adjoint transport calculations. Using the forward and adjoint solutions, Tsumani-1D calculates the sensitivity coefficients, which indicates the sensitivity of a system response due to uncertainties in the nuclear data. This calculation is performed using generalized perturbation theory.

A Tsunami-1D model was generated for a typical target, representative of those irradiated in campaign 75. This model was run including a filter composed of 2 grams of each potential filter material. The total uncertainty in k-effective in this model was determined to be 6.95 %. Although the targets themselves are not a critical experiment, uncertainty in k-effective can be used as a general guideline for uncertainty in fission reactions. A higher uncertainty in k-effective would indicate greater uncertainty in the number of fission reactions, which in turn leads to uncertainty in the consumption of feedstock material. The Tsunami-1D model was also used to calculate the contributions to the uncertainty in k-effective, as a percentage of the total uncertainty (6.95 %), for each nuclide reaction. Table 25 lists the top 10 contributions to uncertainty in k-effective listed from highest to lowest contribution.

Table 25: Relative Contributions to Uncertainty in Keff

Reaction	Contributions to Uncertainty in k-eff (%)
^{244}Cm fission	4.60E+00
^{247}Cm fission	3.48E+00
^{246}Cm fission	3.08E+00
^{248}Cm nubar	1.58E+00
^{248}Cm fission	1.41E+00
^{27}Al n,n'	7.30E-01
^{1}H elastic	5.49E-01
^{245}Cm fission	3.84E-01
^{243}Am fission	2.40E-01
^{27}Al n,n'	2.17E-01

As can be seen from Table 25, the fission reactions in Cm-244 through Cm-248 comprise five of the top ten contributors to uncertainty in k-effective. This is expected, as curium comprises the largest mass in the target composition. Additionally, as indicated in Table 25, there exists a significant amount of uncertainty associated with the fission cross sections for curium. In terms of filter materials, the (n,γ) cross section for Eu-151 ranked 11th with a contribution to the uncertainty in k-effective of 1.7753E-01, or about 10% the average contribution for curium isotopes. Thus it can be inferred that the greatest uncertainty attributed to cross sections comes from the curium isotopes.

The other main source of uncertainty in the calculations performed as a part of this research comes from the calculated neutron flux. The neutron flux used in this research is based upon the static neutron flux calculated at the start of irradiation in the moderator inside the flux trap. This neutron flux was calculated using the KENO-VI 3-D model and also includes a calculation of the flux uncertainty, for each geometric region, for each energy bin. Weighting each uncertainty by the flux within the geometry region and energy bin, the average uncertainty associated with the neutron flux in the moderator inside the flux trap is 9.36%.

Although there are minor uncertainties associated with the depletion calculations performed in ORIGEN-S, such as assuming the removal of short lived nuclides and the discretizing of the time steps, the uncertainties associated with the nuclear data is dominant for typical reactor cases [35].

12. Reaction Rate Optimization Routines

As described in Section 3, it is possible to alter the transcurium yields by modifying the target composition, which in turn perturbs the flux spectrum. The long-term objective of this research was to develop a methodology for systematically perturbing the flux spectrum in order to optimize transcurium production. The optimization of a problem this complex in nature is no simple feat. The minimum for a typical multi-variable equation can be determined by setting the partial derivatives to zero. However, the equation for the amount of curium feedstock consumed during a production run cannot be conveniently described by one equation.

The approach taken for this optimization is that of an iterative framework in which directed perturbation of target materials is combined with cross-section and flux-spectrum analysis,

simulated depletion, analysis of transmutation parameters, and subsequent (iterative) perturbations to converge upon an optimal solution. The process for such an optimization takes place in the phases shown in Figure 35.

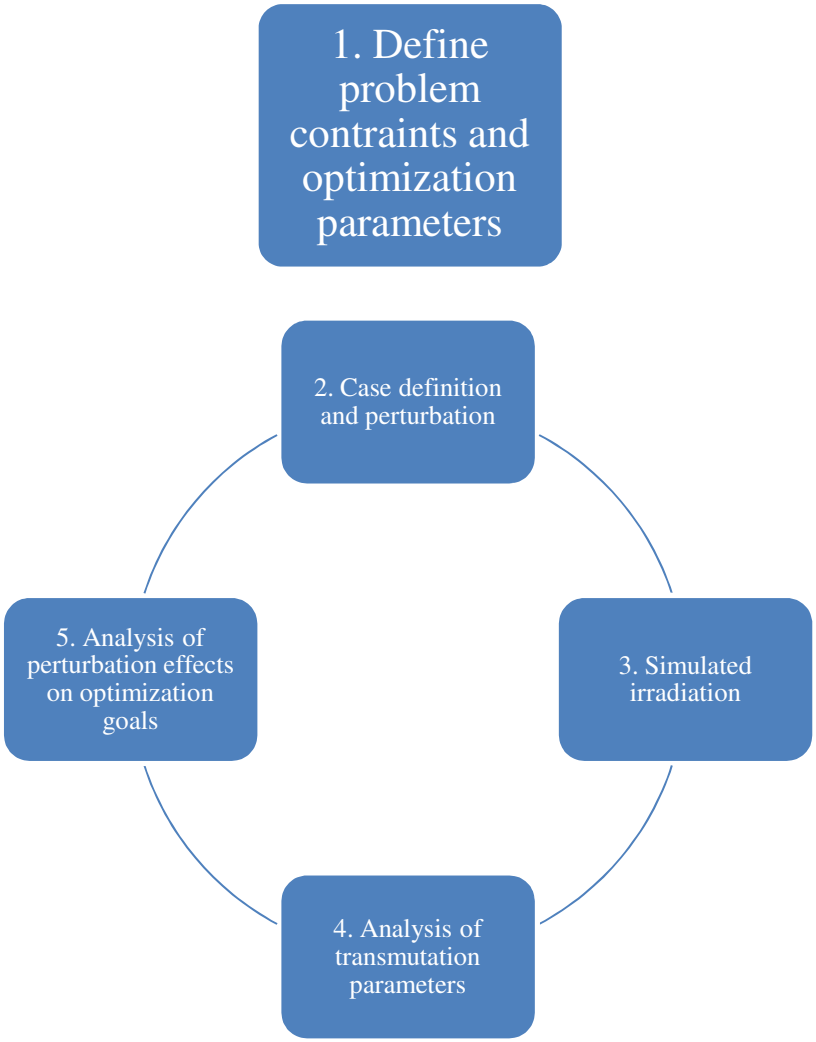


Figure 35: Iterative optimization routine

The process proceeds in five phases, as described below:

1. Define the problem constraints and optimization parameters (control variables) including target composition and geometry, available filter materials, maximum and/or minimum bounds for filter materials, and available irradiation time.
2. Within the bounds of the control variables defined in step 1, prepare one or more cases for simulation, perturbing the composition of the target filter as well as the irradiation time.
3. Perform calculations to simulate irradiation of the proposed cases. Gather key parameters regarding the transmutation for determination of the "fitness" of the case. Additional data saved for possible future analysis.
4. Analyze the transmutation parameters (the yields and losses) for each of the analyzed cases. Determine the "fitness" of the case in terms of reaching the optimization goals.
5. Compare the "fitness" of the cases to previous cases, and how perturbations have affected the goal of the optimization. Examine correlations between input perturbations and final "fitness" to identify future cases. If optimal conditions are achieved, end process, otherwise iterate to step 2 to perturb the target filter and irradiation conditions.

Iterative optimization can be carried out used a number of different algorithm types, each with different benefits and drawbacks. One such algorithms is called a "Genetic Algorithm", as discussed in section 4.1.7. Genetic algorithms are applicable to optimization cases where the "fitness" or "goodness" of a solution can be described by a single equation or value. Genetic algorithms are highly flexible, and can be applied to problems with large numbers of both discrete and continuous variables. The ability to handle discrete variables is one of the particularly attractive benefits of genetic algorithms.

In order for genetic algorithms to converge upon a global minimum for the optimization it is necessary to analyze a large number of potential solutions spanning the full range of possibilities. In a typical analysis, many thousands of irradiation cases may be analyzed. In order for these optimizations to be carried out in a reasonable amount of time, the results of the irradiation must be able to be estimated as quickly as possible. For this reason, the genetic algorithm has been developed in conjunction with a neural network solver, as discussed previously in section 4.1.6 and below in section 12.3, which is applicable to problems for which the range of variables is well-defined and for which large quantities of data spanning the variable range are available.

Both the genetic algorithm and the neural network have been programmed in MATLAB and have been designed to be as flexible as possible, allowing user control over the data to be used, the fitness function, and the filter materials to be considered.

12.1. Problem Definition

The first phase of the optimization routine involves problem definition. This phase takes place only once for the routine and involves setting all of the global constraints and conditions for the optimization.

The problem definition phase begins with the definition of the fitness function for the optimization. The algorithm contains a default customizable fitness functions for the user to select, or allows the user to generate their own function. The default fitness function is a linear combination of the primary factors in the optimization:

1. amount of Cf-252 produced,
2. amount of Bk-249 produced,
3. amount of total curium consumed,
4. amount of total actinides consumed, and
5. number of irradiation cycles.

If the user selects this fitness function they may apply weights to each of these five amounts to indicate the importance of optimizing each particular measure. The fitness function is wholly de-coupled from the genetic algorithm, returning only the result of the evaluation. Therefore the algorithm can easily substitute any function, or series of functions, that returns a single value for minimization. If the user does not wish to use the default linear combination fitness function, they may substitute their own fitness function in the form of a MATLAB .m file. The flexibility to use a custom fitness function means that the value to be minimized can be customized, and that other conditions may be added to the function, depending upon the desired outcome for the campaign. For example, if it was known that there were only 5 targets available for irradiation and that it was necessary to produce at least 150 mg of Cf-252 by the end of the irradiation, a condition could be added to the fitness function evaluator to ensure that the Cf-252 yield of an irradiated target was at least 30 mg. A simple if statement could be inserted that returned the

evaluation of the fitness function if the 30 mg quantity were reached, and returned a sufficiently high value if it were not.

The next step of the problem definition phase involves entering the initial target composition. The user may load a pre-set vector containing the masses of the actinides in the target, in a certain order. If no vector is defined when the optimization routine is called, the user is prompted to enter the weights of each of the typical major actinide in the target.

The next step of the problem definition phase involves entering the bounds for the optimization variables, which include the mass of each of the potential filter materials, and the number of irradiation cycles. The algorithm contains a set of default bounds for the filter materials and number of cycles. The user may input alternative bounds in the form of an upper bounds vector and a lower bounds vector, which are includes as arguments when the routine is initiated. If no bounds are indicated when the argument is initiated then the defaults will be used. Setting bounds on each of the potential filter materials adds an additional level of customization flexibility to the optimization routine, allowing the user to indicate if they wish to not use any of certain filter materials, due to unavailability, manufacturing concerns, or for other reasons. Setting bounds on the number of irradiation cycles also allows the user to limit the scope of the optimization to within a certain time frame.

The final step of the problem definition phase involves either loading the data to be used as the basis for the neural network in the genetic algorithm, or loading a pre-trained neural network. One of the major benefits of neural networks is that they need only be trained once, and can then be used to make unlimited predictions within the range of data. There is no need to re-train a neural network unless additional data is available to add to the training basis. As part of this research a large database of curium target irradiation cases has been developed and used to train, test and validate the neural network. Each of the cases in this database were evaluated under identical circumstances, including the same geometry and the same incident flux, varying only the filter composition and the number of cycles. This allows the optimization routine to isolate and optimize based upon the effects of the filter.

The user may opt to use the network already trained and tested, or to input a new data-set and re-train the neural network. The option to re-train the neural network provides the user with the

ability to expand the range of the model, should alternative feed or filter materials, or alternative irradiation schemes be used which are outside the range of the data used as part of this research.

This optimization algorithm has been developed for the purpose of analyzing the production of transcurium isotopes in the flux trap, however, the optimization algorithm itself is very generic, and could easily be modified to analyze other sorts of optimization problems. Almost all of the changes that would be necessary to analyze other optimization problems would take place during this first phase of the optimization, simply by changing the database to be used to generate the neural network used to solve each case evaluation.

12.2. Case Preparation

The second phase of the optimization routine involves case preparation. This portion of the optimization is controlled via the genetic algorithm, not by the user. In the first iteration of the routine, with no prior knowledge of the fitness of each case, a uniformly distributed random population sample is generated.

Each population sample consists of the filter isotopic composition, in grams, and the number of irradiation cycles. When this information is combined with the problem definitions provided in the first phase, it comprises the full information necessary for evaluating a case, which is carried out in phase 3.

The number of sample cases in the population is a function of the algorithm, and can be modified as needed. In general, a small population per generation reduces the possibility of finding a good solution; however, large population per generation may unnecessarily increase the calculation time [55]. The more variables to be considered in the optimization problem, the greater the population per generation that is needed to provide sufficient diversity. The default population size has been set at 50, and the user may increase the population as needed, depending up on the calculation resources available to them.

Upon subsequent iterations the population of the new generation is based upon the results of the evaluations of the population of the previous generation. The new population includes the individuals from the previous population with the best fitness function evaluation, as well as "children" of the individuals in the previous population with the best fitness. These "children" are produced by making random changes to the individual "parents" based upon a Gaussian

distribution, called mutation, and by combining pairs of individual "parents", called crossover. Over subsequent generations, the diversity of the population, that is, the average distance between individuals within the population, decreases, as the algorithm converges upon an optimal solution. Parameters affecting the production of subsequent population can be modified by the user if desired, such as the number of children produced by mutations and crossover, and the distribution of random changes.

12.3. Case Evaluation

The third phase of the optimization involves the evaluation of the cases selected in the second phase. The optimization algorithm has been set up in a modular manner such that the case evaluation may be wholly modified by the user with little change to the overall routine. The genetic algorithm only accesses the single value returned by the fitness function, with no regard for the methods used to determine that value. This allows the user of the optimization algorithm to use different means of evaluating the cases and determining the fitness function if they so choose, and would only necessitate modifying a single line of code within the genetic algorithm to call a different evaluation function.

For the purposes of this research, the evaluation of the cases was done using a neural network. The neural network was set up in the manner shown in Figure 36:

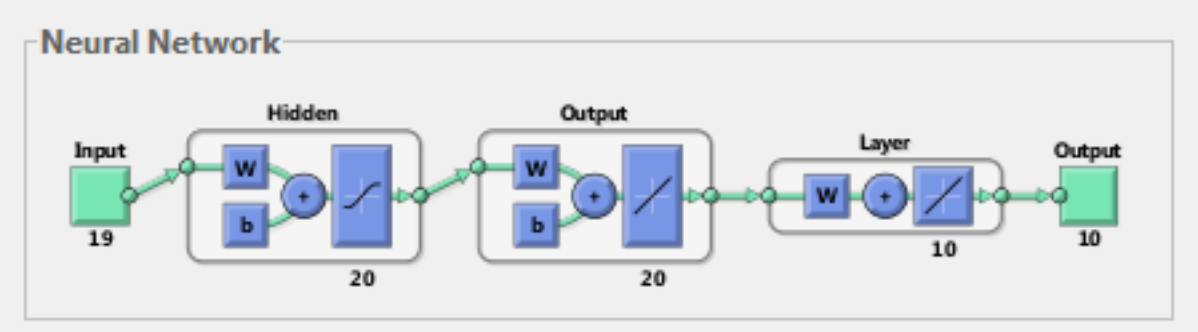


Figure 36: Neural Network Layout

Figure 36 displays the flow of information through the neural network. The start of the case evaluation begins with the input of the individual from the population. This input consists of nineteen pieces of information: the weights (in grams) of the typical isotopes present in a transcurium production target, the weights (in grams) of each of the potential filter materials, and the number of irradiation cycles.

These inputs are then passed through to the first layer within the network, which contains twenty neurons, represented by the number 20 below the box enclosing the layer after the input. Each of the nineteen inputs are combined with a series of weights and biases (represented by the "w" and "b" boxes, respectively) and sent to each of the twenty neurons in this first layer. In each of these neurons the inputs, weights and biases are processed through a sigmoid transfer function, represented by the wavy line in the third box of this layer. Each of the neurons of this layer produces a single output, resulting in twenty outputs to be sent to the next layer.

The twenty outputs from the first layer are then sent to the second layer, which are again combined with the series of weight and biases. In this layer each input is sent to each of the twenty neurons, where they are processed with the weights and biases through a linear transfer function, represented by the positive sloped straight line. Again, in this layer there are twenty neurons, which result in twenty outputs.

Finally, these twenty outputs are sent to the third layer in the neural network. Each of the twenty inputs to this layer are sent to each of the ten neurons in the output layer where they are combined with their relative weights and processed through a linear transfer function. These ten neurons produce ten outputs, which represent the output from the neural network. These ten outputs are the yields (in grams) of the typical isotopes in the transcurium production target following the irradiation described in the input data.

This neural network was trained using a dataset consisting of 2500 irradiation cases. These cases were generated using the previously described iterative CENTRM/ORIGEN model. The starting target composition for each case was selected at random based upon a perturbation of the typically available feedstock materials. The starting filter composition for each case was also selected at random from within the set bounds on the amount of filter materials. Finally, the number of irradiation cycles was selected at random, with a minimum of four and a maximum of nine. A simple algorithm was generated to create new cases, and could easily be modified to create additional data should the scope of the optimization search be changed.

Each of the 2500 cases was evaluated using the CENTRM/ORIGEN model and the isotope yields for the major actinides were extracted from the output. This resulted in a set of 2500 data

vectors, each of which consisted of the target and filter compositions, number of irradiation cycles, and the final post-irradiation yields of the major actinides.

With the database consisting of 2500 data vectors, the previously described neural network was able to be trained. The neural network was trained by analyzing the ability of the neural network to accurately predict the known post-irradiation yields for the data vectors. During an iterative process the weights and biases were systematically perturbed. With each iteration the performance of the neural network was evaluated, as well as the gradient of the performance. The neural network training performance failed to significantly increase with additional perturbations to the weights and biases and when a series of validation checks were achieved.

Part of the performance evaluation involves evaluating the mean-squared-error of the predicted yields (when compared to the known yields). This evaluation was performed by separating the database into three sets: training, testing and validation. The training set was used to train the neural network, the testing set was used to test the performance of the network and modify the weights and biases, and the validation set was used to validate the performance of the network, with none of the inputs of this set used to modify the network parameters (and thus to simulate entirely new data). The performance of each data set is shown in Figure 37.

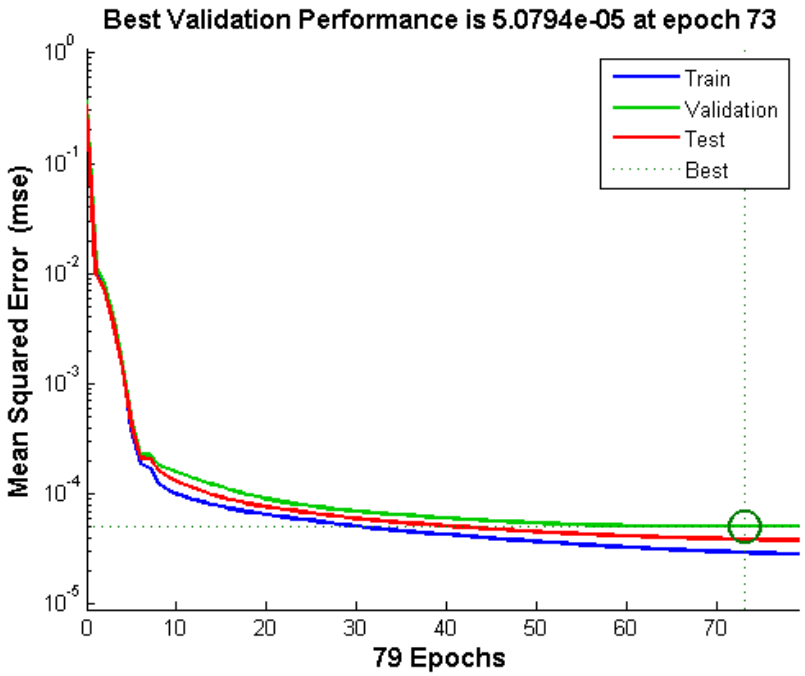


Figure 37: Neural Network Mean Squared Error

As can be seen from Figure 37, the mean squared error for the performance of each dataset falls dramatically within the first 15 iterations, or epochs. Around 70 iterations the mean squared error for the validation set has leveled out, and no longer continues to decrease. It can be seen that the mean squared error of the validation set is always later than the training and testing sets, but all three sets show very high performance. The performance of the neural network can also be seen in Figure 38 which displays a histogram of the errors associated with each evaluation of the neural network:

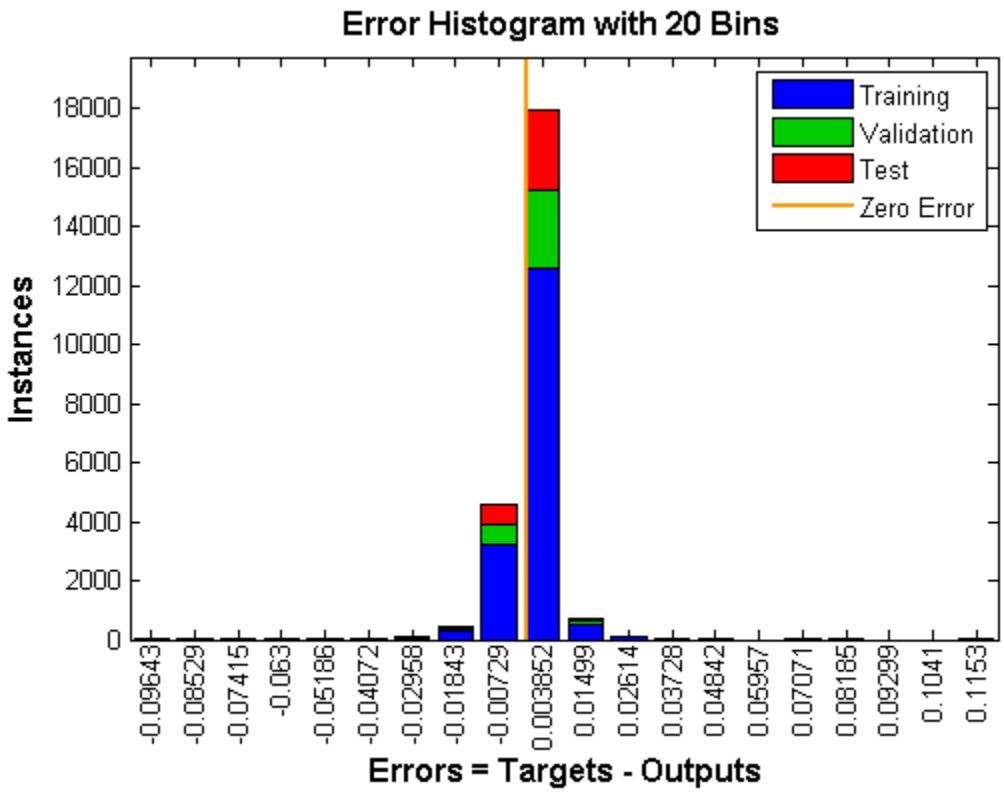


Figure 38: Neural Network Error Distribution

As can be seen from Figure 38, during training the neural network was evaluated over 20,000 times. Of these evaluations, approximately 18,000 of these results contained an error centered on 0.003852. It can be seen that the error distribution is Gaussian, centered just on the positive side of zero.

The neural network discussed in this section was used to evaluate a five-cycle irradiation for a target with composition representative of the most irradiation campaign. This is the same target

and irradiation configuration evaluated in section 6 using both the KENO-VI and CENTRM/ORIGEN models. The results of this evaluation are shown in Table 26.

Table 26: Neural Network Target Yields

	KENO-VI	CENTRM	Neural Network
Cm-244	1.291	1.196	1.154
Cm-246	3.860	3.805	3.649
Cm-248	0.838	0.856	0.868
Bk-249	0.004	0.004	0.003
Cf-252	0.023	0.024	0.025

As can be seen from Table 26, the neural network predicts the target yields with similar accuracy as the CENTRM/ORIGEN model. As such, the neural network was considered an applicable tool for performing case evaluations within the context of the genetic algorithm. The result is a highly accurate prediction tool, capable of performing thousands of evaluations in only seconds.

The neural network as described in this section was used to evaluate all of the individual cases in the population, as selected in phase 2. The post-irradiation transcurium yields were predicted and the results of the case evaluation were sent to phase 4.

12.4. Analyze Transmutation Parameters

The fourth phase of the optimization involves analyzing the transmutation parameters from all of the cases evaluated in phase three to determine the "fitness" of each case. This phase is relatively simple, and relies on the fitness function defined in phase 1. The fitness function is executed using the yields determined in phase 3 as the parameters, and returns a quantitative value for the fitness for each individual case in the population. The fitness function is set up such that a lower value indicates a more optimal result. For example, the default fitness function appears as follows, illustrated by Eq. 13.

$$F = -w_1\left(^{252}Cf\right) - w_2\left(^{249}Bk\right) + w_3(Loss\ Cm) + w_4(Loss\ Act) + w_5(Ncycles)$$

(Eq. 13)

In this example, the weights for the first two terms are negative, because these are values that are desired to be maximized, while the remaining three terms are positive, indicating a preference for minimizing these values. As discussed in section 12.1, the fitness function can be modified by the user to evaluate any of the parameters returned during the case evaluation.

12.5. Analyze Fitness

The final phase of the iterative optimization loop involves analyzing the fitness of the evaluated cases. In this phase the fitness of the cases are analyzed and compared both to each other and to the fitness of the previous cases to determine if the optimal state has been achieved, or if it is necessary to proceed to another generation. If it is necessary to proceed to another generation, the fitness of the individuals in the population is sent to phase two, so that the population of the next generation can be selected.

The genetic algorithm determines whether the optimal state has been achieved by analyzing the change in fitness of the population over many generations. In each generation the average fitness for the population is calculated and over subsequent generations, the change in the average fitness for the population is compared. When the total change in the average fitness function over a certain number of generations is less than a set tolerance the genetic algorithm ends and returns the solution with lowest fitness function evaluation. The number of generations to be considered, called the number of "stall generations" is set to a default of 50, and the tolerance is set to a default of 1E-6. Both of these values may be altered should the genetic algorithm not perform adequately for a given problem.

The genetic algorithm also employs a stopping criteria based on the number of generations. If the stopping criteria for the change in the average fitness of the population is not met within a set number of generations the algorithm will end and return the solutions with the lowest fitness function evaluation determined so far, and will indicate that the fitness function stopping criteria was not met. If this occurs it may indicate a lack of sufficient information for the optimization to proceed. The default value for the maximum number of generations is 100, however, if the genetic algorithm ends with the fitness function stopping criteria not being met this value can be increased and the algorithm can be run again.

12.6. Performance

The genetic algorithm as described in this section was developed for the purposes of optimizing the reaction rates for the production of transcurium isotopes. This algorithm has been tested and is proposed to work within the following bounds:

- Actinide target mass between 2 and 8 grams
- Plutonium weight percent between 5-10%
- Americium weight percent between 10-15%
- Cm-244 weight percent between 15-25%
- Cm-246 weight percent between 45-60%
- Cm-248 weight percent between 8-12%
- Number of 25-day irradiation cycles between 4 and 9
- Filter mass between 1 and 15 grams consisting of some combination of the following elements in their natural abundances:
    - Rhodium, Indium, Samarium, Europium, Dysprosium, Erbium, Lutetium, Hafnium, Tantalum, Rhenium, Iridium

Should the user wish the analyze cases outside the bounds specified above this would require analyzing additional cases using the CENTRM/ORIGEN model to cover the expanded range and adding this information to the neural network database.

In order to analyze the performance of the genetic algorithm the typical curium target analyzed previously in this research was selected for optimization. The default fitness function was selected and selections of different weights were utilized in order to examine the different ways in which the problem can be optimized.

For the first case a weight of 1 was applied to the production of Cf-252, and a weight of zero was applied to all other factors. In this case we would expect a solution from the genetic algorithm that produces the most possible Cf-252, with no regard to production efficiency. Running the genetic algorithm with standard upper and lower bounds for all potential filter materials resulted in a suggested filter of approximately 6 grams of indium and the projected yields as shown in Table 27:

Table 27: Optimized Projections weighted for Cf production with 6 g indium

	Charge (g)	Base Projection (g)	Optimized Projection (g)
Pu-240	0.565	0.033	0.023
Am-243	0.706	0.130	0.094
Cm-244	1.580	1.154	1.095
Cm-246	4.043	3.649	3.797
Cm-248	0.858	0.868	0.923
Bk-249	0	0.003	0.003
Cf-252	0	0.025	0.026

As can be seen from Table 27 these projected results include slightly elevated yields of the heavier isotopes of curium and increased consumption of Cm-244. The yield of Cf-252 is only slightly increased, within the margin of error of the projections. These results are as expected, as it is predicted that the majority of potential gains from incorporation of filter materials is in reduction of curium consumption, as opposed to increased gross yields of heavy actinides.

Due to the stochastic nature of genetic algorithms, the suggested "optimal" case may vary on subsequent iterations as the genetic algorithm may find a local minimum, instead of a global minimum. More complex problems, with many factors contributing to the final state, may result in more variation in the suggested optimal case. Running this same optimization problem a second time resulted in a suggested filter of approximately 3 grams of indium mixed with 12 grams of tantalum, and the projected yields as shown in Table 28:

Table 28: Optimized Projections weighted for Cf production with 3 g indium and 12 g tantalum

	Charge (g)	Base Projection (g)	Optimized Projection (g)
Pu-240	0.565	0.033	0.039
Am-243	0.706	0.130	0.119
Cm-244	1.580	1.154	1.278
Cm-246	4.043	3.649	3.864
Cm-248	0.858	0.868	0.951
Bk-249	0	0.003	0.003
Cf-252	0	0.025	0.026

As can be seen from Table 28 these projected results are identical to the projected results for the previous case for Cf-252, although the consumption of curium feedstock is slightly lower. As the fitness function was weighted only for Cf-252, the fitness function sees no difference between these two cases, and measures them both as equally optimal. It can be seen that there are multiple ways to achieve the same outcome for an irradiation problem, and in order to narrow down the selection it is necessary to include more factors than simply the production of Cf-252. Running this optimization ten more times resulted in only minor variations on the previous two results, with the suggested filter of 6 g of indium being returned 8 times out of 10.

Looking at a second optimization case, using the same target, the fitness function weights were adjusted to have equal weighting for Cf-252 production and curium consumption. Running the genetic algorithm with standard upper and lower bounds for all potential filter materials resulted in a suggested filter of approximately 6 grams of tantalum and 5 grams of dysprosium, and the projected yields as shown in Table 29.

Table 29: Optimized Projection Weighted for Cf production and Cm consumption with 6 g tantalum and 5 g dysprosium

	Charge (g)	Base Projection (g)	Optimized Projection (g)
Pu-240	0.565	0.033	0.046
Am-243	0.706	0.130	0.194
Cm-244	1.580	1.154	1.538
Cm-246	4.043	3.649	3.857
Cm-248	0.858	0.868	0.941
Bk-249	0	0.003	0.004
Cf-252	0	0.025	0.024

As can be seen from Table 29 the projected yield of Cf-252 in the optimized case is only slightly decreased, within the margin of error of the projections. However, looking at the total mass of primary curium isotopes (the yields of Cm-245 and Cm-247 are negligible in comparison and so not listed) it can be seen that the total mass of curium decreased by only 0.145 grams in the optimized projection, from a charge of 6.481 grams to a final yield of 6.336 grams, while in the base case the final yield of curium was 5.671 grams, for a total loss of 0.810 grams. This increased conservation of curium results in a much higher yield of ^{252}Cf per unit curium consumed. Running this optimization again, resulted in a suggested filter of approximately 10 grams of tantalum and 3 grams of dysprosium, with actinide yields nearly identical to the previous case. Running this algorithm ten more times resulted in variations on the amount of tantalum and dysprosium utilized in the filters, varying between 4 and 12 grams for tantalum and between 2 and 6 grams for dysprosium. In each case the actinide yields were similar to the original case, indicating that there are multiple combinations of tantalum and dysprosium filters which will result in the same "fitness", when examining only curium consumption and californium production. No other filter materials were suggested in significant (>1g) amounts.

When the weighting factor for californium production was increased to double that of curium consumption, the suggested filter returned from the optimization algorithm was similar to that where both factors were weighted equally, but with the addition of 2 grams of indium. Further increasing the weighting of californium production resulted in increasing amounts of indium suggested as a filter material, and decreasing amounts of dysprosium and tantalum. The yield of

californium slowly increased (though by very small margins, from 0.024 g to 0.026 g) while the consumption of curium also slowly increased. This is to be expected as it was shown from the original optimization, where only californium production was considered, that indium was the filter material chosen by the algorithm for increasing californium production when feedstock material consumption is not a factor.

Looking at the total consumption of actinides instead of the total consumption of curium, the optimization case was run again, using the same target and fitness function weights of equal value of Cf-252 production and total actinide consumption. The genetic algorithm suggested a filter composition of 6 grams of dysprosium, 2 grams of hafnium, and 6 grams of indium, and the projected yields as shown in Table 30.

Table 30: Optimized Projection Weighted for Cf production and Actinide Consumption with 6 g dysprosium, 2 g hafnium and 6 g indium

	Charge (g)	Base Projection (g)	Optimized Projection (g)
Pu-240	0.565	0.033	0.051
Am-243	0.706	0.130	0.212
Cm-244	1.580	1.154	1.537
Cm-246	4.043	3.649	3.851
Cm-248	0.858	0.868	0.939
Bk-249	0	0.003	0.004
Cf-252	0	0.025	0.024

Comparing this case to that where californium production and curium consumption were weighted equally it can be seen that the californium yields are identical. In the curium consumption optimization case the total consumption of curium was 0.145 g and the total consumption of actinides was 1.176 g. In the actinide consumption optimization case the total consumption of curium was 0.154 g and the total consumption of actinides was 1.162 g. In both cases the californium yield was identical, but in the case of optimizing for actinide consumption, less plutonium and americium was converted to curium, and less total actinide feed was consumed. The genetic algorithm was run ten additional times with the same parameters, and each result returned a filter composition and actinide yield similar to the first result.

Just as in the previous case, when the weighting factor for californium production was increased, the amount of indium suggested by the algorithm for the filter composition was increased, and the amount of other filter materials decreased. The californium yields rose slightly, as did the amount of actinides consumed.

Allowing for different weights in the fitness function allows the user to optimize for different campaign goals. If the goal of the campaign is to increase the weight percent of heavier isotopes in the feedstock, converting lighter plutonium and americium into curium, then the user may choose to optimize for total curium consumption, while if the goal of the campaign is to conserve total actinide inventories, they may select to optimize for total actinide consumption.

13. Conclusions

The main goal of this research is to identify the primary sources of feedstock material consumption, and to propose methods to reduce these losses so as to optimize the production of transcurium isotopes. It is shown that filtering of the neutron flux to perturb the spectrum incumbent upon the target is a means available to optimize the reaction rates for transcurium production.

It has been shown that by incorporating materials with resonances in the thermal and epithermal range that are much higher than their overall cross section, that the flux spectrum can be locally depressed in this energy range. It has also been shown that there are energy bands where the ratio of fission absorptions per (n,γ) absorption are exceptionally high. It follows that a local reduction of the flux spectrum in these energy ranges, by way of incorporating materials with high resonances in these energy ranges, would result in less overall fission absorptions per (n,γ) absorption.

To present this theory, a number of models of the High Flux Isotope Reactor were developed with the SCALE code modules which have provided valuable insight into the reactions rates throughout the transmutation process. A full 3-D Monte Carlo model of the reactor has been developed in KENO and an analysis of this model has been shown that while the flux in the target region is dependent upon the composition of the target, the flux in the moderator surrounding the target region is relatively constant. This information has been used to generate a

CENTRM model of the flux trap assuming a constant fixed source in the moderator with the ability to perform quick calculations. This model is most accurate when analyzing only small changes within the flux trap, and has been compared against the results of the high fidelity Monte Carlo model when analyzing irradiation periods of 4 to 9 cycles.

The data obtained from the CEMTRM and KENO models have helped identify isotopes which are high contributors to feedstock material loss, as well as to determine the energy bands where absorptions in these isotopes are most likely to cause fission. Analysis of isotope cross sections and physical properties uncovered a number of materials with potential to act as filter materials for optimization of transcurium isotopes. An initial proof-of-concept model confirmed that incorporating these isotopes into the target increased the retention of curium feedstock, and the amount of californium produced per unit of feedstock material consumed. This research has evaluated the effects of placement of the filter material both inside the target pellets, and in the exterior target cladding, to account for ease of filter construction, as well as ease of post-irradiation target processing. It has been shown that there is great potential to reduce the consumption of curium feedstock material with modifications to the target cladding material, reducing complications with target fabrication and post-irradiation isotopic separations.

The neural network developed as part of this work was trained using over 2000 data cases run using the CENTRM model and it was shown to perform exceptionally well within the boundaries of the analyzed (training) data. Expanding the range of the neural network to cover different target or filter compositions requires providing additional training data.

The genetic algorithm developed for this research was paired with the neural network in order to perform thousands of case analyses in a few minutes, to select a filter composition for the user supplied target. The filter composition selected by the algorithm depends upon both the fitness function, and the problem boundary conditions, both of which can be modified by the user.

Analysis of the performance of the genetic algorithm showed how the results of the algorithm varied, depending upon the fitness function. The fitness function used in this research allows the user to vary the weighting of californium production, berkelium production, curium consumption, actinide consumption and number of cycles. Allowing for different weights in the fitness function allows the user to optimize for different campaign goals. Alternate fitness

functions can easily be added by the user without affecting overall function of the genetic algorithm.

Although the user would be cautioned about using the genetic algorithm as the sole source of predictions regarding transcurium yields, as this model has yet to receive experimental validation, it is an extremely useful tool for determining patterns, and providing options, which may then be studied in higher fidelity using the CENTRM and/or KENO models.

14. Summary of Future Work

There are currently proposals underway to continue the work described in this paper by performing experimental validation. This validation will involve preparing experimental targets, to be irradiated in the hydraulic tube of the high flux isotope reactor, followed by analysis of the resulting actinide and fission product yields. The information from these irradiations should provide valuable insight into both the effectiveness and the longevity of various filter materials.

List of References

[1] Oak Ridge National Laboratory. (2011). *Scale: A Comprehensive Modeling and Simulation Suite for Nuclear Safety and Design*

[2] I. I. Bondarenko, "Group Constants for Nuclear Reactor Calculations", Consultants Bureau, New York (1964).

[3] D. F. Hollenback and P. B. Fox, "CENTRM Validation", ORNL/TM-2004/66, Oak Ridge National Laboratory, May 2006.

[4] R. C. Martin, R. R. Laxson, J. B. Knauer, "Proposed Californium-252 user facility for neutron science at Oak Ridge National Laboratory" Applied Radiation and Isotopes Volume 48, Issues 10–12, , Pages 1691–1695, October–December 1997.

[5] C. W. Alexander, "TCOMP Users Manual", NMP-TCOMP-MA Revision 1, Oak Ridge National Laboratory, May 2007.

[6] Californium Human Health Fact Sheet, Argonne National Laboratory, August 2005

[7] C. Alexander, D. Benker, E. Collins, J. Ezold, S. Hogle, B. Lewis, B. Patton, R. Taylor, "Feedstock Cases for ^{252}Cf Production", Oak Ridge National Laboratory, March 2012.

[8] R. C. Martin, J. B. Knauer, and P. A. Balo, "Production, Distribution and Applications of Californium-252 Neutron Sources", IRRMA 4th Topical Meeting on Industrial Radiation and Radioisotope Measurement Applications, October 1999

[9] T. Tacev, B. Ptackova, V. Stmad, "Cf-252 vs conventional gamma radiation in the brachytherapy of advanced cervical carcinoma", Strahlenther Onkol, 179: 377-384, 2003.

[10] Yu. Ts. Oganessian et al "Synthesis of a New Element with Atomic Number Z=117", Physical Review Letters, 104, 142502 (2010).

[11] R. A. Penneman and T. K. Keenan, "The Radiochemistry of Americium and Curium" National Research Council Nuclear Science Series, US Atomic Energy Commission, January 1960.

[12] G. H. Higgins, "The Radiochemistry of the Transcurium Elements" National research Council Nuclear Science Series, US Atomic Energy Commission, October 1960.

[13] D. L. Massart "Cation-Exchange Techniques in Radiochemistry" National Research Council Nuclear Science Series, US Atomic Energy Commission, December 1971.

[14] Y. Nagame and M. Hirata, "Production and Properties of Transuranium Elements", Radiochm Acta 99, 377-393 (2011).

[15] J.E. Bigelow, B.L. Borbett, L.J. King, S.C. McGuire and T.M. Sims, “Production of Transplutonium Elements in the High Flux Isotope Reactor,” Ch 1, pp 3-18, ACS Symposium Series, No 161, Washington DC, 1981.

[16] W. M. Stacey “Nuclear Reactor Physics”, Wiley-VCH Verlag GmbH & Vo. KGaA, Weinheim, 2007.

[17] http://neutrons.ornl.gov/facilities/HFIR/data

[18] R. T. Primm, III and N. Xoubi, ―Modeling of the High Flux Isotope Reactor Cycle 400, ORNL/TM-2004/251, Oak Ridge National Laboratory, August 2005

[19] N. Xoubi, ―Characterization of Exposure-Dependent Eigenvalue Drift Using Monte Carlo Based Nuclear Fuel Management, A Dissertation Presented for the Doctor of Philosophy Degree, University of Cincinnati, November 2005

[20] Chandler, David, "Spatially-Dependent Reactor Kinetics and Supporting Physics Validation Studies at the High Flux Isotope Reactor." PhD diss., University of Tennessee, 2011.

[21] D. F. Hollenbach, L. M. Petrie, S. Goluoglu, N. F. Landers, and M. E. Dunn, ―KENO-VI: A General Quadratic Version of the KENO Program, ORNL/TM-2005/39, Version 6, Vol. II, Oak Ridge National Laboratory, January 2009

[22] D. Chandler, R. T. Primm, III, and G. I. Maldonado, ―HFIR Post-Irradiation Curium Target Rod Nuclide Inventory Calculations, Transaction American Nuclear Society, Vol. 102, 560 – 561, ANS 2010 Annual Meeting, San Diego, CA, June 2010Chandler KENO

[23] M. D. DeHart and L. M. Petrie, “A Radioisotope Depletion Method Using Monte Carlo Transport with Variance Reduction and Error Propagation,” in *Proc. of PHYSOR 2004 - The Physics of Fuel Cycles and Advanced Nuclear Systems: Global Developments*, April 25–29, 2004, Chicago, Illinois, on CD-ROM, American Nuclear Society, La Grange Park, Illinois (2004).

[24] X-5 Monte Carlo Team, ―MCNP—A General Monte Carlo N-Particle Transport Code, Version 5, LA-CP-03-0245, Los Alamos National Laboratory, April 24, 2003

[25] G. Youinou et al, “MANTRA: An Integral reactor Physics Experiment to Infer Actinide Capture Cross-sections from Thorium to Californium with Accelerator Mass Spectrometry”, Journal of Korean Physical Society, Vol. 59, No. 2, pp 1940-1944, August 2011.

[26] R. J. Ellis, J. C. Gehin, J. L. McDuffee, R. W. Hobbs, "Analysis of a fast spectrum irradiation facility in the high flux isotope reactor," International Conference on the Physics of Reactors "Nuclear Power: A Sustainable Resource," Casino-Kursaal Conference Center, Interlaken, Switzerland, September 14-19, 2008.

[27] A. Ouardia, R. Alamia, A. Bensitela, A. Hommada, "GEANT4 used for neutron beam design of a neutron imaging facility at TRIGA reactor in Morocco", Nuclear Instruments and Methods in Physics Research Section A: Accelerators, Spectrometers, Detectors and Associated Equipment, Volume 651, Issue 1, 21, Pages 21–27, September 2011

[28] J. J. Duderstadt, L. J. Hamilton "Nuclear Reactor Analysis", Wiley, January 1976.

[29] M. L. Williams and M. Asgari, "Computation of Continuous-Energy Neutron Spectra with Discrete Ordinates Transport Theory," *Nuclear Science Engineering*, **No 121**, pp 173-201, (1995).

[30] N. M. Greene, L. M. Petrie, M. L. Williams, "XSDRNPM: A One Dimensional Discrete-Ordinates Code for Transport Analysis", ORNL/TM-2005/39, Version 6.1 Section F3, Oak Ridge National Laboratory, June 2011.

[31] S. Goluoglu, N. F. Landers, L. M. Petrie, and D. F. Hollenbach, "CSAS5: Control Module for Enhanced Criticality Safety Analysis Sequences with KENO V.A", ORNL/TM-2005/39, Version 6, Vol. I, Oak Ridge National Laboratory, January 2009.

[32] S. Goluoglu, D. F. Hollenbach, and L. M. Petrie, "CSAS6: Control Module for Enhanced Criticality Safety Analysis Sequences with KENO-VI", ORNL/TM-2005/39, Version 6, Vol. I, Oak Ridge National Laboratory, January 2009.

[33] N. M. Greene, "BONAMI: Resonance Self-Shielding by the Bondarenko Method", ORNL/TM-2005/39 Version 6.1 Section f1, Oak Ridge National Laboratory, June 2011.

[34] I. C. Gauld, D. Wiarda, "COUPLE: A Nuclear Decay and Cross Section Data Processing Code for Creating ORIGEN-S Libraries", ORNL/TM-2005/39, Version 6.1 Section F6, Oak Ridge National Laboratory, June 2011

[35] I. C. Gauld, O. W. Hermann, and R. M. Westfall, "ORIGEN-S: SCALE System Module to Calculate Fuel Depletion, Actinide Transmutation, Fission Product Buildup and Decay, and Associated Radiation Source Terms", ORNL/TM-2005/39, Version 6, Vol. II, Oak Ridge National Laboratory, January 2009.

[36] H. Demuth, and M. Beale, “Neural Network Toolbox for Use with Matlab”, MathWorks, Inc. (1992).

[37] A. J. Chipperfield and P. J. Flemming, “The MATLAB Genetic Algorithm Toolbox”, IEE Colloquium Applied Control Techniques Using MATLAB, pp 10/1 – 10/4, January 1995.

[38] S. M. Bowman, M. E. Dunn, “SCALE Cross-Section Libraries”, ORNL/TM-2005/39, Version 6.1 Section M4, Oak Ridge National Laboratory, June 2011

[39] M.B. Chadwick, et. al. ENDF/B-VII.1 Nuclear Data for Science and Technology: Cross Sections, Covariances, Fission Product Yields and Decay Data, Nuclear Data Sheets, Volume 112, Issue 12, 2887-2996 (2011).

[40] http://www.mathworks.com

[41] Perl 5 version 14.2: http://perldoc.perl.org

[42] S. Hogle and G.I. Maldonado, “Modeling of the High Flux Isotope Reactor with KENO-VI,” *Transactions American Nuclear Society*, **No 104**, pp 915–917 (2011).

[43] D. Chandler, G.I. Maldonado, R.T. Primm III, “Startup Reactivity Accountability Attributed to Isotopic Transmutations in the Irradiated Beryllium Reflector of the High Flux Isotope Reactor”, PHYSOR 2010.

[44] S. Hogle, G. I. Maldonado, “Development and Comparison of High Flux Isotope Reactor Actinide Target Models,” Transactions American Nuclear Society, **No 106**, (2012)

[45] S. Hogle, G. I. Maldonado, I. C. Gauld, J. G. Ezold, “Calculating Transcurium Production Yields at the High Flux Isotope Reactor,” Transactions American Nuclear Society, **No 103**, pp 766-767 (2010)

[46] S. Hogle, G. I. Maldonado, C. Alexander, “The Effects of Flux Spectrum Perturbation on Transmutation of Actinides: Optimizing the Production of Transcurium Isotopes” PHYSOR 2012.

[47] K. Shibata, O. Iwamoto, T. Nakagawa, N. Iwamoto, A. Ichihara, S. Kunieda, S. Chiba, K. Furutaka, N. Otuka, T. Ohsawa, T. Murata, H. Matsunobu, A. Zukeran, S. Kamada, and J. Katakura, "JENDL-4.0: A New Library for Nuclear Science and Engineering," J. Nucl. Sci. Technol.. 48(1), 1-30 (2011).

[48] Internal communications – Radiochemical Engineering Development Center

[49] T. Sekine and H. Baba, “Reactor-neutron-capture cross sections of 165Dy isomers”, Journal of Inorganic and Nuclear Chemistry, Volume 43, Issue 6, 1981, Pages 1107–1113

[50] R. D. Cheverton, T. M. Sims, "HFIR Core Nuclear Design", ORNL-4621, Oak Ridge National Laboratory, 1971.

[51] G. Ilas, R.T. Primm III, "Methodology for Simulating the Irradiation of the Control Elements in HFIR," Transactions, American Nuclear Society, 101 696, 2010.

[52] “Present Status of Minor Actinide Data,” NEA/WPEC-8,OECD/NEA (1999)

[53] G. Aliberti, G. Palmiotti, M. Salvatores, and C. G. Stenberg, “Impact of Nuclear Data Uncertainties on Transmutation of Actinides in Accelerator-Driven Assemblies”, Nuclear Science and Engineering: **146**, 13–50 (2004).

[54] B. T. Rearden, M. A. Jessee, and M. L. Williams, “TSUNAMI-1D: Module for One-Dimensional Cross-Section Sensitivity and Uncertainty”, ORNL/TM-2005/39, Version 6.1 Section C8, Oak Ridge National Laboratory, June 2011

[55] A. Piszcz and T. Soule, “Genetic programming: Optimal population sizes for varying complexity problems,” in *Proceedings of the Genetic and Evolutionary Computation Conference,* 2006, pp. 953-954.

Vita

Susan Hogle was born on April 28, 1982 is Napanee, Ontario, Canada to her parents Anne and Hubert Hogle. She attended Napanee District Secondary School, graduating with honors in the spring of 2000. Susan attended the University of Toronto in Toronto, Ontario, Canada from 2000 to 2004 where she studied Mechanical Engineering. During the summer of 2003 she was fortunate enough to be offered an internship with Atomic Energy of Canada in Chalk River, Ontario. It was during this summer that Susan developed an interest in nuclear physics and engineering. After obtaining her bachelors of applied science in 2004 Susan elected to obtain work experience before choosing a field for graduate studies.

After continuing to work in the nuclear industry, in 2008 Susan returned to school to focus on nuclear engineering, obtaining her Masters of Science from the University of Tennessee in 2009. Susan continued her studies with the University of Tennessee under the guidance of her advising professor Dr. G. Ivan Maldonado working in the area of reactor physics. Susan will graduate with her Ph. D. in nuclear engineering in the fall of 2012.